Electronic Supporting Information

Heterometallic NIR-emitting nanothermometers by click-reaction between two lanthanide complexes

Daniil .S. Koshelev *[a,b], Alexey V. Medved'ko [c], Alexander.S. Goloveshkin [d], Yulia V. Nelubina [d], Olga A. Maloshitskaya[b], Elnara S. Safiullina[d],[g], Yulia A. Gracheva[b], Evgeny A. Nikitin[b], Leonid S. Lepnev [e], Sergey Z. Vatsadze,[c] and Valentina V. Utochnikova *[a,b]

a) Faculty of Material Sciences, Lomonosov Moscow State University
1/73 Leninskie Gory, Moscow, 119991, Russia

b) Department of Chemistry, Lomonosov Moscow State University
1/3 Leninskie gory, Moscow, 119991, Russia

c) Zelinsky Institute of Organic Chemistry RAS, 47 Leninsky Prospekt, Moscow, 119991, Russia

d) A.N.Nesmeyanov Institute of Organoelement Compounds, Russian Academy of Sciences, 119334 Vavilova St. 28, bld. 1, Moscow, Russia

e) P.N. Lebedev Physical Institute of the Russian Academy of Sciences, GSP-1, Moscow, Leninsky Prospekt, 53, GSP-1 Moscow, 119991, Russia

f) A.V. Topchiev Institute of Petrochemical Synthesis, RAS, 29 Leninskiy pr., 119991, Moscow, Russia.

daniil.s.koshelev@gmail.com

valentina.utochnikova@gmail.com

Experimental section

Materials and Methods

All solvents and chemicals were purchased from commercial sources.

Powder X-ray diffraction (PXRD) was performed by using Bruker D8 Advance [λ(Cu-Kα) = 1.5418 Å; Ni filter] and Bruker D8 Advance Vario diffractometers [λ(Cu-$K\alpha_1$) = 1.54060 Å; Ge(111)-monochromator] with a step size of 0.020°. The patterns were indexed using SVD-Index [1] as implemented in the TOPAS 4.2 software. Then, the powder patterns were refined by using the Pawley method. **Thermal analysis** was carried out on an STA 409PC Luxx thermoanalyzer (NETZSCH, Germany) in the temperature range of 20-1000°C in air, at the heating rate of 10 (°)/min. The evolved gases were simultaneously monitored during the TA experiment using a coupled QMS 403C Aeolos quadrupole mass spectrometer (NETZSCH, Germany). **The mass spectra** were registered for the species with the following m/z values: 17, 18 (corresponding to OH^-, H_2O), 30 (corresponding to CH_2O, CH_3NH^{-2}, $C_2H_5^{-2}$, $^{15}N_2$), 44 (corresponding to CO_2), 64 (corresponding to SO_2). **MALDI MS spectra** were carried out on a Bruker Autoflex II instrument (resolution FWHM 18000) equipped with a nitrogen laser with an operating wavelength of 337 nm and a time-of-flight mass analyzer operating in the reflectron mode. Accelerating voltage 20 kV. The samples were applied to a polished steel substrate without matrix or with CHCA (alpha-cyano-4-hydroxy-cinnamic acid). The spectra were recorded in the positive ion mode. The resulting spectrum was the sum of 50 spectra obtained at different points in the sample. The **FTIR spectra** were recorded on a Thermo Scientific™ Nicolet™ iS50 FTIR Spectrometer as a powder at ATR in attenuated total reflectance mode in the wavenumber range of 400 - 4000 cm^{-1} with Universal ATR accessory (diamond/KRS-5 crystal).

^{1}H and diffusion-ordered (DOSY) NMR spectra were recorded from DMSO-d_6 and $CDCl_3$ solutions on a Bruker Avance 300 FT-NMR spectrometer (^{1}H frequency 300.15 MHz) and Bruker Ascend 400 spectrometer (^{1}H frequency 400.1 MHz). The residual solvent signals were used as internal references.

DOSY experiments were acquired using the Bruker ledbpgp2s pulse program (2D LED experiment using bipolar gradients). The gradient pulse length δ was optimised and was set as 0.04 s. The diffusion delay was set to 50 ms. For all experiments, gradients were linearly sampled from 0.68 $G \cdot cm^{-1}$ to 32.35 $G \cdot cm^{-1}$ in 32 points and the gradient pulses were sine. Eight scans were acquired on 32k data points (3 s recycle time). Fourier transform was applied to the free induction decays (FIDs) using the Topspin software (Bruker) and an automatic baseline

correction routine was applied. For all pulse sequences, the experimental signal amplitude (*I*) of an NMR resonance is given by the Stejskal–Tanner equation [2].

$$I = I_0 exp\left(-D\gamma^2 g^2 \delta^2 \left(\Delta - \frac{\delta}{3} - \frac{\tau}{2}\right)\right)$$

where I_0 is the reference amplitude (at zero gradient strength), *D* is the diffusion coefficient, γ is the gyromagnetic ratio of the observed nucleus, τ is the time between the bipolar gradient pulses, *g* is the gradient strength, δ is the gradient pulse length, and Δ is the diffusion time (self-diffusion).

Absorption spectra of Yb(**L**)(H**L**) and K[Yb(**L**)$_2$](H_2O)$_n$ (**L=**L1, L2) in the ranges 200–600 nm and in 950-1100 nm were obtained using Perkin-Elmer Lambda 35 UV/vis Spectrometer (Perkin Elmer). The registration of **luminescence spectra** in the NIR range and the measurement of **quantum yields** were carried out with Maya2000 Pro spectrofluorimeter (Ocean Optics) as detector and xenon lamp as excitation source at room temperature; excitation was performed through a ligand (λ_{ex} = 380 nm). The **quantum yield** was measured by the absolute method in the integrating sphere. The **observed luminescence lifetimes** in the NIR range were determined using a Boxcar Averager system (model 162) including gated integrators (model 164), a monochromator MDR-3, a filter KS-19 and a photomultiplier FEU-106 and a wide-band preamplifier (model 115) from EG&G Princeton Applied Research. Lifetimes were calculated from the luminescence decay curves recorded upon excitation with a nitrogen laser LGI-21 (337 nm).

Crystal structure determination

Colourless crystals of H_2L2 and yellow crystals of K[Nd(L1)2](THF) were obtained by n-Hexane diffusion to the solution of the corresponding compounds in THF.

The suitable crystals were selected and mounted on a Bruker Quest D8 diffractometer equipped with a Photon-III area-detector (graphite monochromator, shutterless ϕ and ω-scans), using MoKα-radiation (λ = 0.71073 Å). The crystals were kept at 120 K during data collection. The structure was solved by direct methods and refined on F2 using SHELXTL and OLEX2 software package [3–5].

Positions of all non-hydrogen atoms and hydrogen atoms of amide groups were found from the electron density difference map. C-H hydrogen atoms were located in calculated positions and refined within the riding model.

Atoms were refined with individual anisotropic (non-hydrogen atoms) or isotropic (hydrogen atoms) displacement parameters. The OLEX2 program suite was used for molecular graphics.

Atomic coordinates, bond lengths, angles and thermal parameters have been deposited at the Cambridge Crystallographic Data Centre with deposition numbers CCDC 2364377.

Crystal Data for K[Nd(L1)$_2$](THF) or $C_{48}H_{44}KN_{12}NdO_7S_2$ (*M* =1148.41 g/mol): monoclinic, space group $P2_1$ (no. 4), *a* = 9.759(3) Å, *b* = 20.683(5) Å, *c* = 12.297(3) Å, *β* = 90.102(7)°, *V* = 2482.1(11) Å^3, *Z* = 2, *T* = 120 K, μ(MoKα) = 1.278 mm^{-1}, *Dcalc* = 1.537 g/cm^3, 18025 reflections measured (3.312° ≤ 2Θ ≤ 52.742°), 9900 unique (R_{int} = 0.0823, R_{sigma} = 0.2034) which were used in all calculations. The final R_1 was 0.0544 (I > 2σ(I)) and wR_2 was 0.1293 (all data).

Yellow tiny crystals of Er(L2)(HL2) were obtained by n-Hexane diffusion to the solution of the compound in THF.

X-ray diffraction data for Er(L2)(HL2) were collected at 100 K at the BL13-XALOC beamline[6] of the ALBA synchrotron (λ = 0.72931 Å). Data reduction and absorption corrections for **1**, and **2** were performed with respectively SAINT and SADABS.[7,8] Data reduction for compounds **3** was done with autoproc package [9] and XDS.[10] Using Olex2,[5] the structure was solved with the ShelXT[11] structure solution program using Intrinsic Phasing and refined with the XL[12] refinement package using Least-Squares minimization against F^2 in anisotropic approximation for non-hydrogen atoms. Hydrogen atoms of NH groups were located from different Fourier syntheses, positions of other atoms were calculated, and they all were refined in the isotropic approximation in the riding model. Crystal data and structure refinement parameters are given in Table S1. CCDC 2367003 contains the supplementary crystallographic information for Er(L2)(HL2).

Table S1: Crystal data and structure refinement details for Er(L2)(HL2).

	Er(L2)(HL2)
Formula	$C_{92}H_{70}Er_2N_{12}O_{12}S_4$
M	1998.36
T, K	100
Crystal system	Monoclinic
Space group	*P21/n*
Z (*Z'*)	4 (2)
a, Å	15.530
b, Å	28.990
c, Å	22.510
α, deg	90

β, deg	106.74
γ, deg	90
V, Å^3	9704.9
dialled, gcm^{-3}	1.368
μ, mm^{-1}	19.82
F_{000}	4008
θ_{max}, deg	50
The number of measured refl.	100934
The number of independent refl. (R_{int})	15136
Observed refl. [$I > 2\sigma(I)$]	12272
Parameters	1142
R_1 and wR_2 [$F^2 > 2\sigma(F^2)$]	0.0626
R_1 and wR_2 (all data)	0.1796
$S(F^2)$	1.017
Residual electron density (d_{max}/d_{min}), eÅ^{-3}	3.658/-1.466

Biological activity. MTT-test

The human HCT116 colorectal carcinoma, A549 non-small cell lung carcinoma, MCF7 breast adenocarcinoma, and WI-38 diploid human cell line composed of fibroblasts were obtained from the European collection of authenticated cell cultures (ECACC; Salisbury, UK). Cells (HCT116, MCF7, WI-38) were grown in a DMEM medium (Gibco™, Ireland) and RPMI medium (A549) supplemented with 10% fetal bovine serum (Gibco™, Brazil). The cells were cultured in an incubator at 37 ◦C in a humidified 5% CO_2 atmosphere and were sub-cultured 2 times a week. The effect of the investigated compounds on cell proliferation was evaluated using a common MTT assay. The cells were seeded in 96-well tissue culture plates («TPP», Trasadingen, Switzerland) at 7 × 10^3 cells/well in 100 μL of the medium. After overnight incubation at 37 ◦C, the cells were treated with the tested compounds in the concentration range of 0 to 100 μM. Cisplatin was used as a standard. After 72 h of treatment, the solution was removed, and a freshly diluted MTT (3-(4,5-dimethylthiazol-2-yl)-2,5-diphenyltetrazolium bromide) (Sigma-Aldrich, St. Louis, USA) solution (100 μL, 0.5 mg/mL in cell medium) was added to the wells, and the plates were further incubated for 50 min. Subsequently, the medium was removed, and the formazan product was dissolved in 100 μL of DMSO (Component Reactive, Moscow, Russia). The number of living cells in each well was evaluated by measuring the absorbance at

570 nm using the «Zenith 200 rt» microplate reader (Biochrom, Cambridge, UK) Each experiment was repeated three times, and each concentration was tested in three replicates. The meanings of 50% inhibition concentration (IC_{50}) with standard deviation were calculated using GraphPad Prism Version 5.03 for Windows.

Synthesis

Synthesis of Schiff bases' precursors

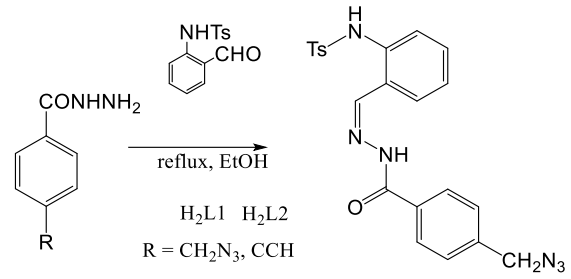

Figure S 1. Synthesis of the substituted hydrazones: 2-tosylaminobenzaldehyde-4-azidomethylbenzoylhydrazone (H_2L1, R = CH_2N_3) and 2-tosylamino-benzaldehyde 4-ethinylbenzoylhydrazone (H_2L2, R = CCH).

For Schiff bases condensation, some precursors were prepared. The 2-(N-tosylamino)benzaldehyde was obtained during the procedure described earlier [13]. The 4-(azidomethyl)-benzohydrazide was obtained by a 3-step procedure described earlier [14–16]. The 4-(ethynyl)-benzohydrazide was obtained by a 3-step procedure described earlier [17,18] .

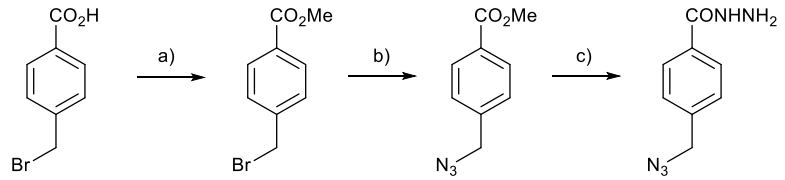

Figure S 2 a) $SOCl_2$, MeOH, reflux, 2.5 h, 75%; b) NaN_3, TBAI, DMF, 60°C, 16 h, 88%; c) N_2H_4*H_2O, EtOH, reflux, 3.5 h, 78%.

After each step, the purity of the products was monitored by ^{1}H NMR spectroscopy (see **Figure S 4 – Figure S 6**).

Methyl 4-(bromomethyl)benzoate was synthesized by known reaction [14]. White powder, 75%. ^{1}H NMR (300 MHz, $CDCl_3$) δ 8.01 (d, J = 8.1 Hz, 2H), 7.45 (d, J = 8.1 Hz, 2H), 4.49 (s, 2H), 3.91 (s, 3H).

Methyl 4-(azidomethyl)benzoate was synthesized by known reaction [15]. White powder, 88%. ^{1}H NMR (300 MHz, $CDCl_3$) δ 8.01 (d, Colorless oil, 88%. ^{1}H NMR (300 MHz, $CDCl_3$) δ 8.06 (d, J = 8.0 Hz, 2H), 7.39 (d, J = 8.0 Hz, 2H), 4.42 (s, 2H), 3.93 (s, 3H).

4-(azidomethyl)benzohydrazide was synthesized by known reaction [16]. White flakes, 78%. ^{1}H NMR (300 MHz, DMSO-d6) δ 9.78 (s, 1H), 7.84 (d, J = 8.2 Hz, 2H), 7.44 (d, J = 8.1 Hz, 2H), 4.50 (d, J = 6.5 Hz, 4H), 3.33 (s, 3H).

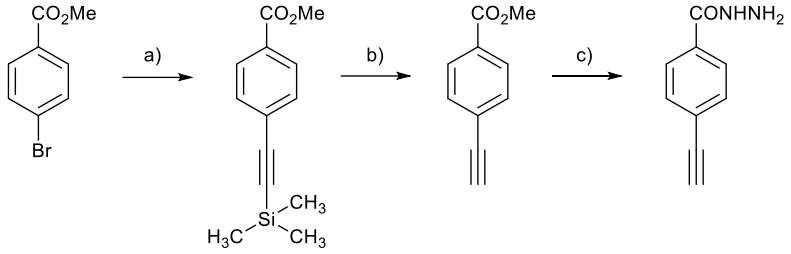

Figure S 3. a) Trimethylsilylacetylene, $Pd(PPh_3)_2Cl_2$, CuI, Et_3N, 50°C, 24 h, 94%; b) K_2CO_3, MeOH, rt, 2 h, 72%; c) $N_2H_4*H_2O$, EtOH, reflux, 1 h, 65%.

Methyl 4-(trimethylsilylethynyl)benzoate was synthesized by a known reaction [17]. Colourless oil, 94%. ^{1}H NMR (300 MHz, Chloroform-*d*) δ 8.04 – 7.93 (m, 2H), 7.59 – 7.48 (m, 2H), 3.93 (s, 3H), 0.28 (s, 9H).

Methyl 4-(ethynyl)benzoate was synthesized by a known reaction [18]. Colourless oil, 72%. ^{1}H NMR (300 MHz, DMSO-d_6) δ 7.95 (d, *J* = 8.3 Hz, 2H), 7.62 (d, *J* = 8.4 Hz, 2H), 4.47 (s, 1H), 3.87 (s, 2H), 1.33 (t, *J* = 7.1 Hz, 1H)

4-(ethynyl)benzohydrazide was synthesized by known reaction [16]. Off-white flakes, 65%. ^{1}H NMR (300 MHz, DMSO-d_6) δ 9.86 (s, 1H), 7.82 (d, *J* = 8.3 Hz, 2H), 7.60 – 7.51 (m, 2H), 4.52 (s, 2H), 4.35 (s, 1H).

After each step, the purity of the products was monitored by ^{1}H NMR spectroscopy (see **Figure S 9– Figure S 11**).

General procedure for Schiff bases

The corresponding hydrazide (14.00 mmol) was dissolved in EtOH (60 mL) with heating. Then the solution of 2-(N-tosylamino)benzaldehyde (14.00 mmol) in EtOH (33 mL) was added and the reaction mixture was refluxed for 3 hours. After that, the reaction mixture was cooled in the ice bath. The precipitated crude product was filtered, washed with a small amount of cold EtOH and dried on air. The obtained products were proved by ^{1}H NMR (Figure S7-8, Figure S12).

N-(2-((2-(4-(azidomethyl)benzoyl)hydrazineylidene)methyl)phenyl)-4-methylbenzenesulfonamide (H_2L1)

White powder, 84%. ^{1}H NMR (300 MHz, DMSO-d6) δ 12.13 (s, 1H), 11.06 (s, 1H), 8.56 (s, 1H), 8.01 (d, J = 8.0 Hz, 2H), 7.74 – 7.50 (m, 5H), 7.37 – 7.13 (m, 5H), 4.59 (s, 2H), 2.32 (s, 3H). ^{13}C NMR (75 MHz, DMSO-d6) δ 162.68, 147.87, 143.60, 139.74, 136.45, 136.22, 132.56, 130.54, 129.69, 128.43, 128.21, 126.99, 124.84, 124.72, 121.52, 53.11, 20.97. HRMS (ESI) for $C_{22}H_{21}N_6O_3S^+$ $[M+H]^+$: m/z calcd. 449.1390; found 449.1395.

N-(2-((2-(4-ethynylbenzoyl)hydrazineylidene)methyl)phenyl)-4-methylbenzenesulfonamide (H_2L2)

Beige powder, 90%. ^{1}H NMR (300 MHz, DMSO-d_6) δ 12.18 (s, 1H), 11.03 (s, 1H), 8.57 (s, 1H), 7.99 (d, *J* = 8.1 Hz, 2H), 7.65 (dd, *J* = 15.2, 7.8 Hz, 6H), 7.33 (d, *J* = 8.0 Hz, 3H), 7.30 – 7.14 (m, 2H), 4.44 (s, 1H), 2.33 (s, 3H).

Click-reaction between Schiff bases

To the solution of **H_2L1** (448 mg, 1 mmol, 1 eq) and **H_2L2** (417 mg, 1 mmol, 1 eq) in methanol (50 ml) solutions of sodium ascorbate (4.3 mg, 0.02 mmol, 0.02 eq) in water (1 ml) and copper (II) sulfate pentahydrate (1.59 mg, 0.01 mmol, 0.01 eq) in water (1 ml) were sequentially added. The reaction mixture was stirred overnight at 50°C under argon. The obtained slightly yellow precipitate was filtered, washed with water and methanol and dried on a rotary evaporator. Slightly yellow powder, 95%. The products obtained were proved by ^{1}H NMR spectroscopy (Figure S 13).

4-methyl-N-(2-((2-(4-(1-(4-(2-((Z)-2-((4-methylphenyl)sulfonamido)benzylidene)hydrazine-1-carbonyl)benzyl)-1H-1,2,3-triazol-4-yl)benzoyl)hydrazono)methyl)phenyl)benzenesulfonamide or di(2-tosylaminobenzylidene-benzoyl)-triazole hydrazone (H_4L3)

^{1}H NMR (300 MHz, DMSO-d_6) δ 12.14 (d, *J* = 8.5 Hz, 2H), 11.07 (d, *J* = 12.2 Hz, 2H), 8.86 (s, 1H), 8.58 (d, *J* = 7.9 Hz, 2H), 8.04 (d, *J* = 23.0 Hz, 6H), 7.73 – 7.51 (m, 9H), 7.38 – 7.14 (m, 11H), 2.33 (s, 6H)

13C NMR (76 MHz, DMSO) δ 162.58, 162.50, 147.90, 147.81, 145.91, 143.55, 139.72, 136.44, 136.21, 134.01, 132.71, 131.92, 130.49, 129.65, 128.52, 128.39, 128.31, 128.17, 128.07, 126.94, 125.13, 124.77, 124.65, 124.60, 122.83, 121.48, 121.37, 52.77, 20.95.

References

1 A. A. Coelho, *J. Appl. Crystallogr.*, 2003, **36**, 86–95.

2 E. O. Stejskal and J. E. Tanner, *J. Chem. Phys.*, 1965, **42**, 288–292.

3 G. M. Sheldrick, *Acta Cryst. A*, 2015, **71**, 3–8.

4 G. M. Sheldrick, *Acta Crystallogr. Sect. C Struct. Chem.*, 2015, **71**, 3–8.

5 O. V. Dolomanov, L. J. Bourhis, R. J. Gildea, J. A. K. Howard and H. Puschmann, *J. Appl. Crystallogr.*, 2009, **42**, 339–341.

6 J. Juanhuix, F. Gil-Ortiz, G. Cuní, C. Colldelram, J. Nicolás, J. Lidón, E. Boter, C. Ruget, S. Ferrer and J. Benach, *J. Synchrotron Radiat.*, 2014, **21**, 679–689.

7 G. M. Sheldrick, *Receiv. July*.

8 L. Krause, R. Herbst-Irmer, G. M. Sheldrick and D. Stalke, *J. Appl. Crystallogr.*, 2015, **48**, 3–10.

9 C. Vonrhein, C. Flensburg, P. Keller, A. Sharff, O. Smart, W. Paciorek, T. Womack and G. Bricogne, *Biol. Crystallogr.*, 2011, **67**, 293–302.

10 W. Kabsch, *Acta Crystallogr. Sect. D Biol. Crystallogr.*, 2010, **66**, 125–132.

11 G. M. Sheldrick, *Acta Crystallogr. Sect. A Found. Adv.*, 2015, **71**, 3–8.

12 G. M. Sheldrick, *Acta Crystallogr. Sect. A Found. Crystallogr.*, 2008, **64**, 112–122.

13 N. I. Chernova, Y. S. Ryabokobylko, V. G. Brudz' and B. M. Bolotin, *Chem. Informationsdienst. Org. Chemie*, 1971, **2**, no-no.

14 K. G. Konya, T. Paul, S. Lin, J. Lusztyk and K. U. Ingold, *J. Am. Chem. Soc.*, 2000, **122**, 7518–7527.

15 L. Mancuso, G. Jürjens, J. Hermane, K. Harmrolfs, S. Eichner, J. Fohrer, W. Collisi, F. Sasse and A. Kirschning, *Org. Lett.*, 2013, **15**, 4442–4445.

16 D. S. Koshelev, L. O. Tcelykh, R. E. Mustakimov, A. V. Medved'ko, E. V. Latipov, A. A. Pavlov, A. S. Goloveshkin, V. E. Gontcharenko, K. Y. Vlasova, A. S. Burlov, L. S. Lepnev, S. Z. Vatsadze and V. V. Utochnikova, *J. Lumin.*, 2023, **263**, 120054.

17 V. Percec, J. G. Rudick, M. Peterca, M. Wagner, M. Obata, C. M. Mitchell, W.-D. Cho, V. S. K. Balagurusamy and P. A. Heiney, *J. Am. Chem. Soc.*, 2005, **127**, 15257–15264.

18 B. Chakraborty, D. Dutta, S. Mukherjee, S. Das, N. C. Maiti, P. Das and C. Chowdhury, *Eur. J. Med. Chem.*, 2015, **102**, 93–105.

19 Y. Zhang, W. Thor, K.-L. Wong and P. A. Tanner, *J. Phys. Chem. C*, 2021, **125**, 7022–7033.

20 A. D. Kovalenko, I. S. Bushmarinov, A. S. Burlov, L. S. Lepnev, E. G. Ilina and V. V. Utochnikova, *Dalt. Trans.*, 2018, **47**, 4524–4533.

21 V. V. Utochnikova, A. Y. Grishko, D. S. Koshelev, A. A. Averin, L. S. Lepnev and N. P. Kuzmina, *Opt. Mater. (Amst).*, 2017, **74**, 201–208.

NMR Spectra of ligands

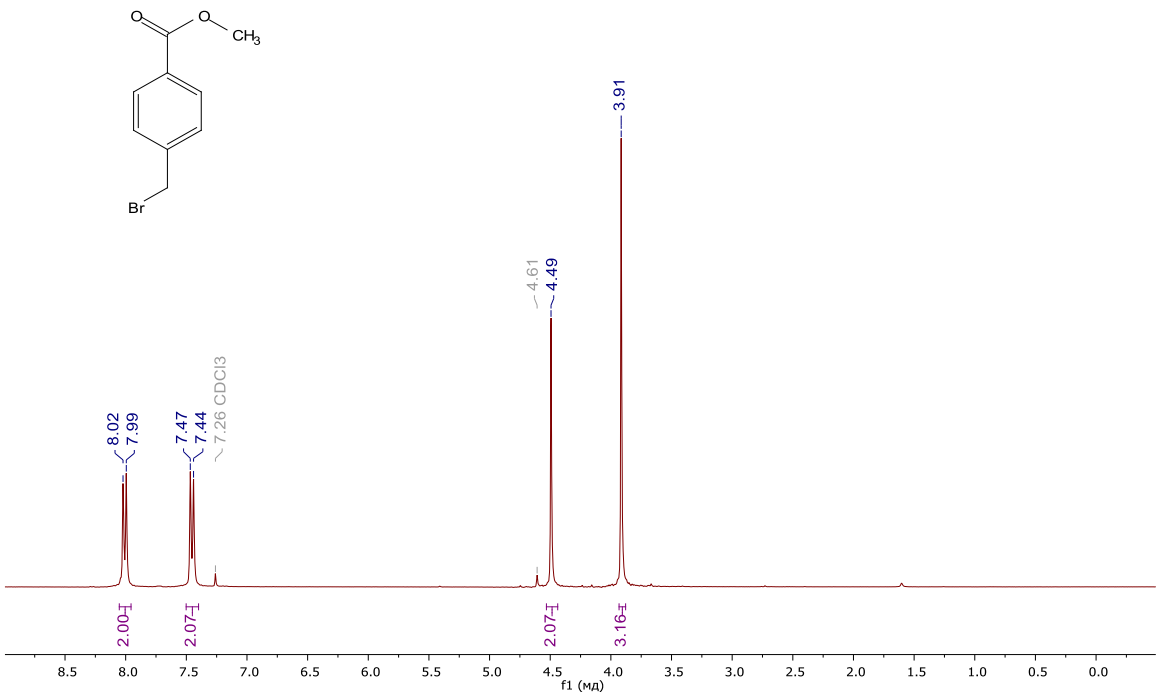

Figure S 4. ^{1}H NMR spectrum (300 MHz, $CDCl_3$) of methyl 4-(bromomethyl)benzoate.

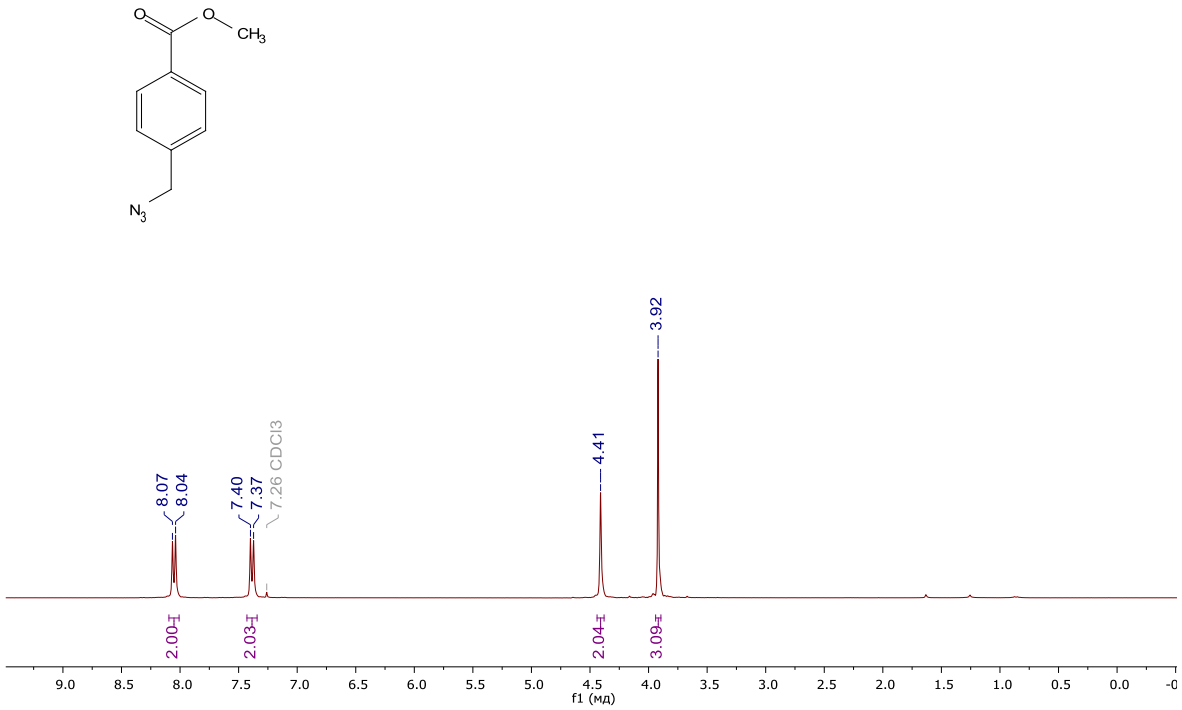

Figure S 5. ^{1}H NMR spectrum (300 MHz, $CDCl_3$) of methyl 4-(azidomethyl)benzoate.

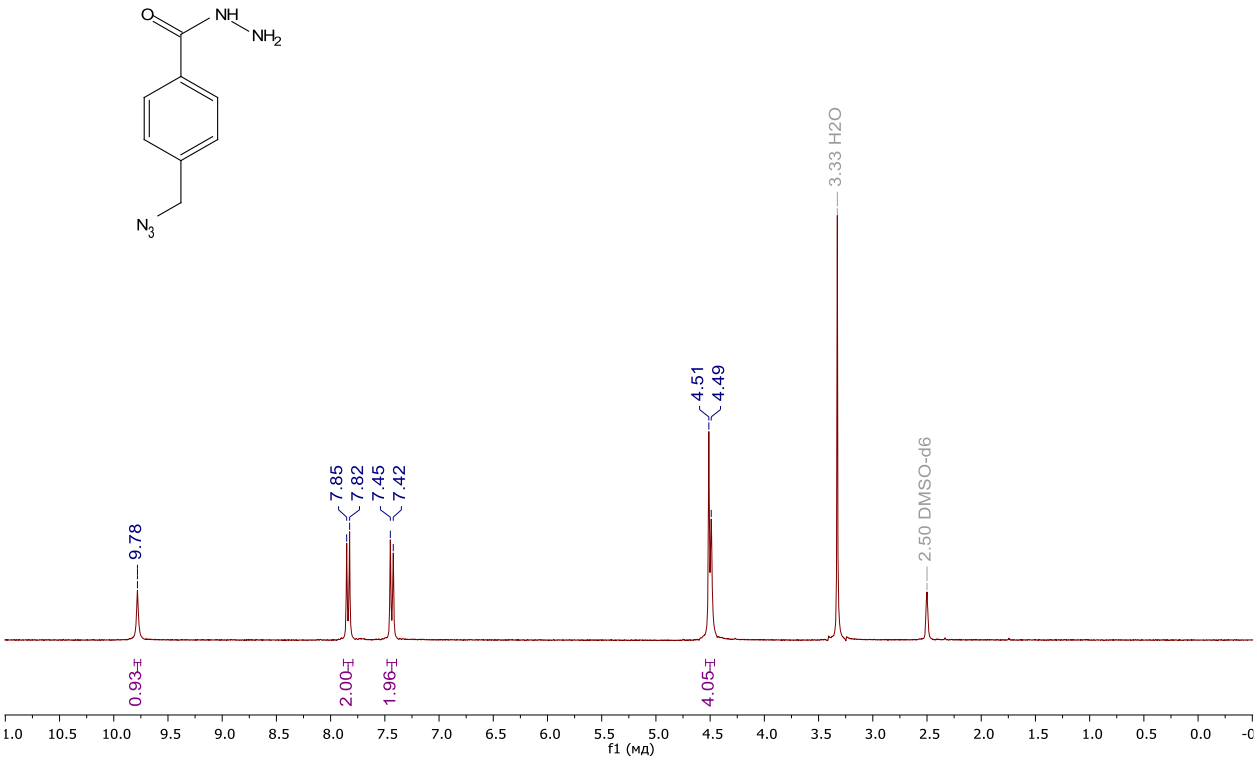

Figure S 6. ^{1}H NMR spectrum (300 MHz, DMSO-d6) of 4-(azidomethyl)benzohydrazide.

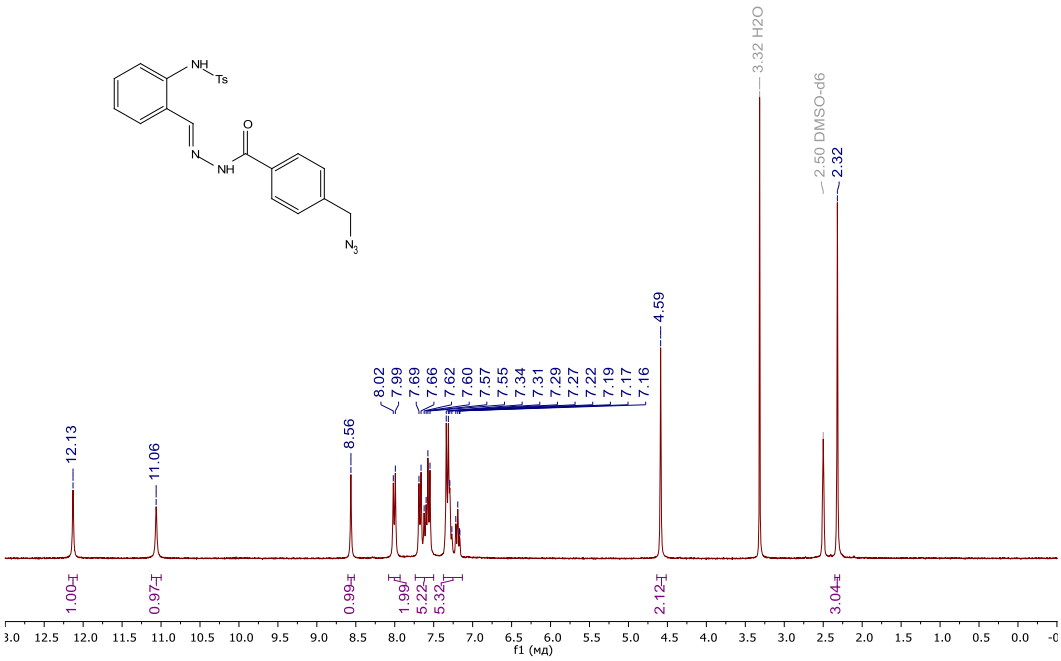

Figure S 7. ^{1}H NMR spectrum (300 MHz, DMSO-d6) of 2-tosylaminobenzaldehyde-4-azidomethylbenzoylhydrazone.

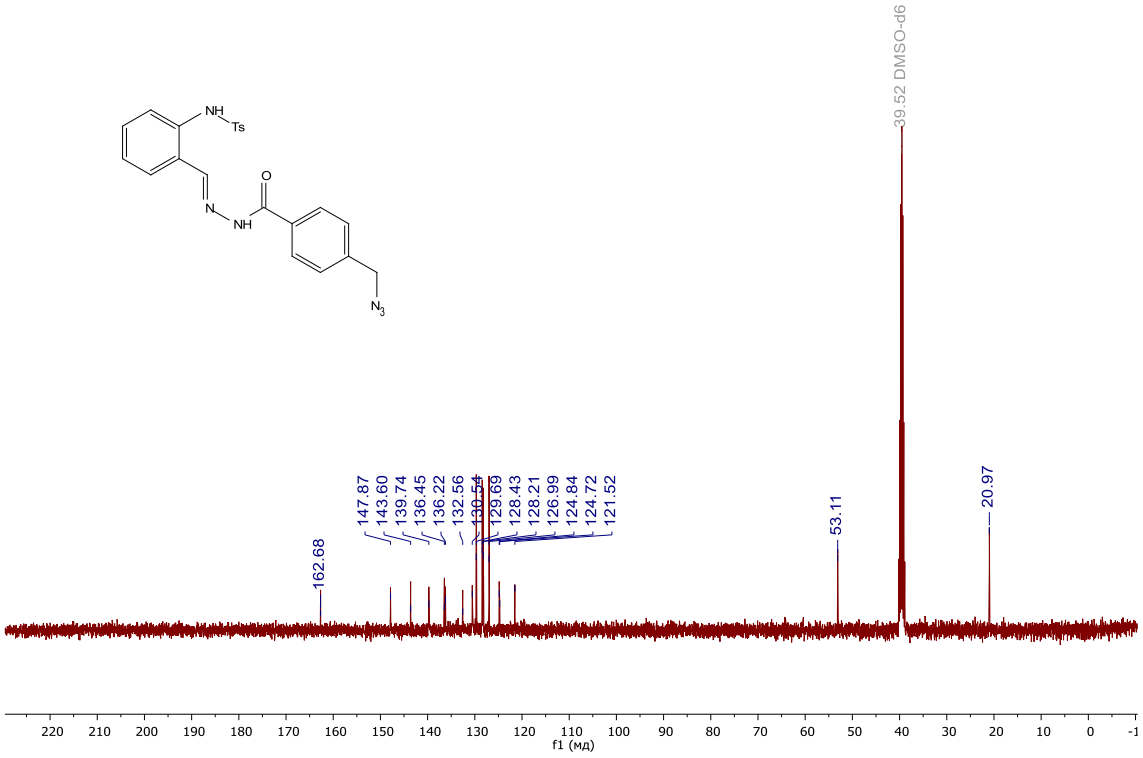

Figure S 8. $^{13}C\{^{1}H\}$ NMR spectrum (75 MHz, DMSO-d_6) of 2-tosylaminobenzaldehyde-4-azidomethylbenzoylhydrazone.

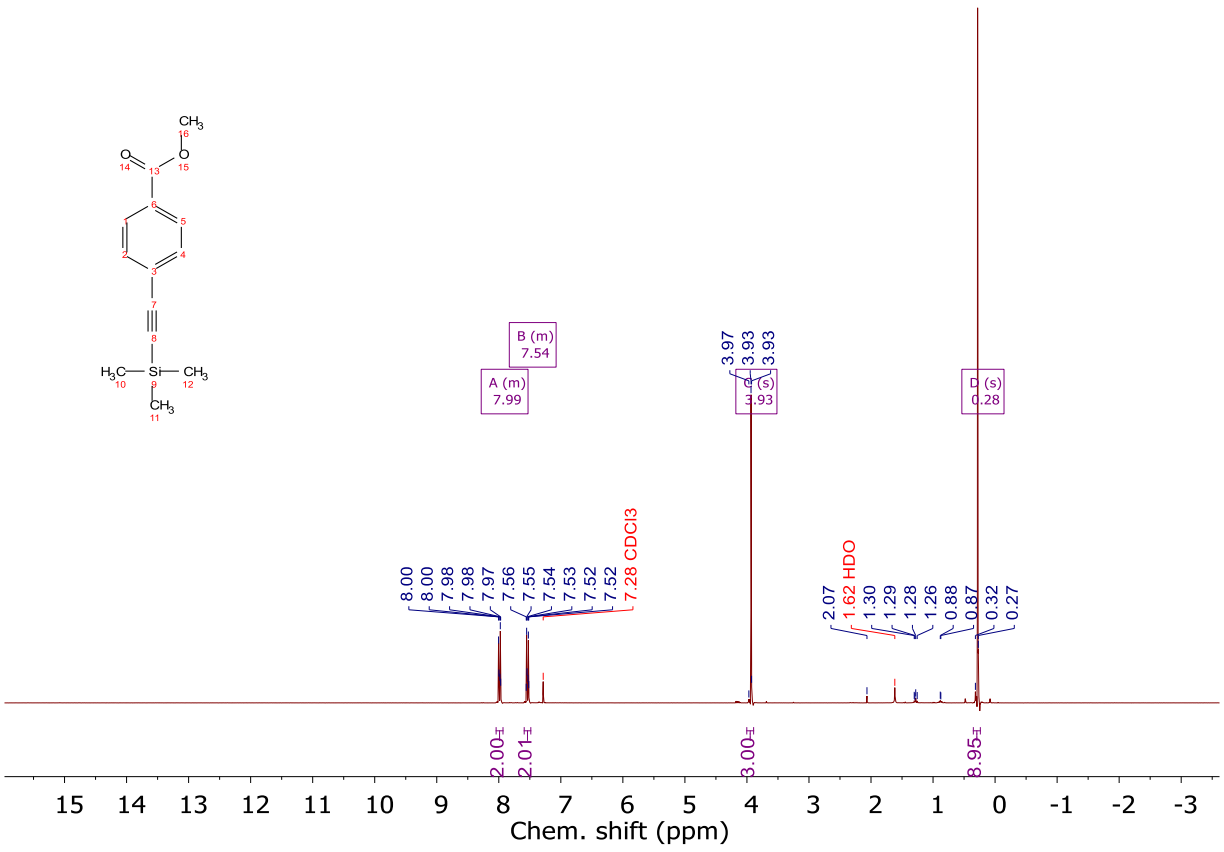

Figure S 9. ^{1}H NMR spectrum (300 MHz, $CDCl_3$) of methyl 4-((trimethylsilyl)ethynyl)benzoate.

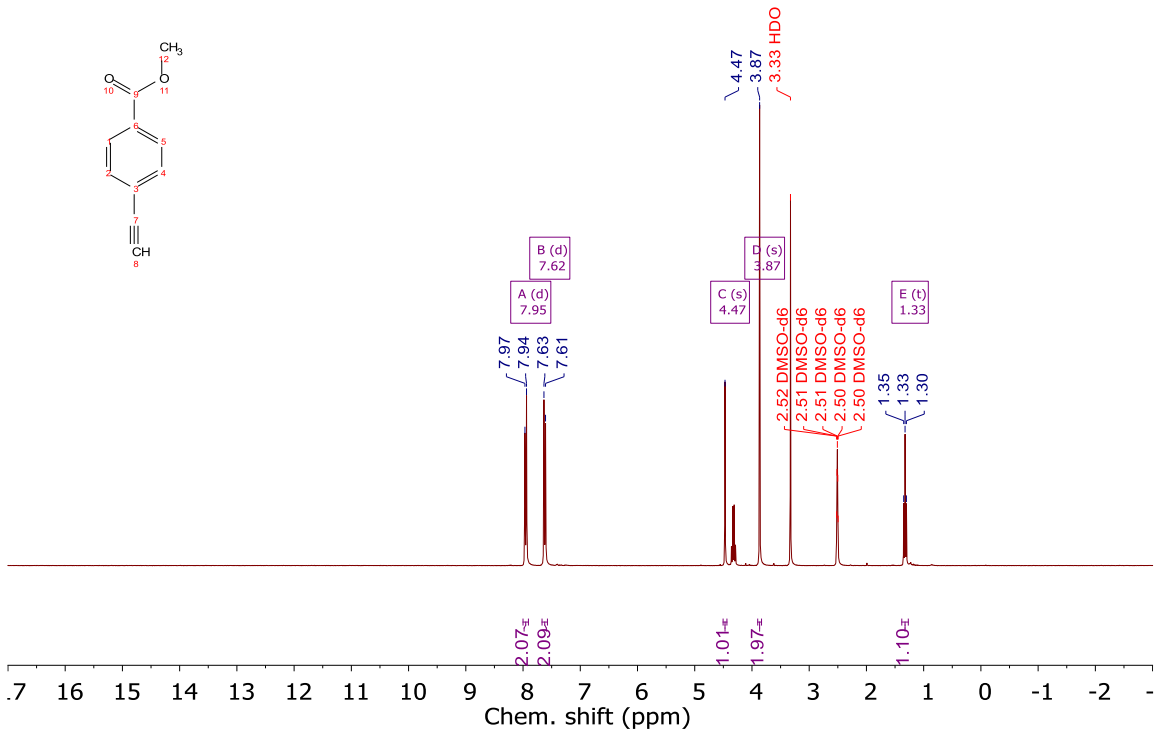

Figure S 10. ^{1}H NMR spectrum (300 MHz, DMSO-d6) of methyl 4-ethynylbenzoate.

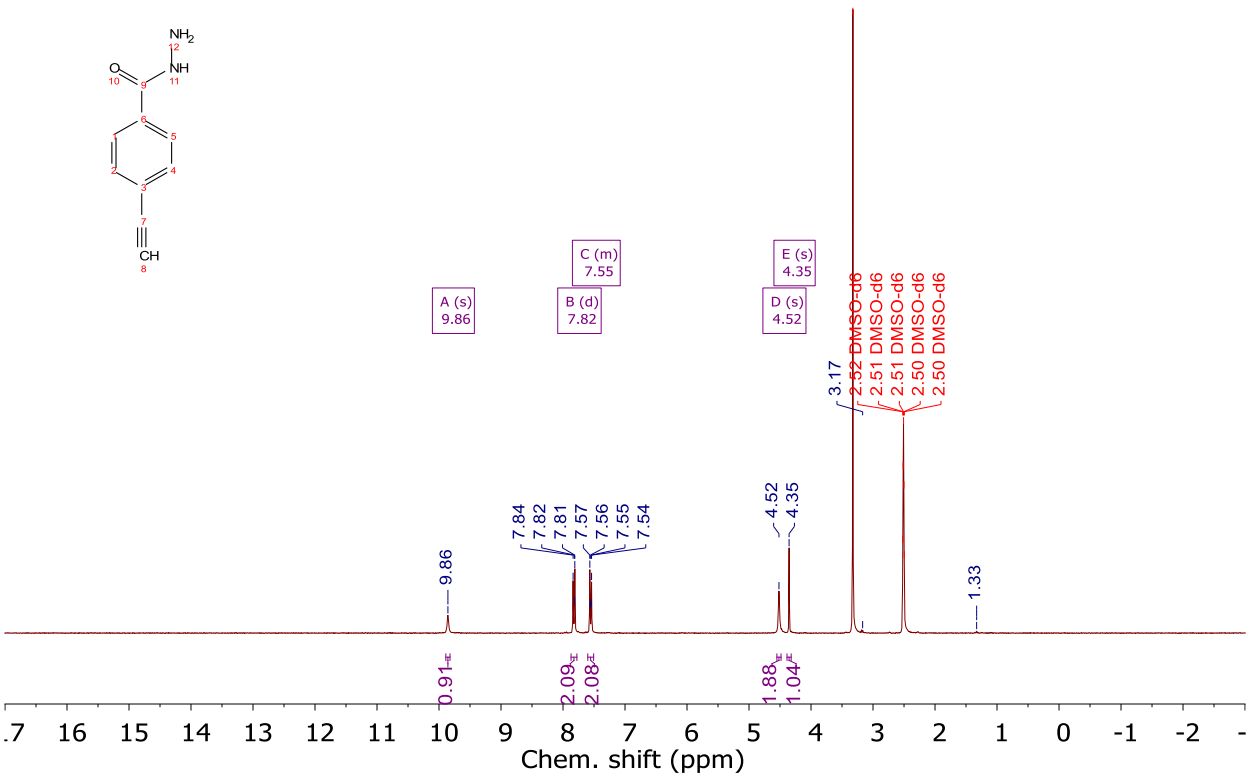

Figure S 11. ^{1}H NMR spectrum (300 MHz, DMSO-d6) of 4-ethynylbenzohydrazide.

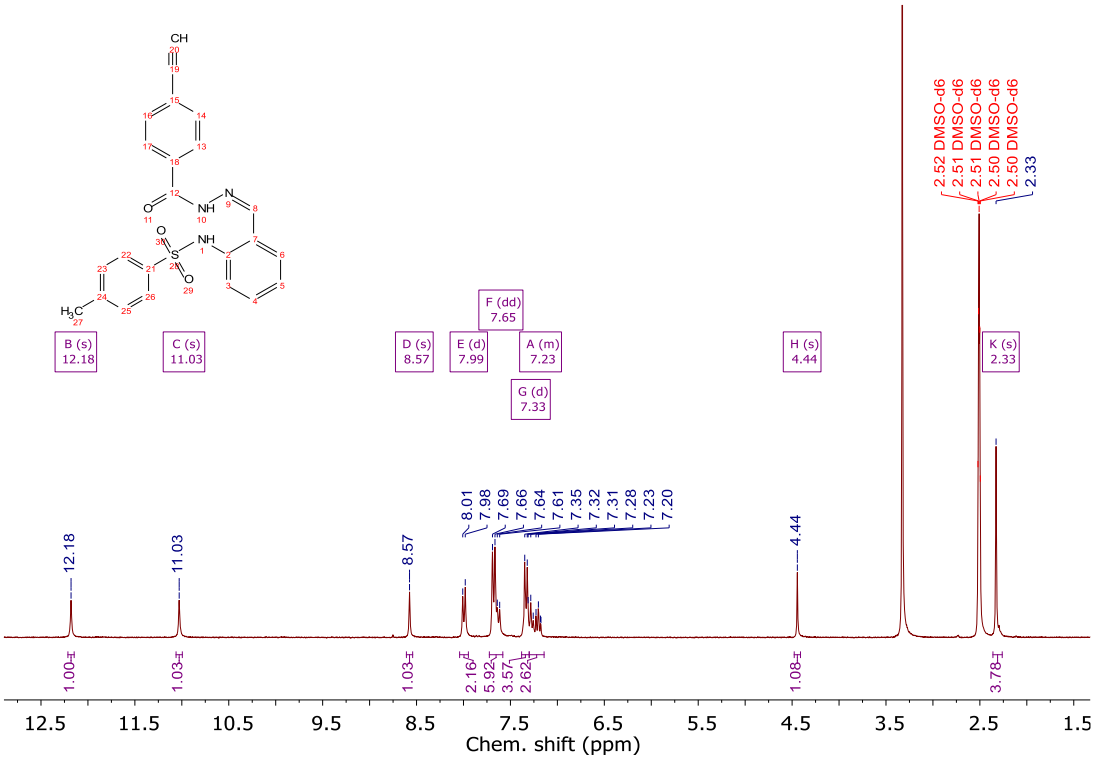

Figure S 12. ^{1}H NMR spectrum (300 MHz, DMSO-d6) of 2-(N-tosylamino)benzylidene (4-ethynyl)benzoylhydrazone.

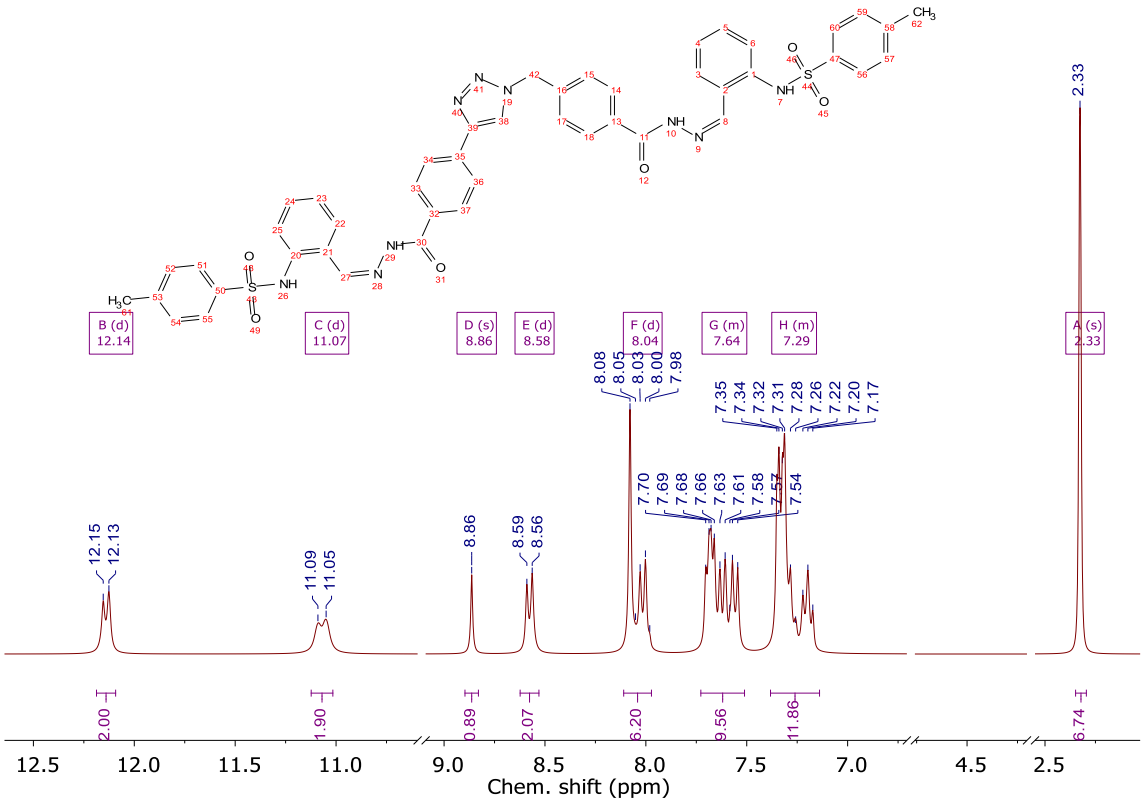

Figure S 13. ^{1}H NMR spectrum (300 MHz, DMSO-d6) of 4-methyl-N-(2-((2-(4-(1-(4-(2-((Z)-2-((4-methylphenyl)sulfonamido)benzylidene)hydrazine-1-carbonyl)benzyl)-1H-1,2,3-triazol-4-yl)benzoyl)hydrazono)methyl)phenyl)benzenesulfonamide or di(2-tosylaminobenzylidene-benzoyl)-triazole hydrazone or H_4L3.

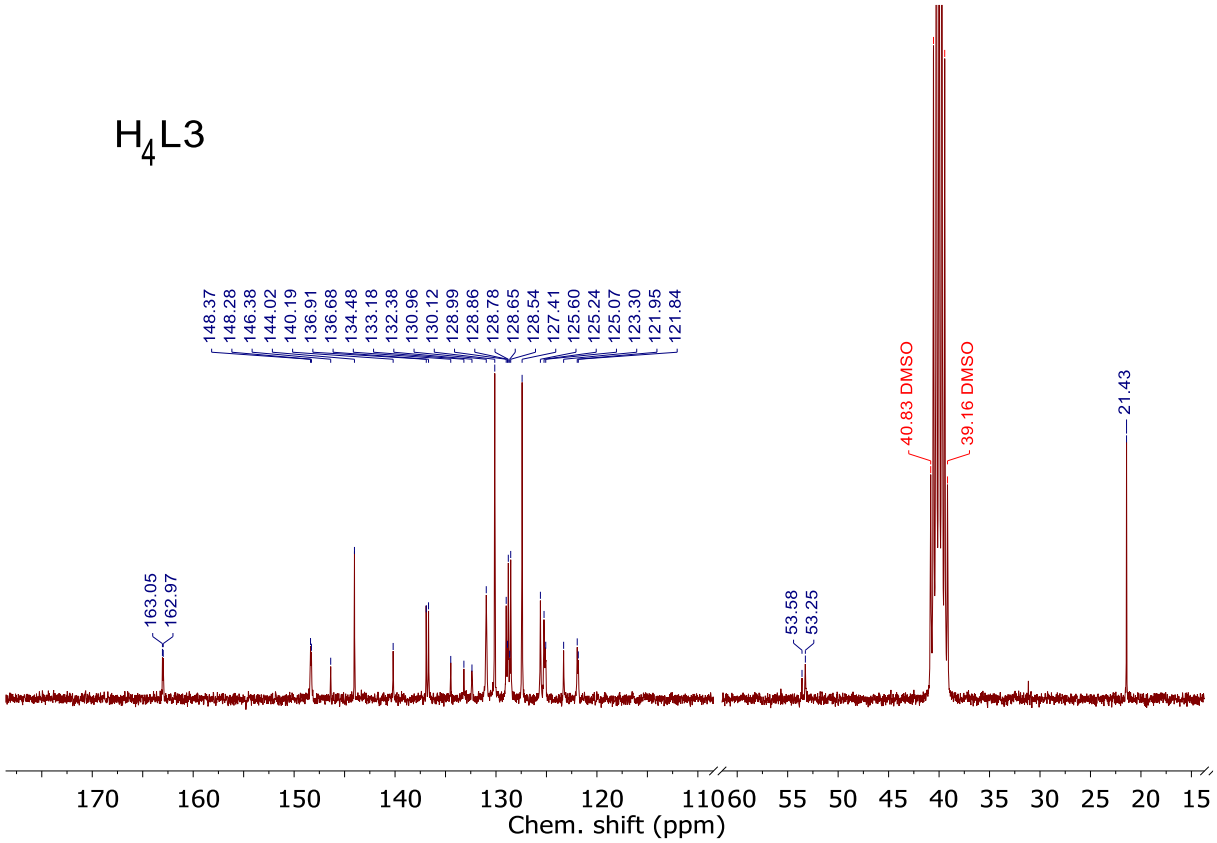

Figure S 14. ^{13}C NMR of H_4L3.

Synthesis of the lanthanide complexes

Synthesis of the Ln(L)(HL) (L=L1, L2). A freshly prepared lanthanide hydroxide (1.0 eq, 0.167 mmol) was added to a hot solution of **H_2L** (L=L1, L2) (2 eq, 0.335 mmol) in a mixture of ethanol:acetonitrile (30 mL, 2:1). The mixture was heated under stirring for 24 h and the solvent was evaporated in half. The precipitate of **Ln(L)(HL)** was filtered off and air-dried. Yellow powder. Yield: 70-80%.

Synthesis of the K[Ln(L)$_2$](H_2O)n (L=L1, L2). To a suspension of Ln(L)(HL) (1.02 eq, 0.075 mmol) in ethanol (4 ml) was added the pre–titrated 40.7 mM KOH solution (1.8 mL, 0.075 mmol). A small excess of the **Ln(L)(HL)** was filtered out and the yellow solution was evaporated to dryness. Recrystallization was carried out from ethanol:water 1:1 solution. Yellow powder. Yield: 70-80%.

Synthesis of the Ln_2(HL3)(Solv). A freshly prepared lanthanide hydroxide (1.0 eq, 0.087 mmol) was added to a hot solution of **H_4L3** (1.03 eq, 0.090 mmol) in THF (100 mL). The mixture was heated under stirring for 48 h and the solvent was evaporated in half. The precipitate $Ln_2(HL3)_2$(Solv) was filtered off and air-dried. Yellow powder. Yield: 80%.

Yield, %	Nd	Gd	Er	Yb	Lu
Ln(L1)(HL1):	81	76	79	77-78	76
K[Ln(L1)$_2$](H_2O)$_2$	72	-	93	45-75	71-72
Ln(L2)(HL2):	62	25	55-82	85	64-74
K[Ln(L2)$_2$](H_2O)$_2$	85	-	82-85	94	70-91
Ln_2(HL3)(Solv)	-	85	-	88	96

PXRD data of complexes

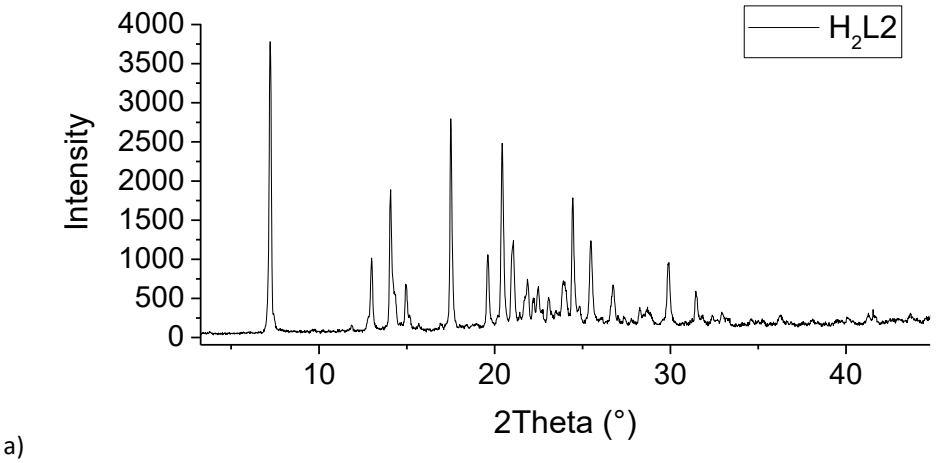

a)

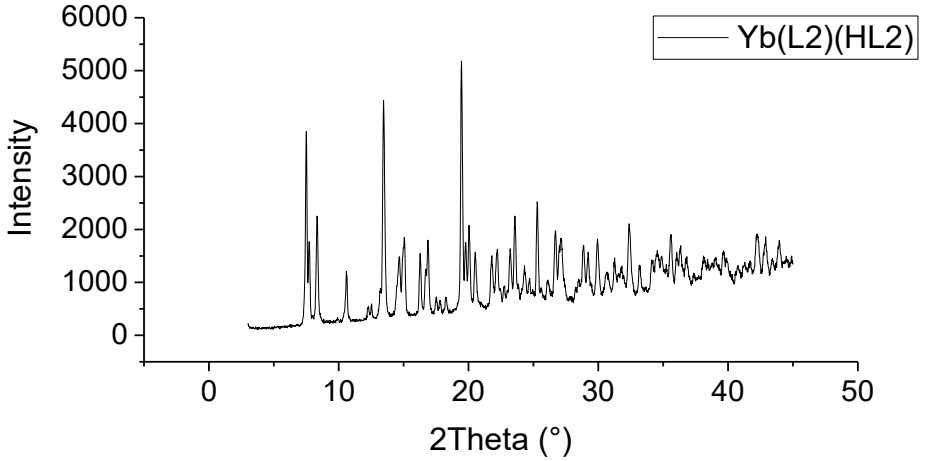

b)

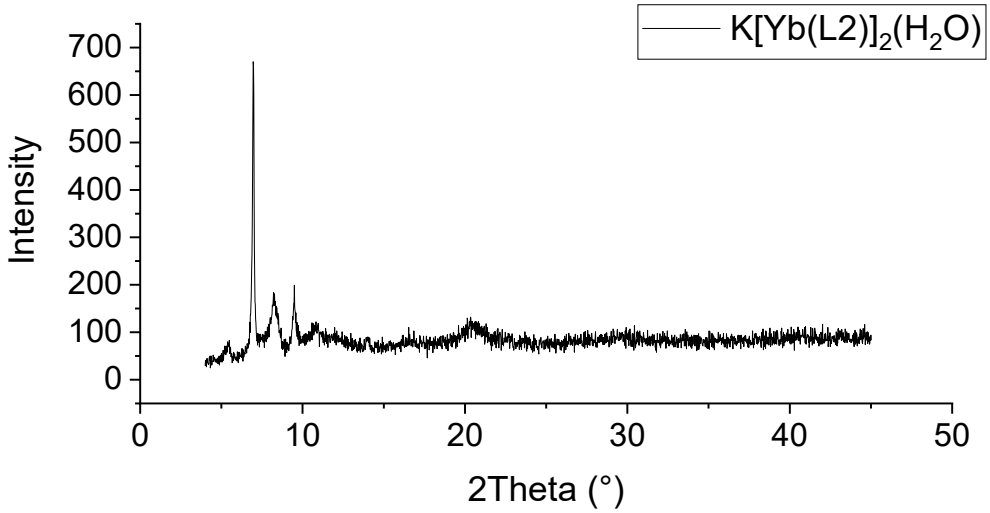

c)

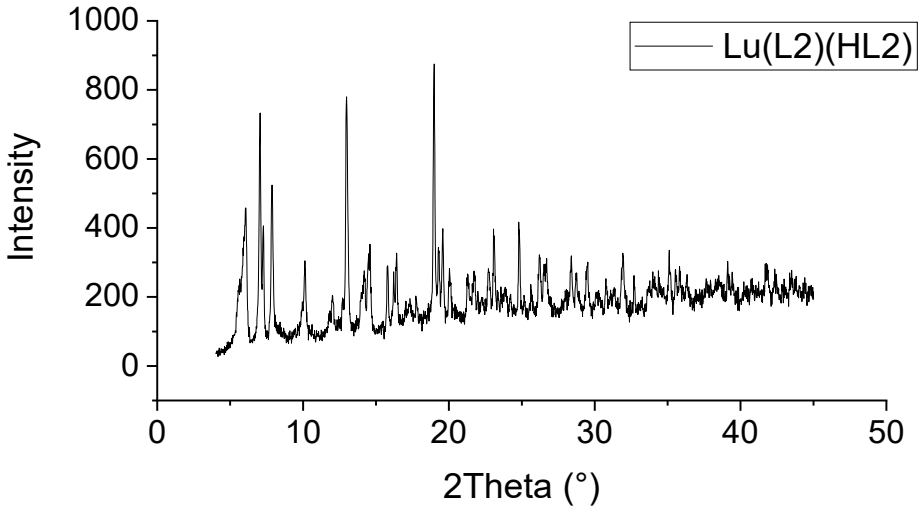
Lu(L2)(HL2)
Intensity
2Theta (°)

d)

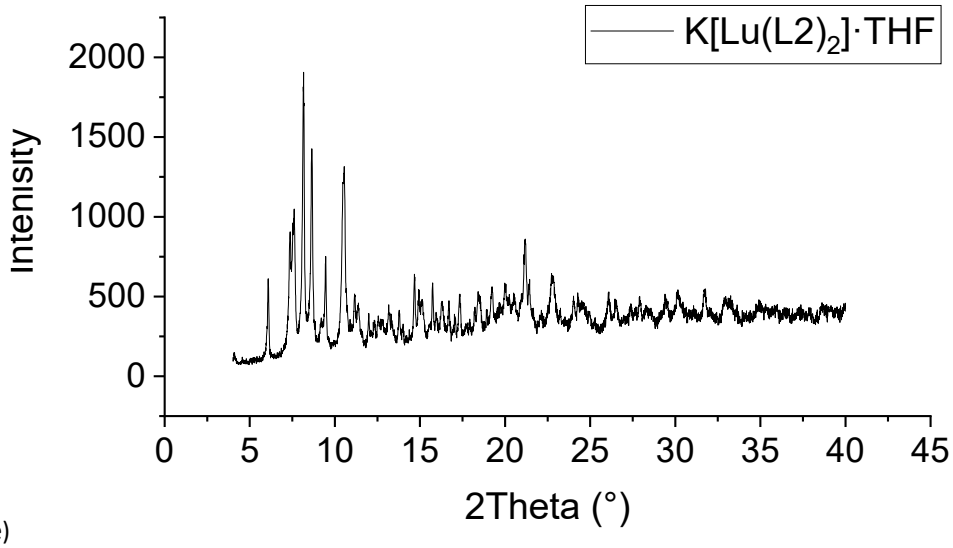
K[Lu(L2)2]·THF
Intenisity
2Theta (°)

e)

f)

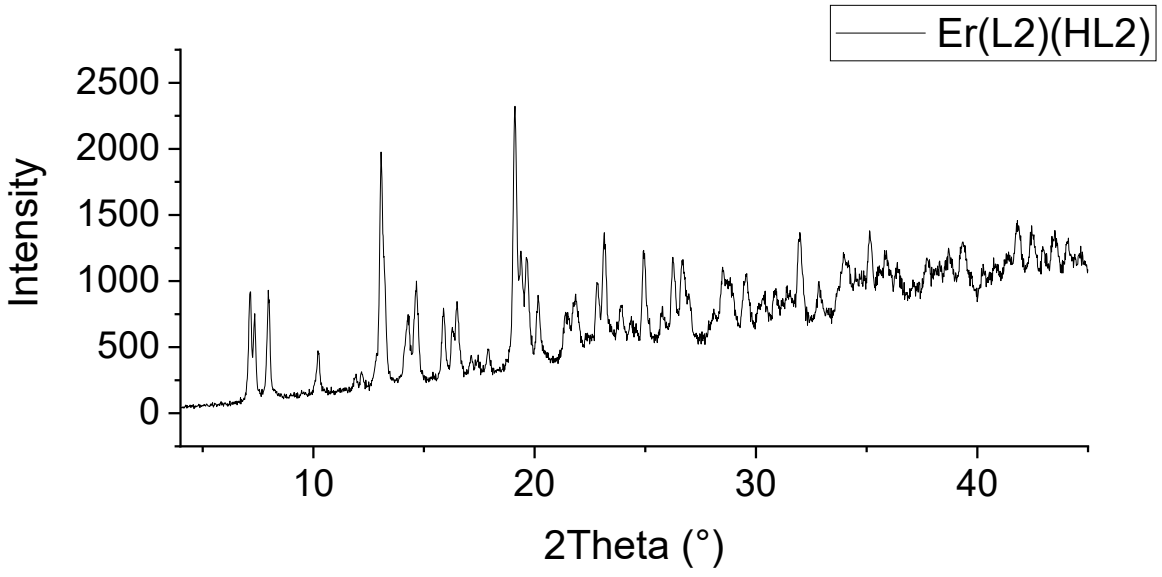
Er(L2)(HL2)
Intensity
2Theta (°)

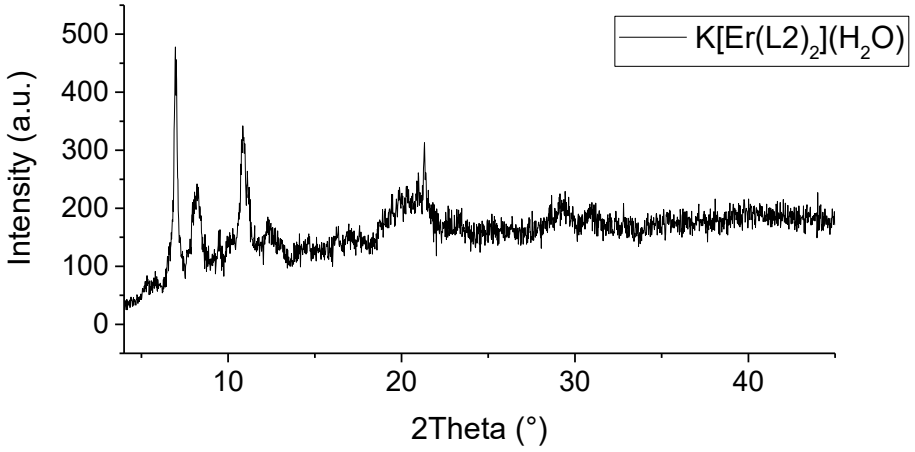
K[Er(L2)2](H2O)
Intensity (a.u.)
2Theta (°)

g)

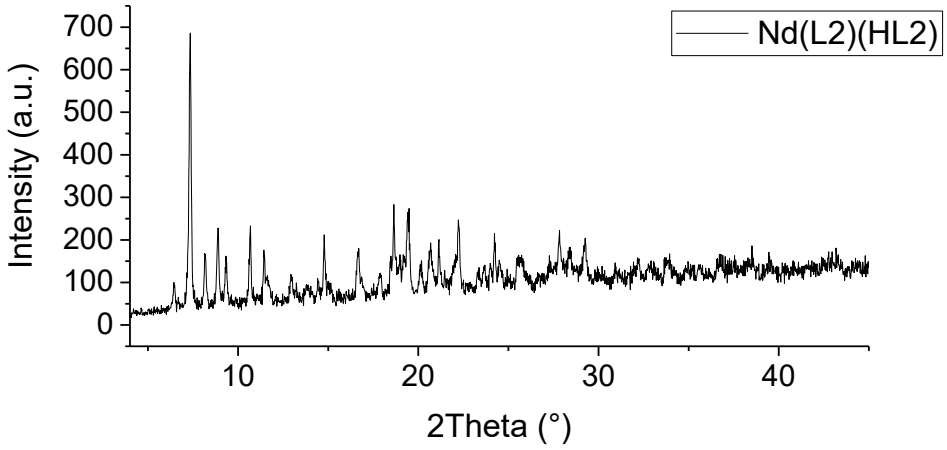
Nd(L2)(HL2)
Intensity (a.u.)
2Theta (°)

h)

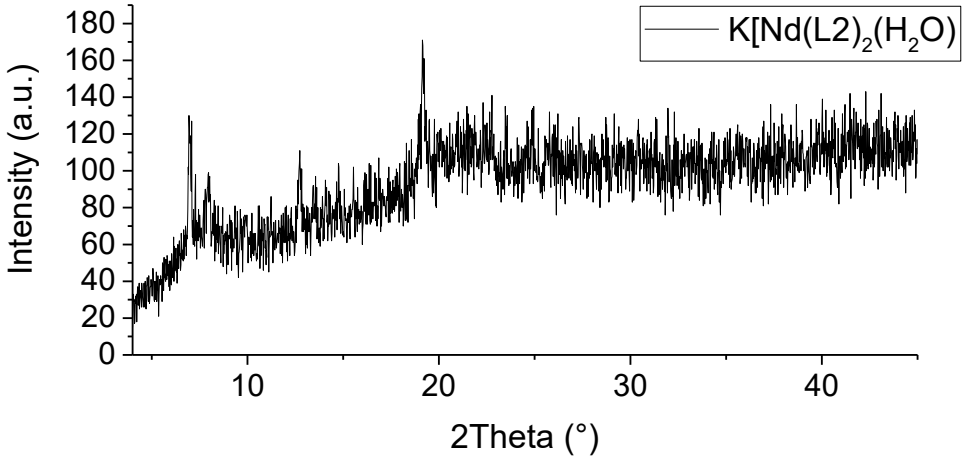
K[Nd(L2)2(H2O)
Intensity (a.u.)
2Theta (°)

i)

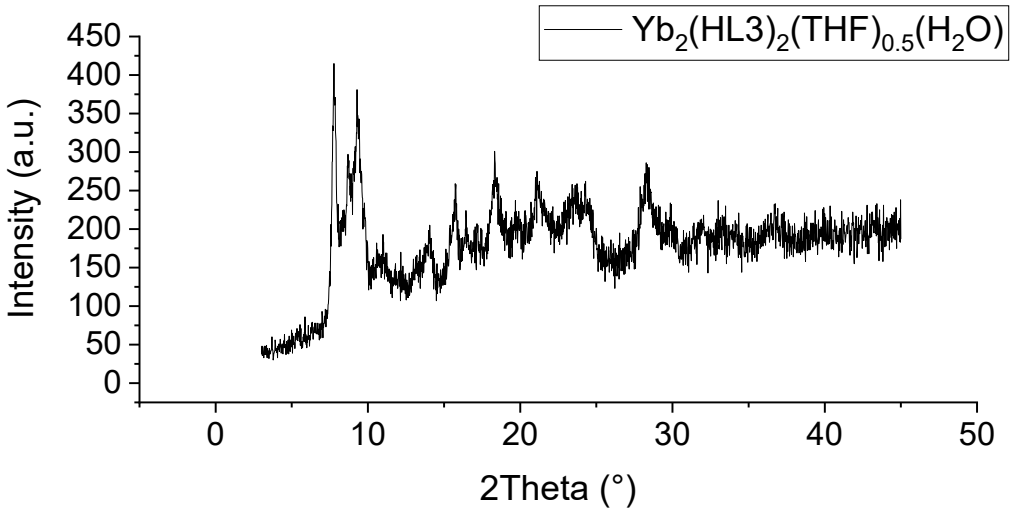

k)

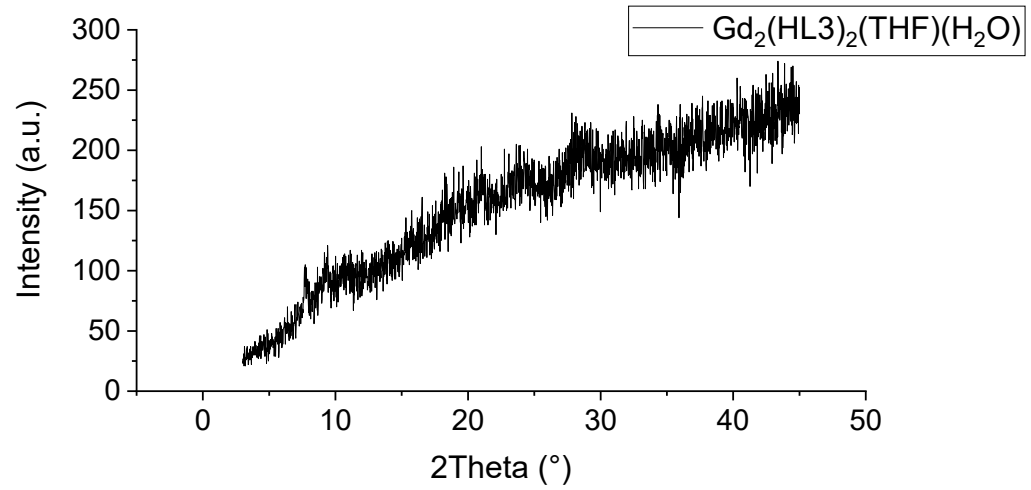

l)

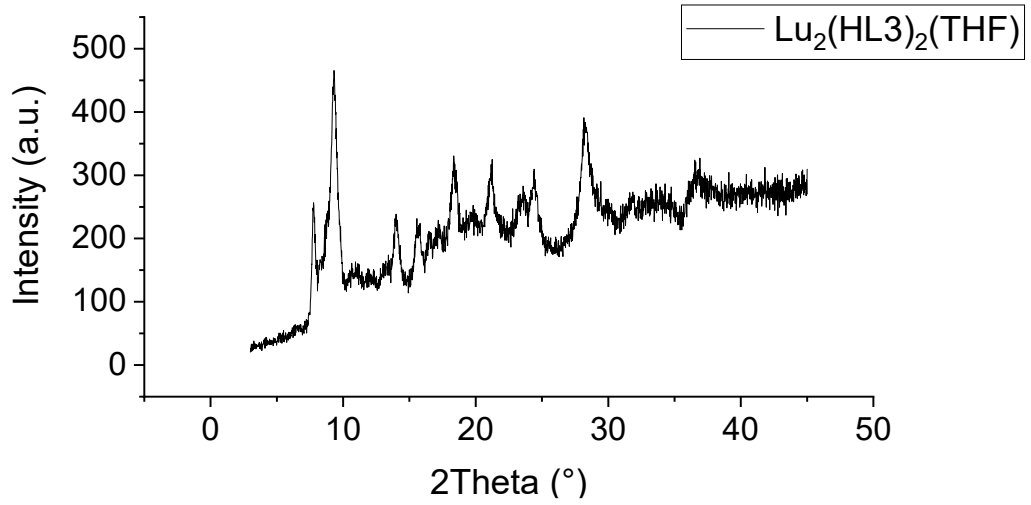

m)

Figure S 15. PXRD data of a) H_2L2, b) Yb(L2)(HL2), c) K[Yb(L2)$_2$](H_2O), d) Lu(L2)(HL2), e) K[Lu(L2)$_2$], f) Er(L2)(HL2), g) K[Er(L2)$_2$](THF)$_{0.5}$, h) Nd(L2)(HL2), i) K[Nd(L2)$_2$](H_2O), k) Yb$_2$(HL3)$_2$(THF)$_{0.5}$(H_2O), l) Gd$_2$(HL3)$_2$(THF)(H_2O), m) Lu$_2$(HL3)$_2$(THF).

IR spectroscopy

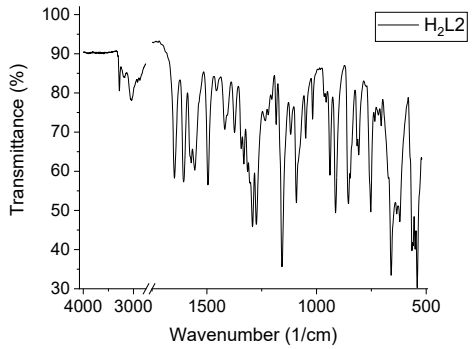

a)

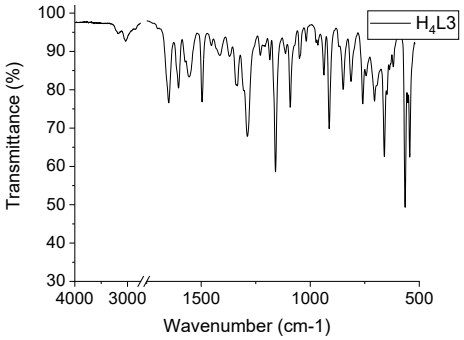

b)

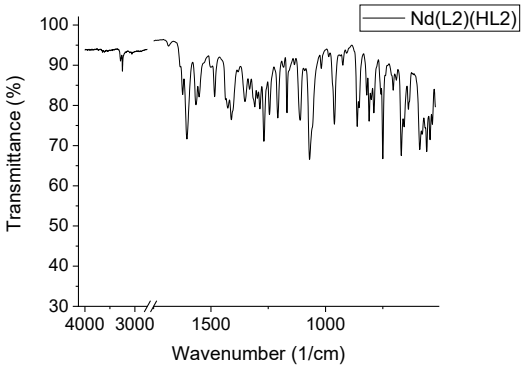

c)

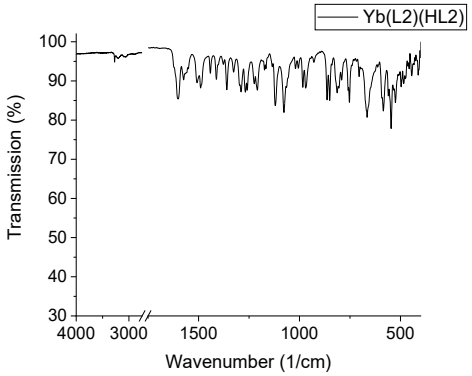

d)

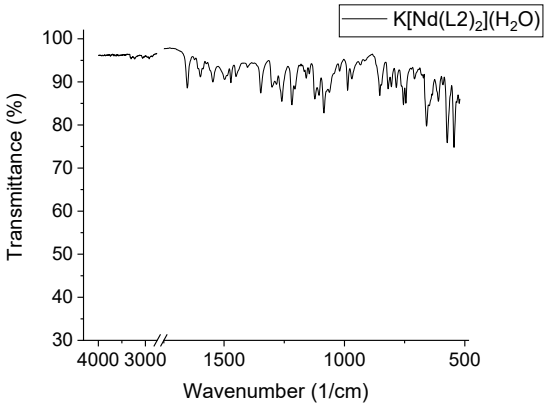

e)

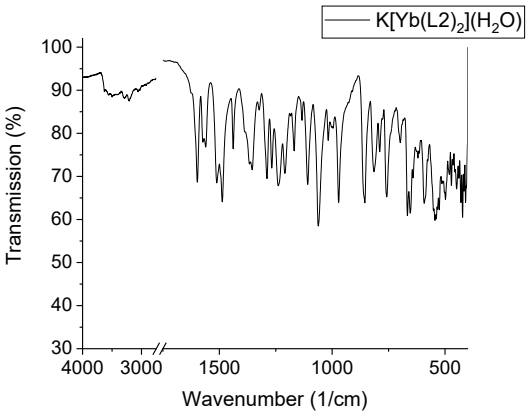

f)

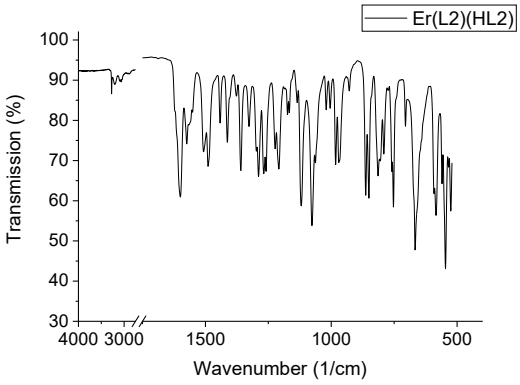

g)

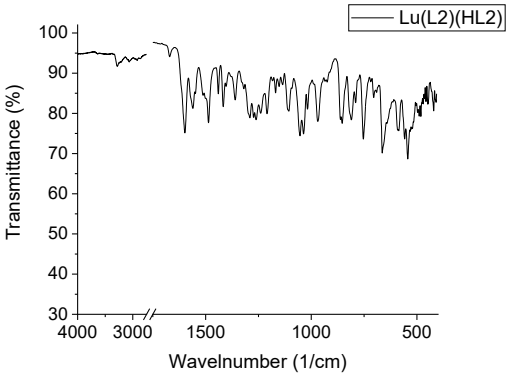

h)

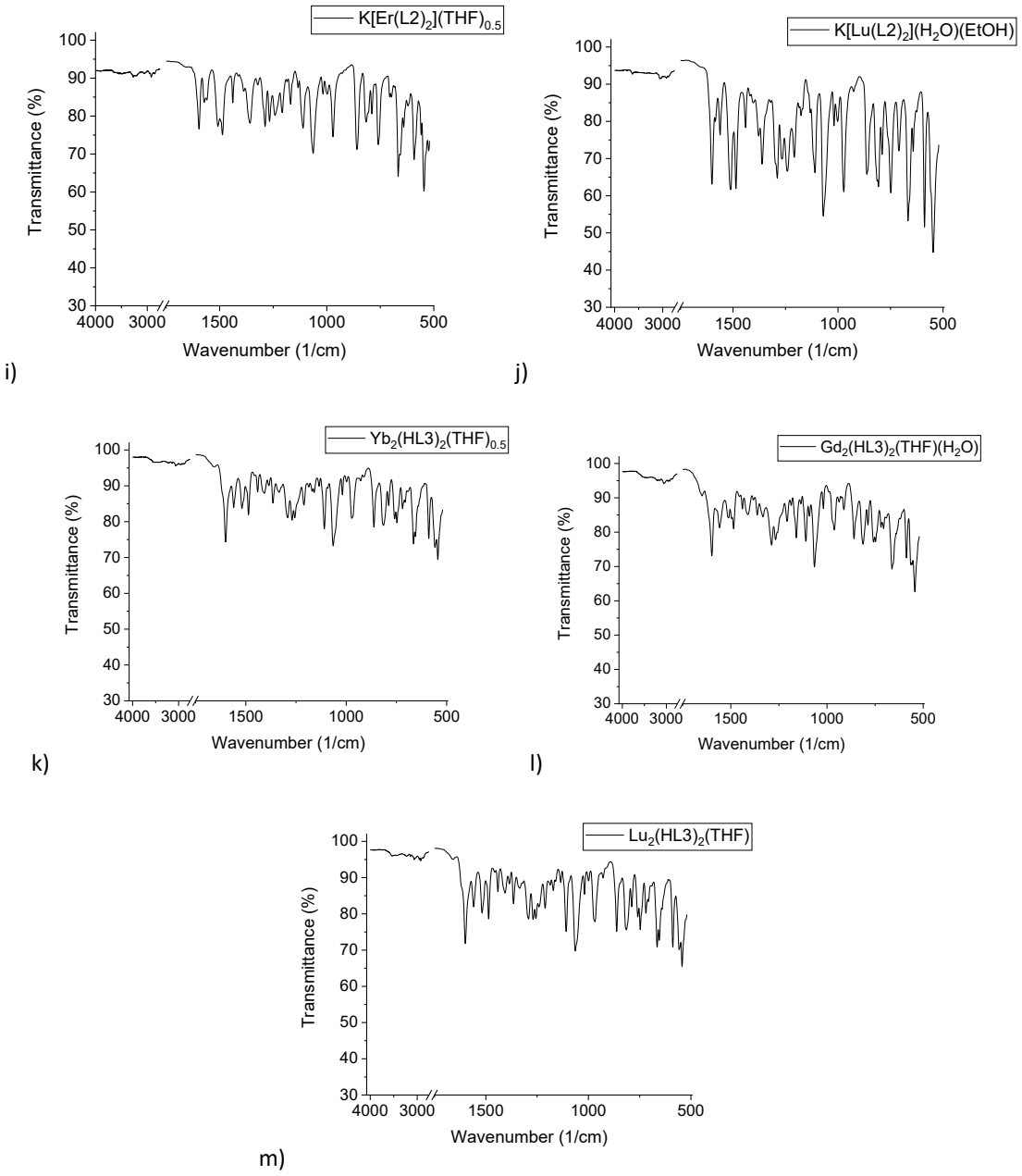

Figure S 16. IR spectroscopy of a) H_2L2, b) H_2L3, c) Nd(L2)(HL2), d) Yb(L2)(HL2), e) $K[Nd(L2)_2](H_2O)$, f) $K[Yb(L2)_2](H_2O)$, g) Er(L2)(HL2), h) Lu(L2)(HL2), i) $K[Er(L2)_2](THF)_{0.5}$, j) $K[Lu(L2)_2](H_2O)(EtOH)$, k) $Yb_2(HL3)_2(THF)_{0.5}(H_2O)$, l) $Gd_2(HL3)_2(THF)(H_2O)$, m) $Lu_2(HL3)_2(THF)$.

FT-IR spectra were studied in the H2L2 - Yb(L2)(HL2) - $K[Yb(L2)_2](H_2O)_2$ row in by analogy with work [16]. Their analysis is demonstrated in Figure S 17. Two broad absorption bands at 3500 and 3200 cm^- most likely correspond to the amide NH vibrations. A very wide absorption band at 3500 cm^{-1} in the $K[Yb(L2)_2](H_2O)$ spectrum corresponds to the H-bonded coordinated water molecules. Shifts and intensity changes in the low energy range of $\nu(SO_2)$, ν(NH), and ν(tosyl-CH_3) are corresponded to the complexation and central metal cation influence.

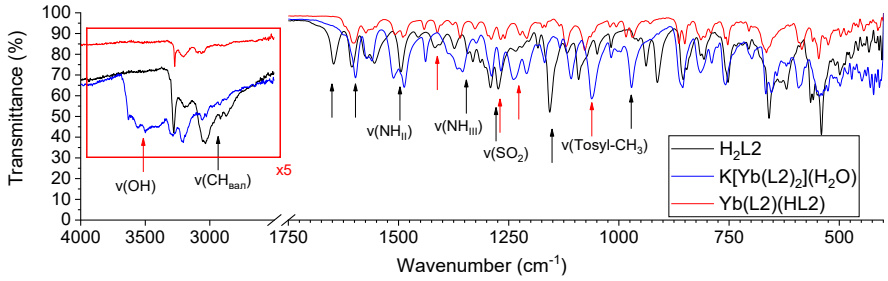

Figure S 17. IR spectra of H_2L1, Yb(L1)(HL1) and $K[Yb(L1)_2](H_2O)_2$. Red arrows(↑) indicate the difference between complexes while black arrows (↑) indicate the difference between complexes and ligand

Thermal analysis and mass-spectroscopy of complexes

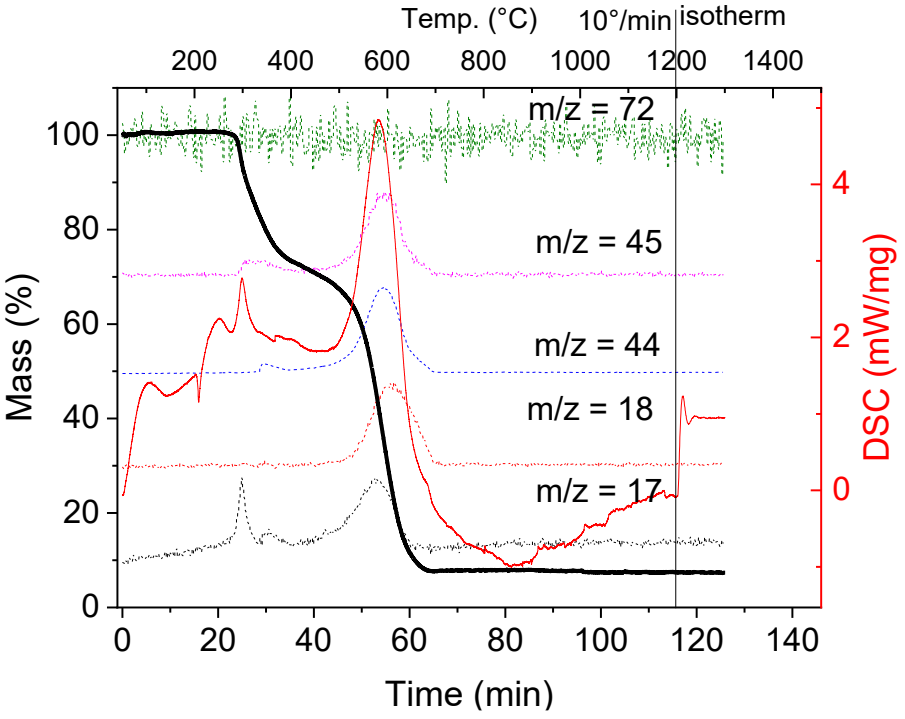

a)

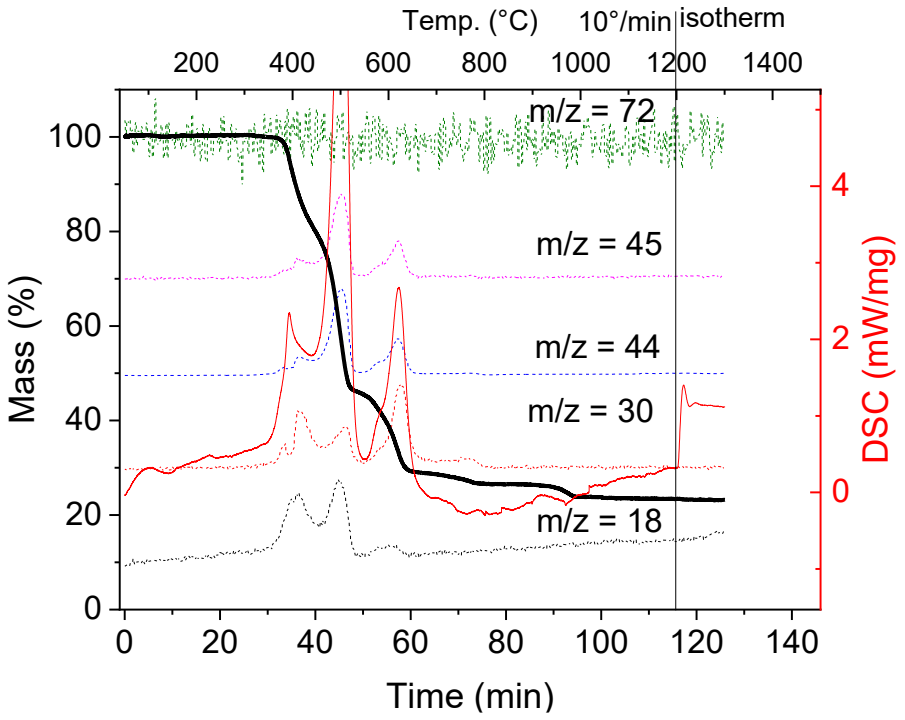

b)

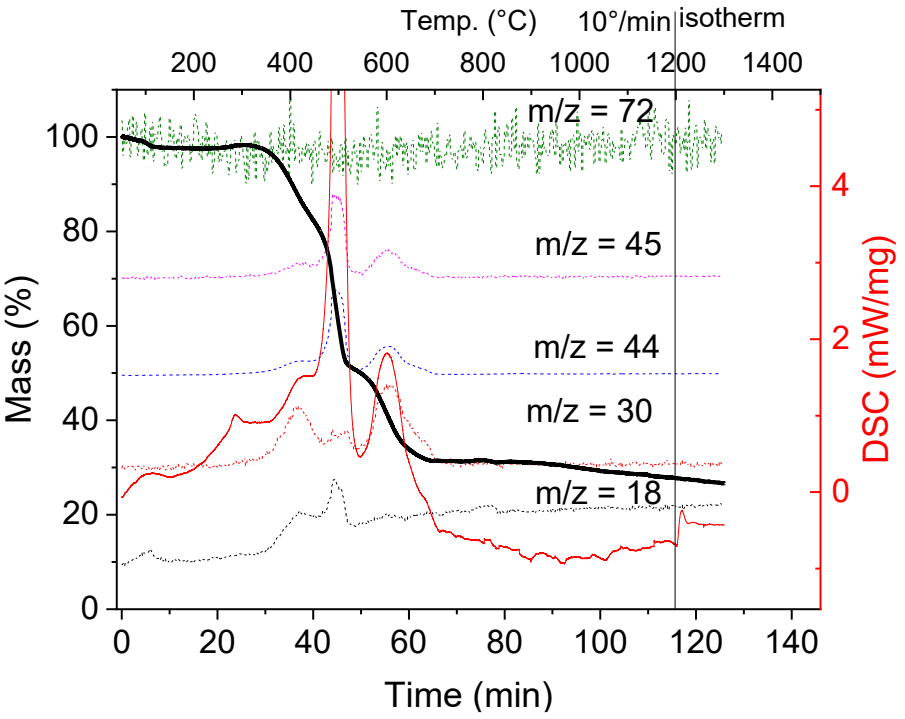
Temp. (°C)
10°/min
isotherm
200
400
600
800
1000
1200
1400
m/z = 72
m/z = 45
m/z = 44
m/z = 30
m/z = 18
Mass (%)
DSC (mW/mg)
Time (min)
0
20
40
60
80
100
120
140
4
2
0

c)

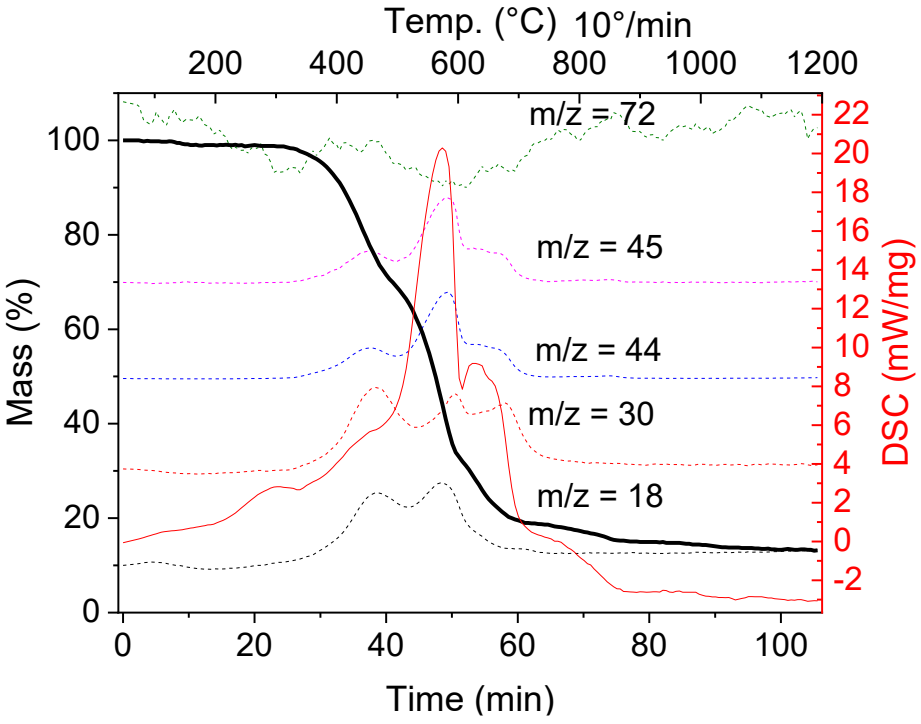
Temp. (°C)
10°/min
200
400
600
800
1000
1200
m/z = 72
m/z = 45
m/z = 44
m/z = 30
m/z = 18
Mass (%)
DSC (mW/mg)
Time (min)
0
20
40
60
80
100
22
20
18
16
14
12
10
8
6
4
2
0
-2

d)

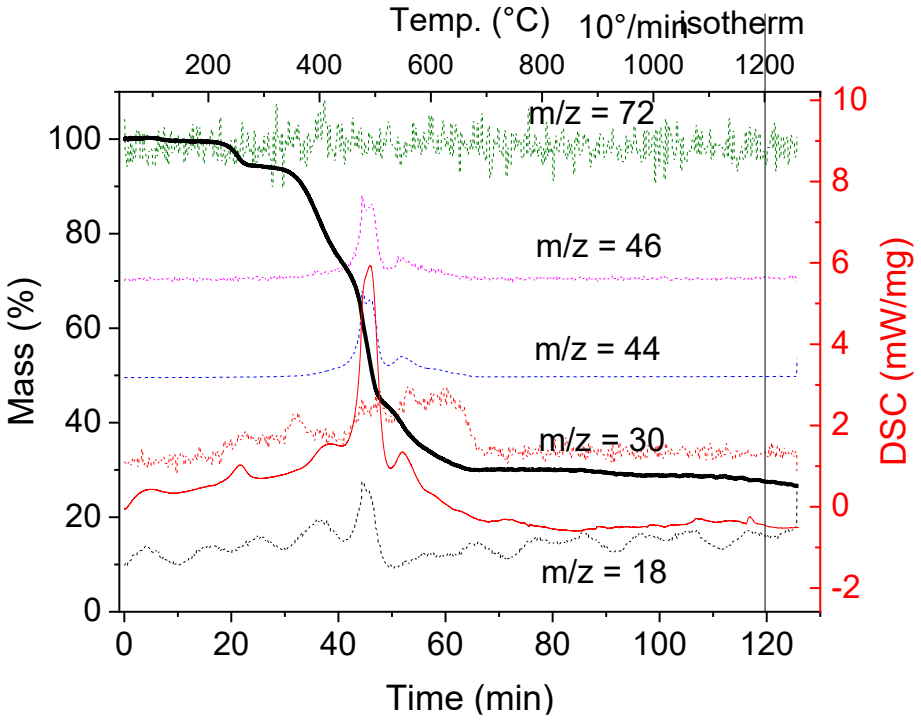
Temp. (°C)
10°/min
isotherm
200
400
600
800
1000
1200
m/z = 72
m/z = 46
m/z = 44
m/z = 30
m/z = 18
Mass (%)
DSC (mW/mg)
Time (min)
0
20
40
60
80
100
120
-2
2
4
6
8
10

e)

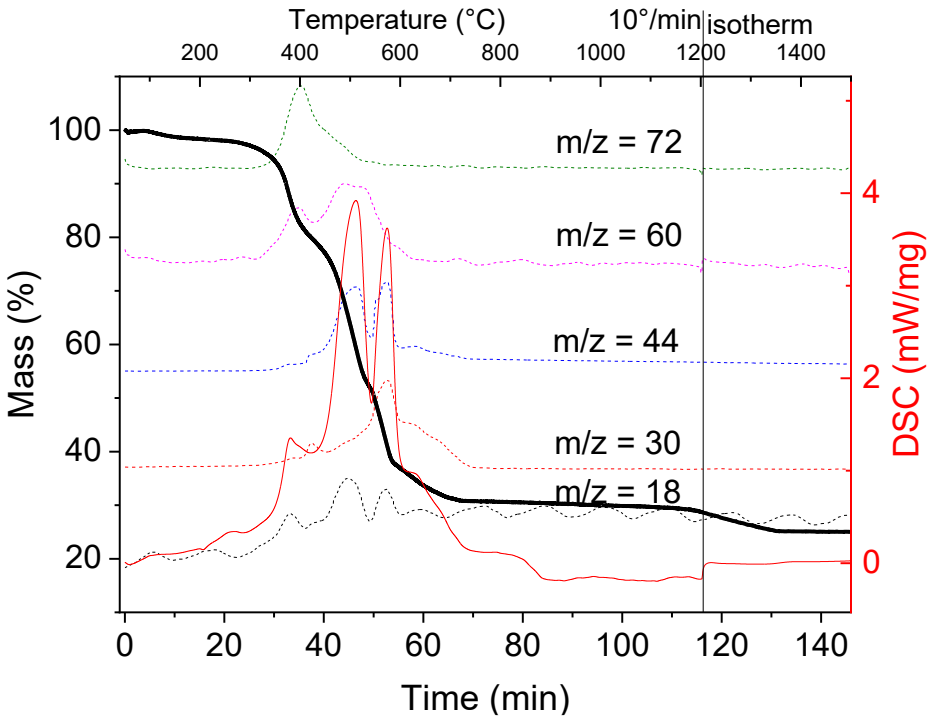
Temperature (°C)
10°/min
isotherm
200
400
600
800
1000
1200
1400
m/z = 72
m/z = 60
m/z = 44
m/z = 30
m/z = 18
Mass (%)
DSC (mW/mg)
Time (min)
0
20
40
60
80
100
120
140
2
4

f)

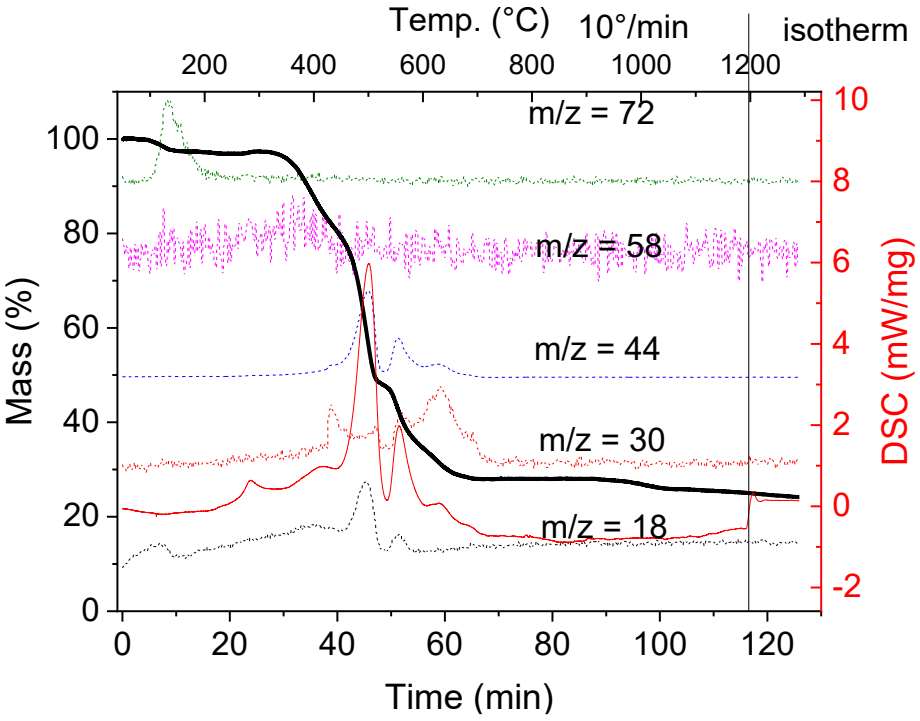
Temp. (°C)
10°/min
isotherm
200
400
600
800
1000
1200
m/z = 72
m/z = 58
m/z = 44
m/z = 30
m/z = 18
Mass (%)
DSC (mW/mg)
Time (min)
0
20
40
60
80
100
120
-2
0
2
4
6
8
10

g)

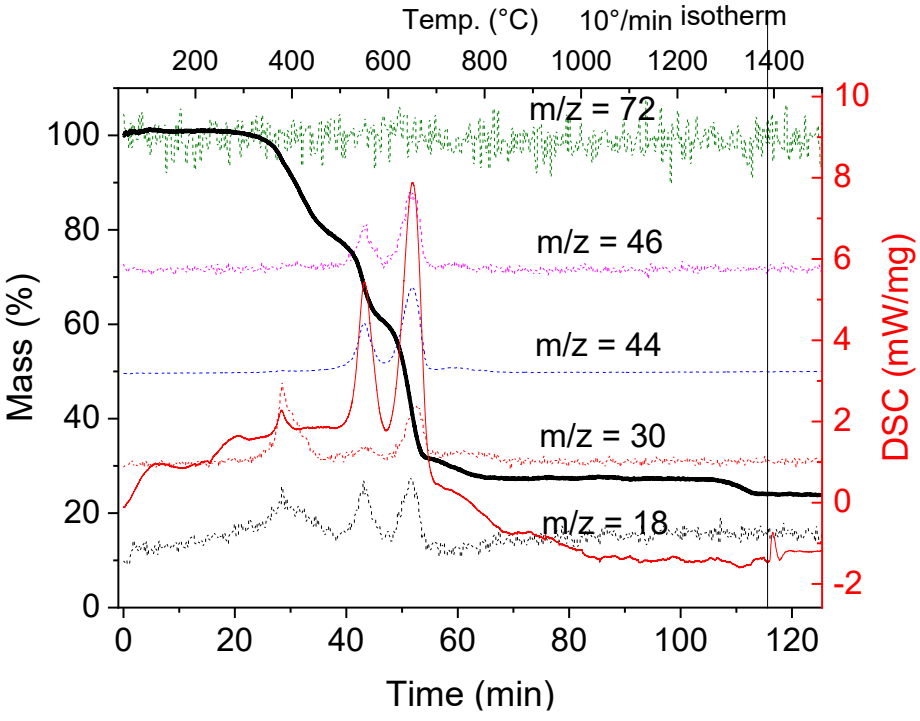
Temp. (°C)
10°/min
isotherm
200
400
600
800
1000
1200
1400
m/z = 72
m/z = 46
m/z = 44
m/z = 30
m/z = 18
Mass (%)
DSC (mW/mg)
Time (min)
0
20
40
60
80
100
120
-2
0
2
4
6
8
10

h)

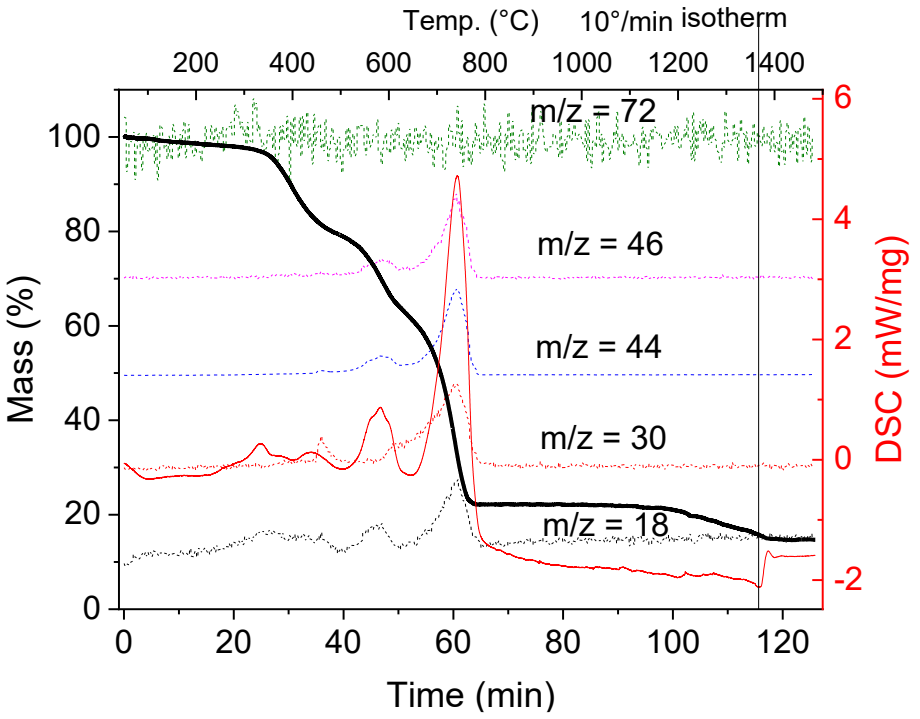
Temp. (°C)
10°/min
isotherm
200
400
600
800
1000
1200
1400
m/z = 72
m/z = 46
m/z = 44
m/z = 30
m/z = 18
Mass (%)
DSC (mW/mg)
Time (min)
0
20
40
60
80
100
120
-2
0
2
4
6

i)

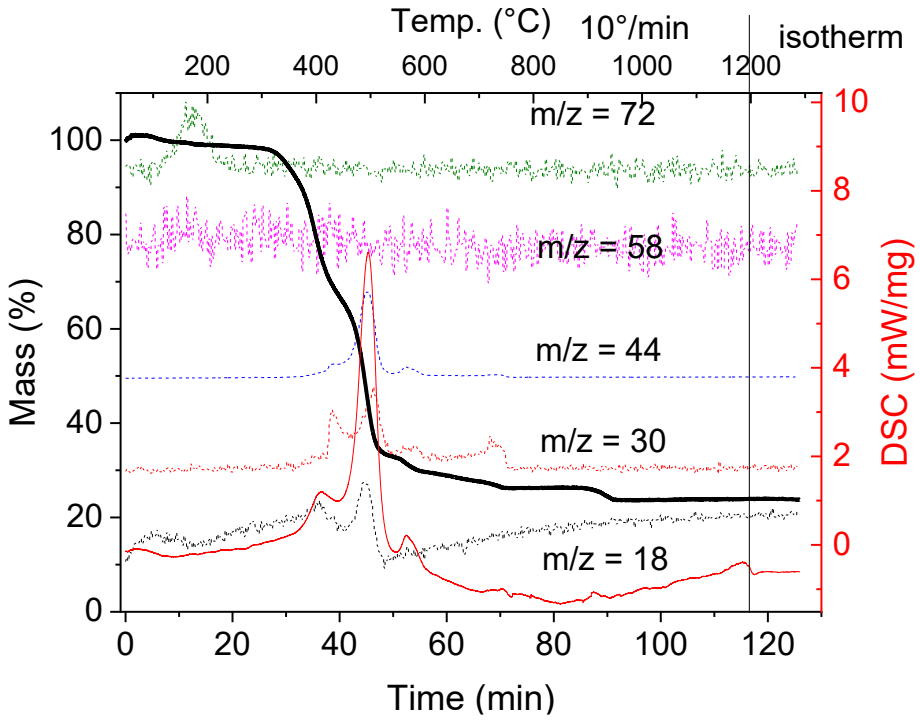
Temp. (°C)
10°/min
isotherm
200
400
600
800
1000
1200
m/z = 72
m/z = 58
m/z = 44
m/z = 30
m/z = 18
Mass (%)
DSC (mW/mg)
Time (min)
0
20
40
60
80
100
120
0
2
4
6
8
10

j)

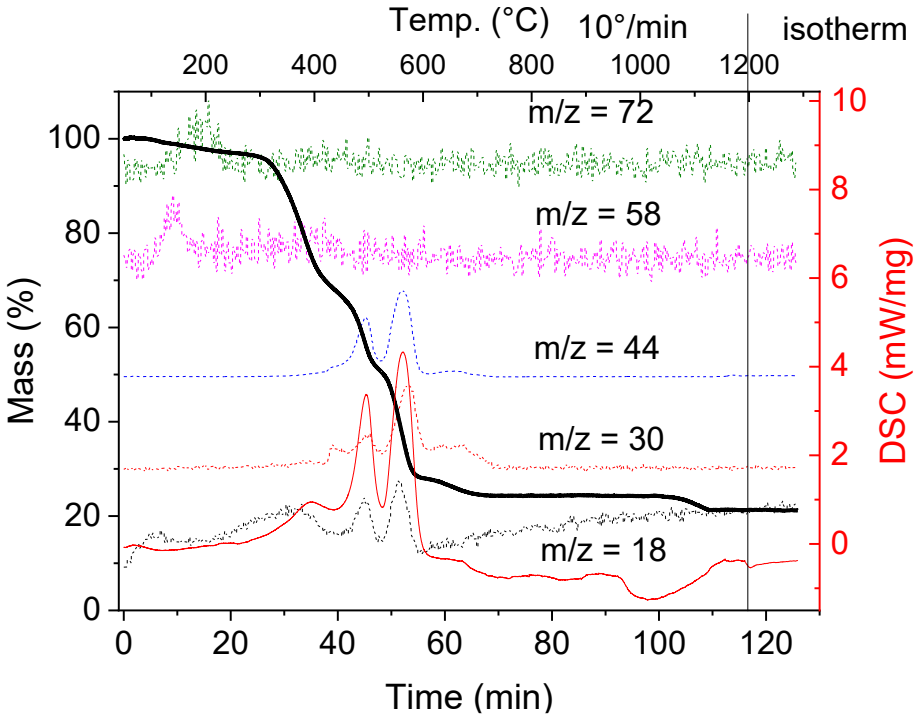

k)

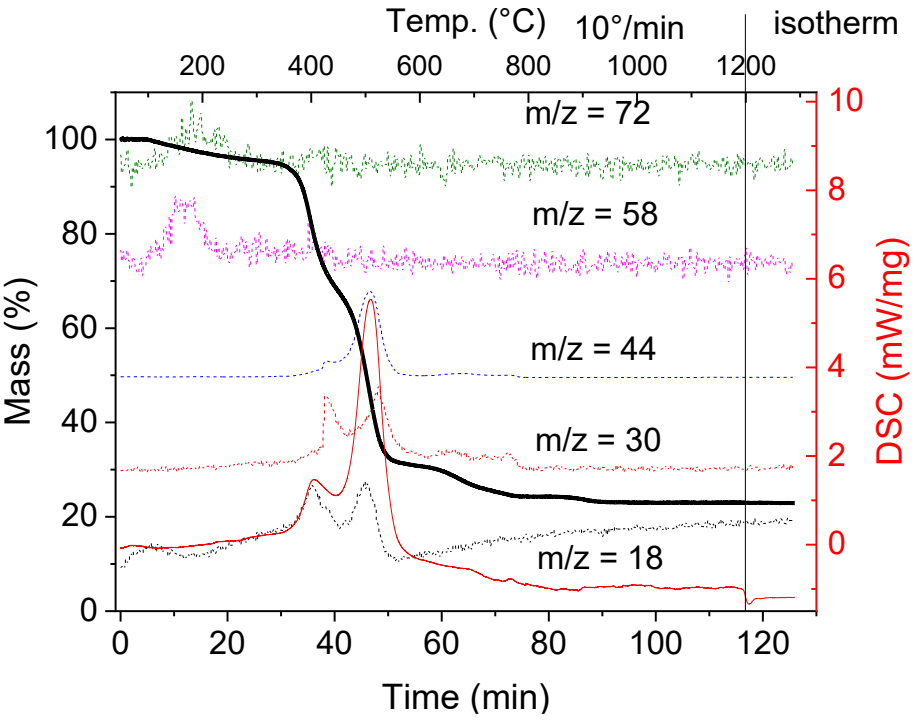

l)

Figure S 18. Thermal analysis and mass-spectroscopy of a) H_2L2 b) Yb(L2)(HL2), c) $K[Yb(L2)_2](H_2O)$, d) Lu(L2)(HL2)(H_2O), e) $K[Yb(L2)_2](H_2O)_2$, f) Er(L2)(HL2)(H_2O), g) $K[Er(L2)_2](THF)_{0.5}$, h) Nd(L2)(HL2), i) $K[Nd(L2)_2(H_2O)$, j)$Yb_2(HL3)_2(THF)_{0.5}(H_2O)$, k) $Gd_2(HL3)_2(THF)(H_2O)$, l) $Lu_2(HL3)_2(THF)$.

MALDI-TOF of complexes

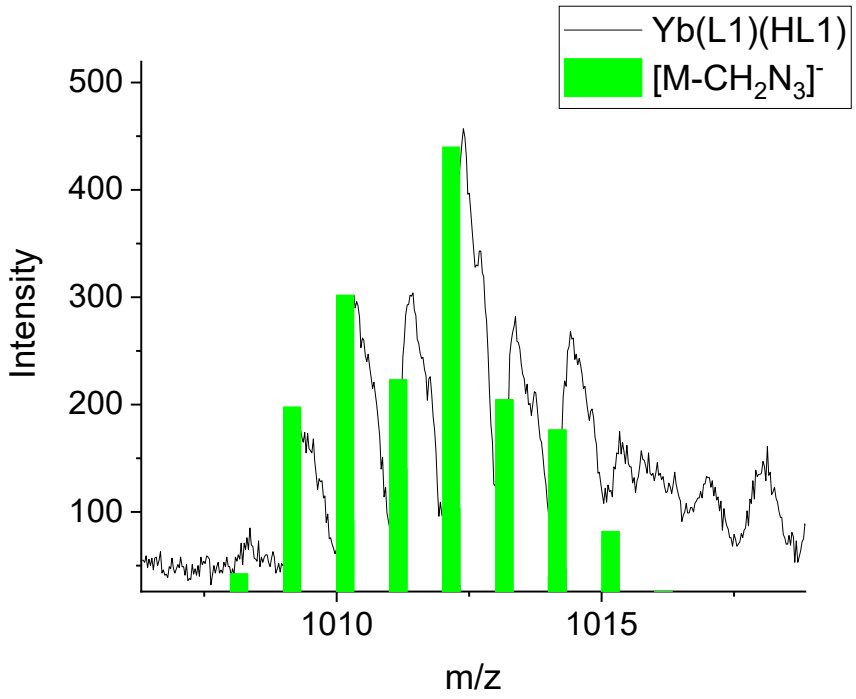

a)

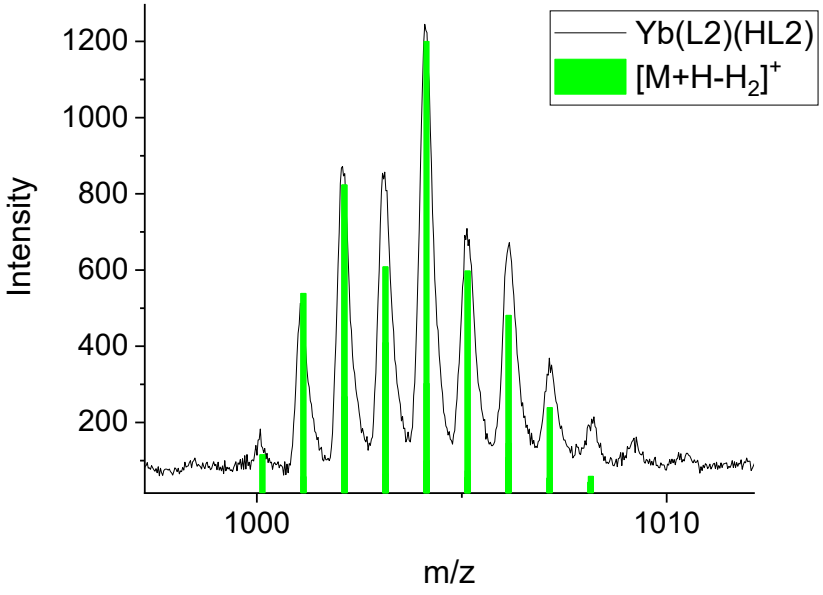

b)

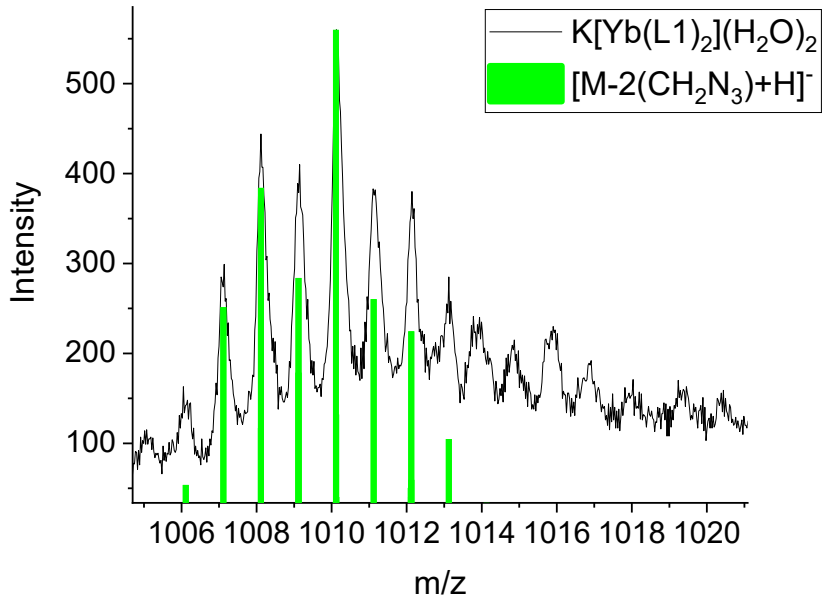
K[Yb(L1)2](H2O)2
[M-2(CH2N3)+H]-
Intensity
500
400
300
200
100
1006 1008 1010 1012 1014 1016 1018 1020
m/z

c)

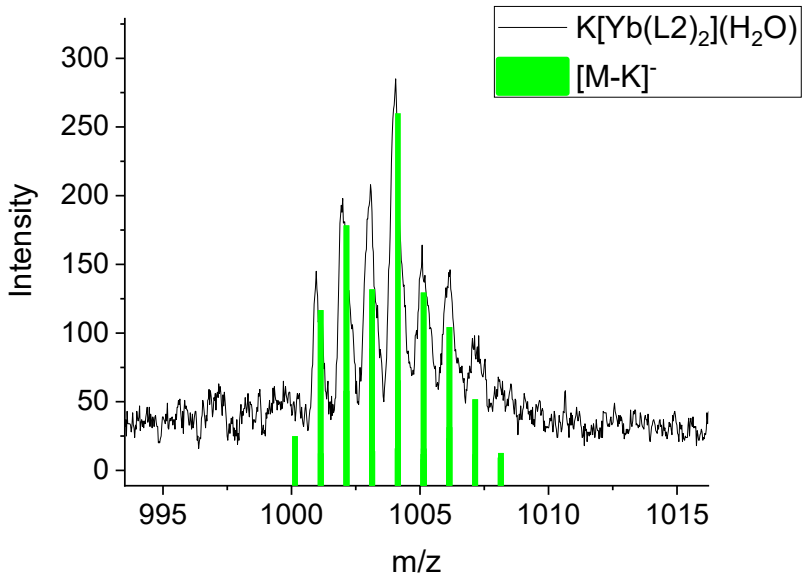
K[Yb(L2)2](H2O)
[M-K]-
Intensity
300
250
200
150
100
50
0
995
1000
1005
1010
1015
m/z

d)

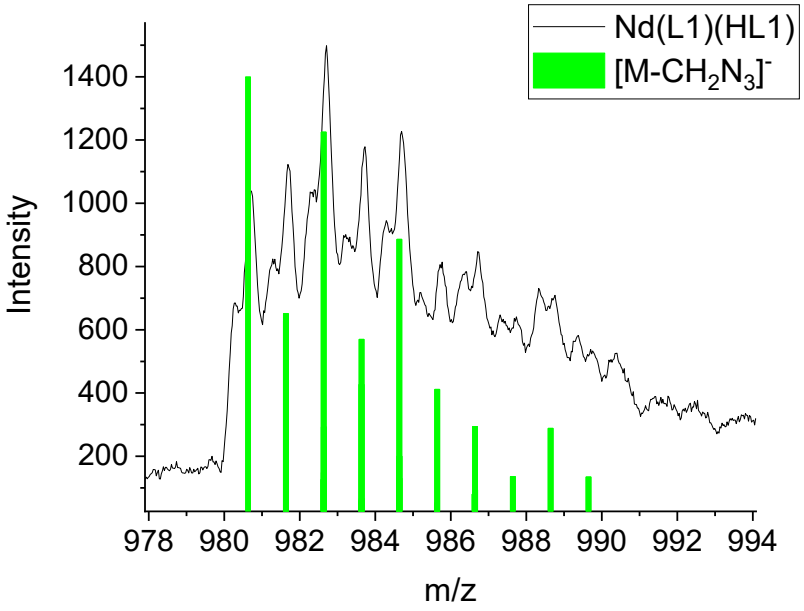
Nd(L1)(HL1)
[M-CH2N3]-
Intensity
1400
1200
1000
800
600
400
200
978
980
982
984
986
988
990
992
994
m/z

e)

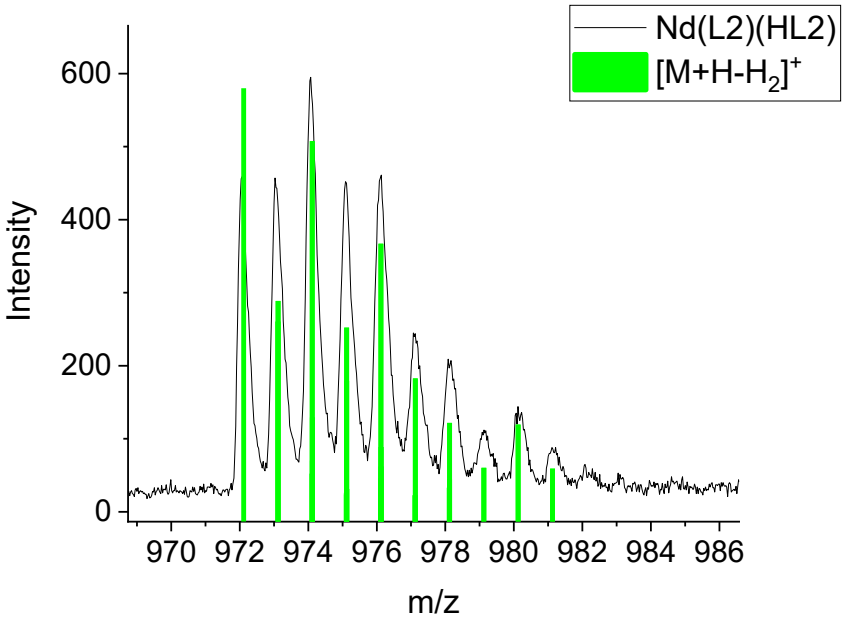
Nd(L2)(HL2)
[M+H-H2]+
Intensity
600
400
200
0
970
972
974
976
978
980
982
984
986
m/z

f)

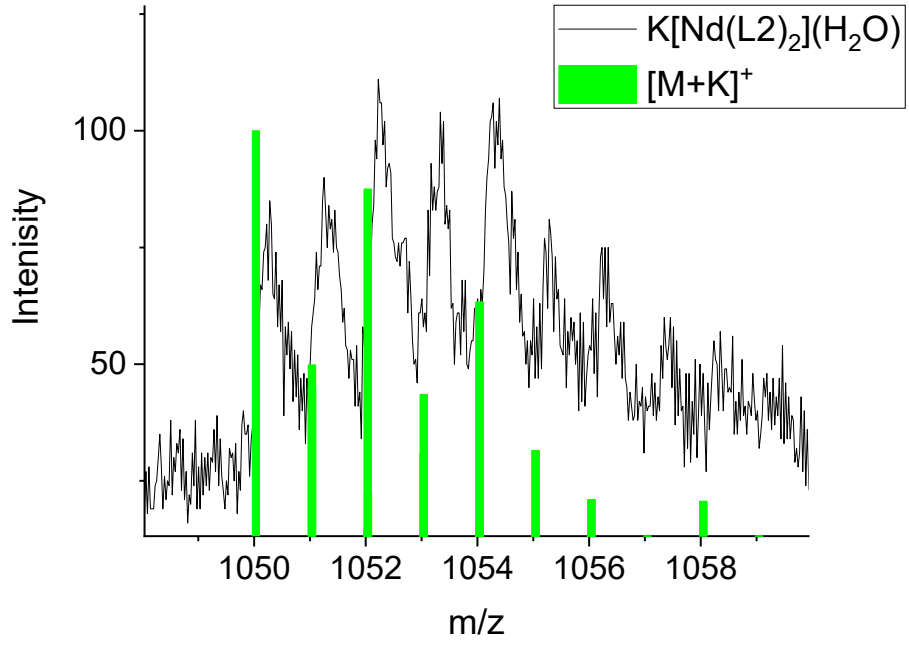
K[Nd(L2)2](H2O)
[M+K]+
100
50
Intenisity
1050
1052
1054
1056
1058
m/z

g)

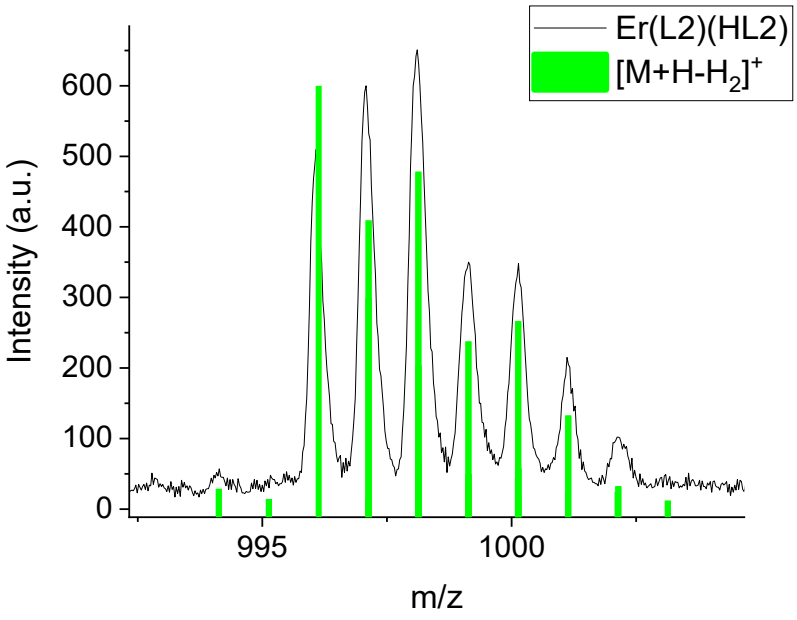
Er(L2)(HL2)
[M+H-H2]+
600
500
400
300
200
100
0
Intensity (a.u.)
995
1000
m/z

h)

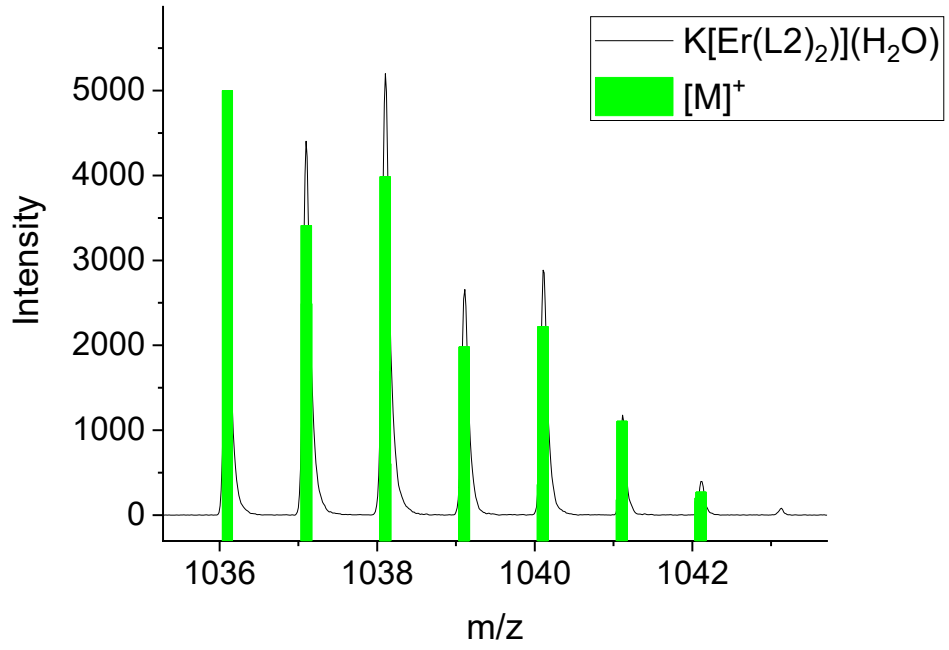
K[Er(L2)2)](H2O)
[M]+
Intensity
5000
4000
3000
2000
1000
0
1036
1038
1040
1042
m/z

i)

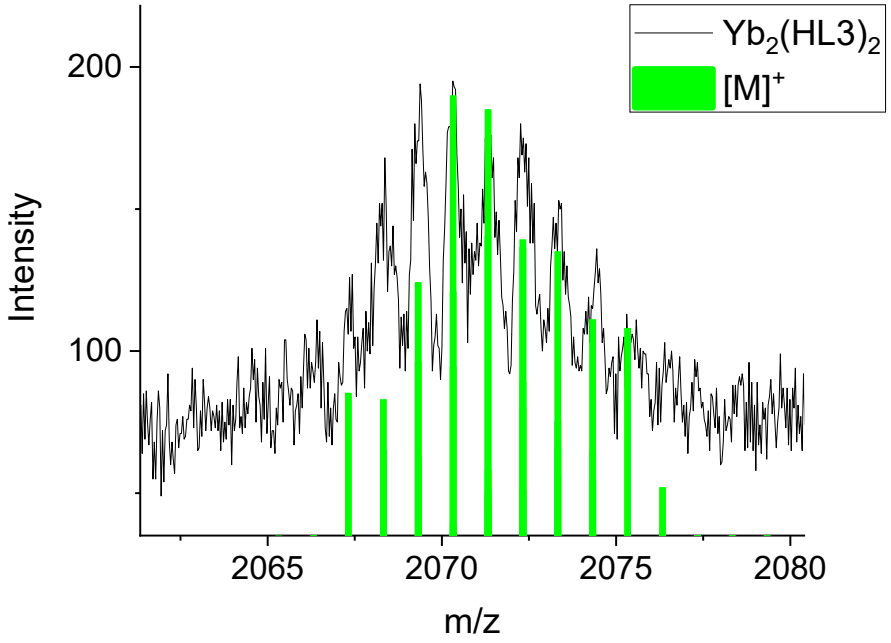
Yb2(HL3)2
[M]+
Intensity
200
100
2065
2070
2075
2080
m/z

j)

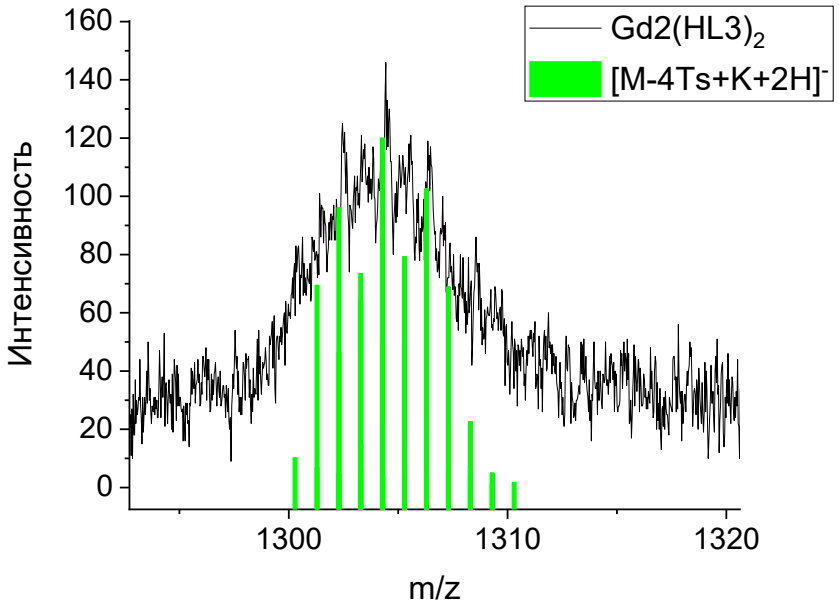

k)

Figure S 19. MALDI-TOF mass-spectra for a) Yb(L1)(HL1), b) Yb(L2)(HL2), c) $K[Yb(L1)_2](H_2O)$, d) $K[Yb(L2)_2](H_2O)$, e)Nd(L1)(HL1), f) Nd(L2)(HL2), g) $K[Nd(L2)_2](H_2O)$, h) Er(L2)(HL2), i) $K[Er(L2)_2](THF)_{0.5}$, j) $Yb_2(HL3)_2(THF)_{0.5}(H_2O)$, k) $Gd_2(HL3)_2(THF)(H_2O)$.

NMR of complexes

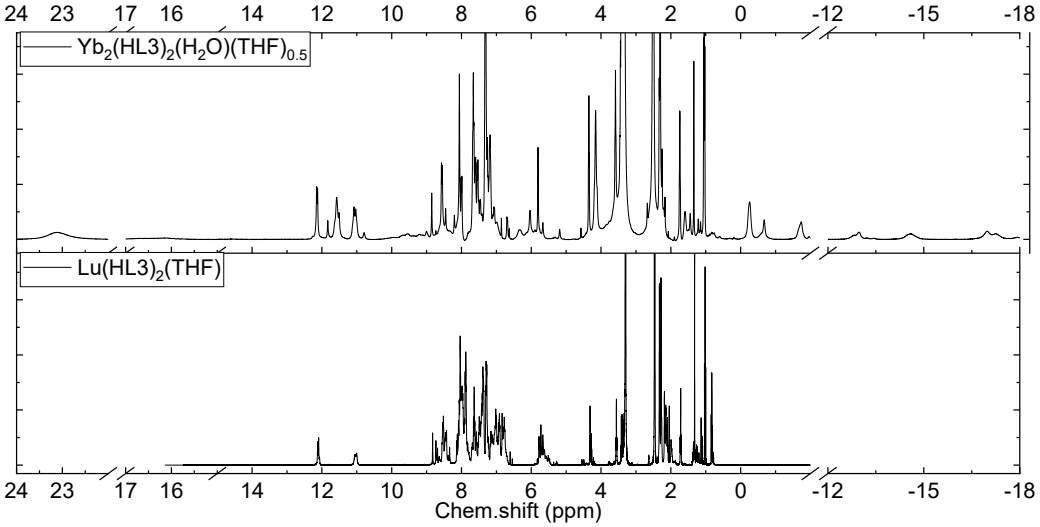

a)

Figure S 20. ^{1}H NMR spectra of a)$Yb_2(HL3)_2(THF)_{0.5}(H_2O)$ and $Lu_2(HL3)_2(THF)$.

NMR table for Lu(L)(HL) and Yb(L)(HL), L = L1, L2

Table S 2. NMR data for for Lu(L)(HL) and Yb(L)(HL), L = L1, L2.

	Lu(L)(HL)						Yb(L1)(HL1)						K[Yb(L1)2						Lu(L2)(HL2)												Yb(L2)(HL2)							
№	H2L		[Lu(L)]+		[Lu(L)2]-		H2L		[Yb(L)]+	18.55	[Yb(L)]2	52.14	H2L		[Yb(L)]+		[Yb(L)]2		№	H2L			[Lu(L)]+			[Lu(L)2]-			№	H2L			[Yb(L)]+		0	[Yb(L)]2	
	ppm	H	ppm	H	ppm	H	ppm	H	ppm	H	ppm	H	ppm	H	ppm	H	ppm	H		ppm	H	J	ppm	H	J	ppm	H	J		ppm	H	J	ppm	H	J	ppm	H
1	2.32	3	2.37	3	2.14	6	2.32	3	2.36	3	2.32	6	2.32		2.36	3	2.32	5	1	2.32	3	s	2.37	3	s	2.18	6	s	**1**	2.32	6.29	s						
											16.35	1					16.61	0.72																	16.45	0.47
2,3	7.32	2	7.43	2	6.85	4	7.34	3.88	11.78	2			7.32		11.78	2	11.83	0.1	2,3	7.33	2	d	6.96	2	d	6.93	4	d	**2,3**	7.34	2	d	11.02	1	s		
4,5	7.67	2	7.93	2	8.02	4	7.7	2.86	23.72	2			7.67		23.72	2	9.72	0.75	4,5	7.67	2	d	6.96	2	d	7.49	4	d	**4,5,14,16**	7.68	4.62	d	23.81	1.89	s	9.64	0.41
											9.64	1.32					9.05	0.79																	9.03	0.48
	12.16	1					12.2	1.04			8.61	1.18	12.16				8.27	3.07																		
											8.24	4.44					8.04	1.2								7.42	1	d								8.21	2.79
7	7.31	1	6.96	1	6.96	2	7.31	1.98	-13.44	1	7.82	3.3	7.31		-13.44	1	7.85	3.55	7	7.32	1	d	6.82	1	d	7.33	1	d	**7**	7.28	1	d					
8	7.27	1	7.57	1	7.28/6.85	1+1	7.27	0.98	-0.18	0.78	7.05	5.25	7.27		-0.18	0.78	7.58	1	8	7.28	1	t	7.04	1	t	7.1	2	t	**8**	7.26	1.5	t	0.02	1.1	s	7.92	2.14
9	7.19	1	7.21	1	7.09	2	7.19	2.33	1.26	0.82	6.83	1.23	7.19		1.26	0.82	7.33	1.38	9	7.19	1	t	6.75	1	t	6.82	2	t	**9**	7.2	1.53	t	0.73	0.68	s	6.76	0.55
10	7.61	1	8.02	1	7.47	2	7.61	1.75	-1.9	0.79	6.46	1.56	7.61		-1.9	0.79	7.16	1.94	10	7.61	1	d	7.49	1	d	8.04	1	d	**10**	7.61	1.07	d	-1.89	0.77	s	6.48	0.45
											5.56	1					7.05	4.18								7.9	1	d								4.51	1.14
11	8.57	1	8.57	1	8.52	2	8.61	1.23	-14.35	1	4.84	5.08	8.57		-14.35	1	6.9	1.43	11	8.57	1	s	8.52	1	s	8.5	2	s	**11**	8.57	0.98	s				4.27	2.87
	11.05	1					11.09	0.72			3.59	10	11.05				6.46	0.97																		
											2.86	1.91					4.94	1.02																	1.98	0.97
											1.97	1.65					4.85	3.15																	1.9	1.16
13,15	8.01	2	8.12	2	8.02	4	8.4	3.38	-16.9	2.4	1.57	1.07	8.01		-16.9	2.4	4.58	1.2	13,1	8.01	2	d	7.42	2	d	7.98	4	d	**13,15**	8	2.4	d	3.55	4.4	d		
14,16	7.56	2	7.43	2	7.38	4	7.56	2.79	-0.62	1.62	0.75	1.15	7.56		-0.62	1.62	2.75	1.69	14,1	7.67	2	d	7.42	2	d	7.98	4	d	**4,5,14,16**	7.68	2	d	-0.19	1.65	s		
											0.25	1.8																					1.62	0.92	s		
17	4.59	2	4.53	2	4.45	4	4.62	2.93	4.28	3.14	-0.62	1.62	4.59		4.28	3.14	1.96	1.16	17b	4.44	1	s	4.35	1	s	4.29	2	s	**17b**	4.45	1.03	s					
											1.26	0.82					1.63	0.25										**6**	12.19	0.9	s					

Luminescence spectra of complexes

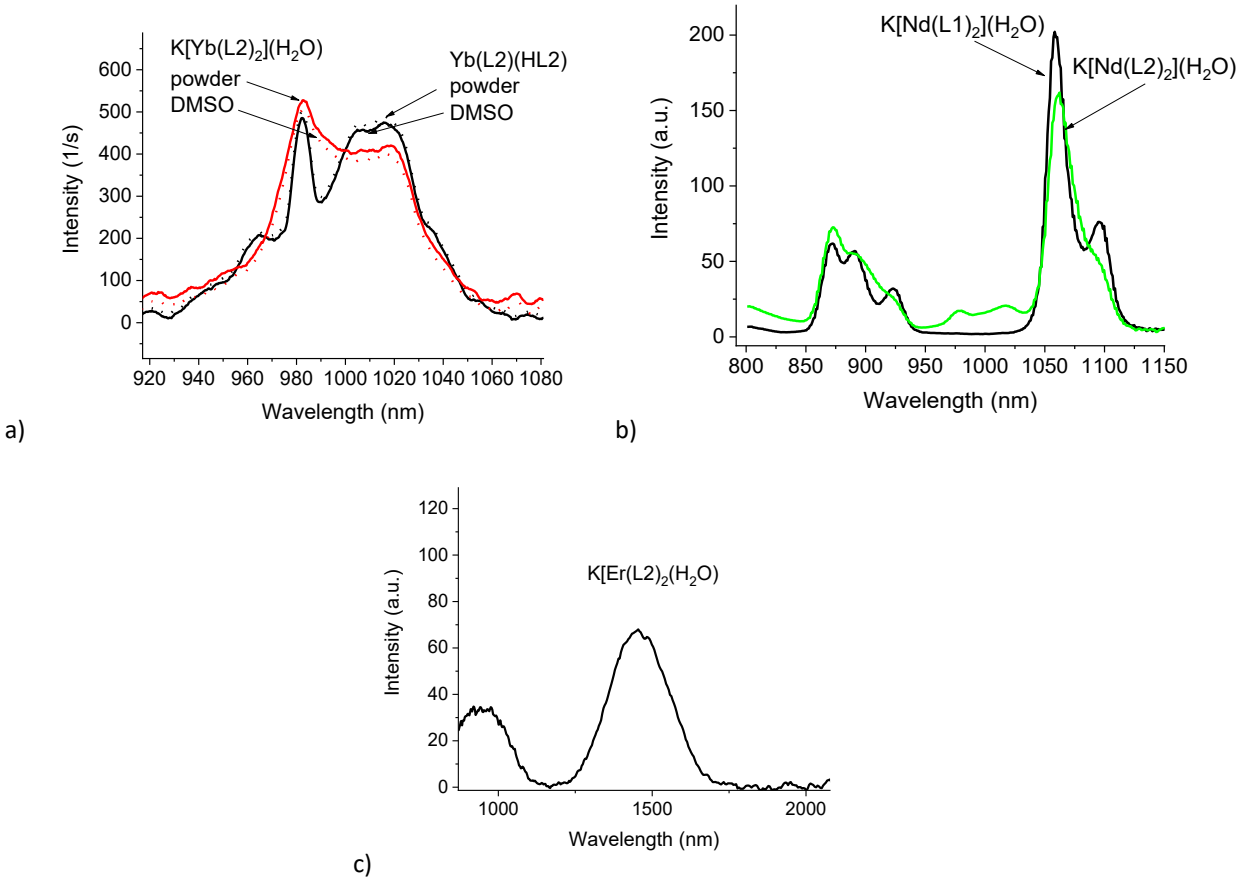

Figure S 21.Luminescence spectra of a) $K[Yb(L1)_2](H_2O)_2$ and $K[Yb(L2)_2](H_2O)$ (powder and DMSO, 20 mM), b) powders of $K[Nd(L1)_2](H_2O)_2$ and $K[Nd(L2)_2](H_2O)$, c) powder of $K[Er(L2)_2](THF)_{0.5}$ under 365 nm excitation.

Luminescence decay of complexes

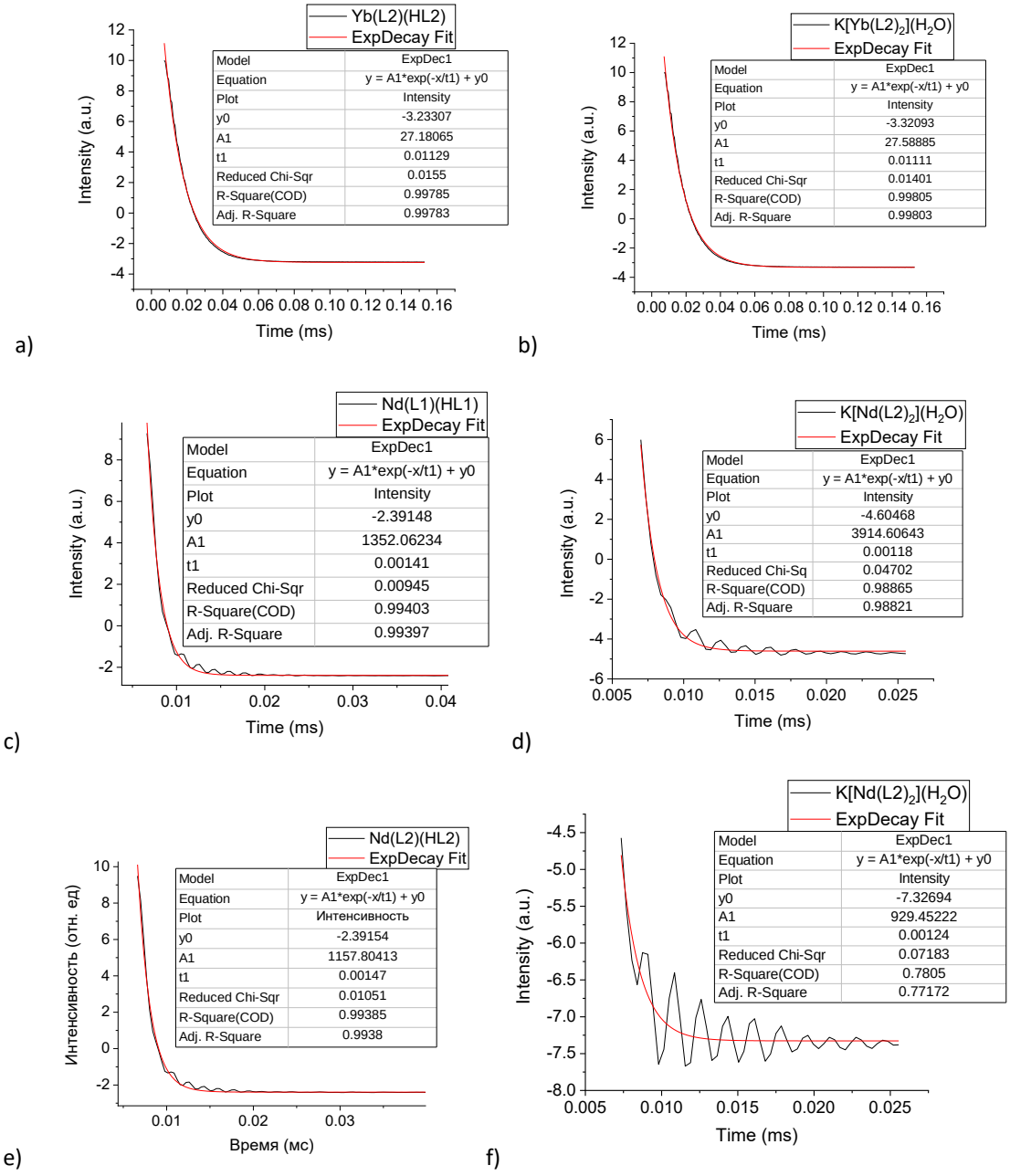

Figure S 22. Lumnescence decay curves of a)Yb(L2)(HL2), b)K[Yb(L2)$_2$](H$_2$O), c) Nd(L1)(HL1), d) K[Nd(L1)$_2$(H$_2$O), e) Nd(L2)(HL2), f) K[Nd(L2)$_2$](H$_2$O).

Synthesis of conjugates

The general procedure of conjugation

To the solution of lanthanide complexes (1 eq, 0.02 mmol each) in methanol (40 ml) sodium ascorbate (0.02 eq, 1 mg) in water (0.1 ml) and $CuSO_4 \cdot 5H_2O$ (0.01 eq, 0.4 mg) in water (0.1 ml) were added sequentially. The reaction mixture was refluxed for 24 h under argon. The suspension was evaporated to dryness and then washed with water (3x1 ml) and methanol (2 x 1 ml) through centrifugation in a 1.5 ml vial. The resulting powder was dried under reduced pressure. Yield: 30 mg of yellow powder.

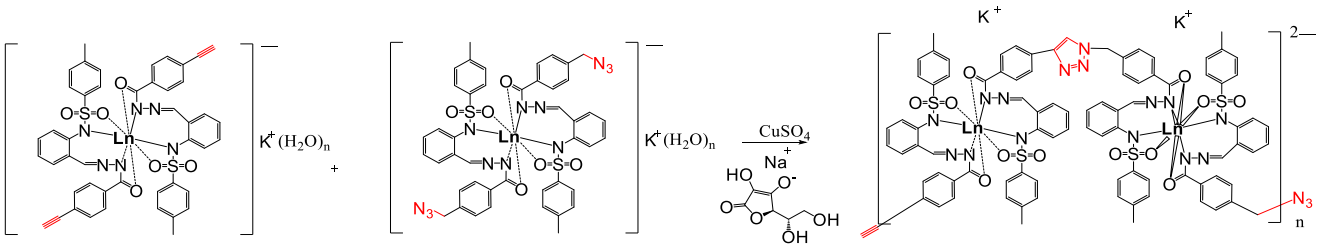

Scheme S 1. Synthesis of the {Ln-Ln} conjugates from **K[Ln(L)$_2$](H$_2$O)** (Ln = Nd, Er, Yb, Lu; **L** = L1 or L2).

MALDI-TOF of conjugates

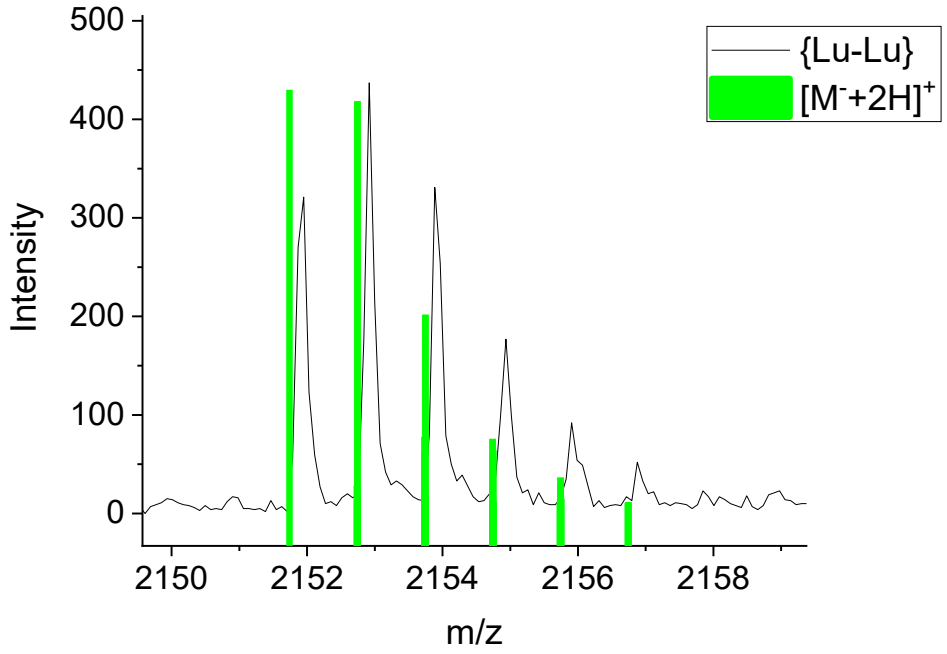

a)

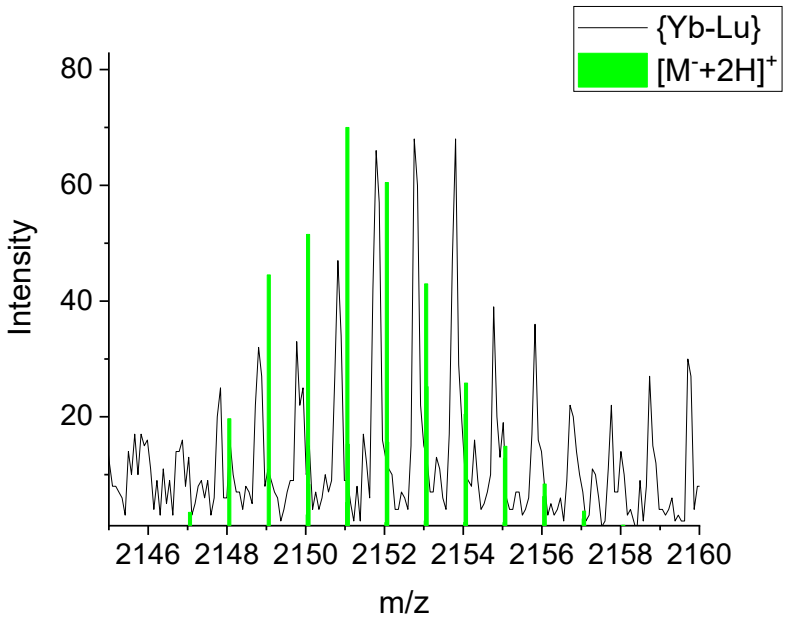

b)

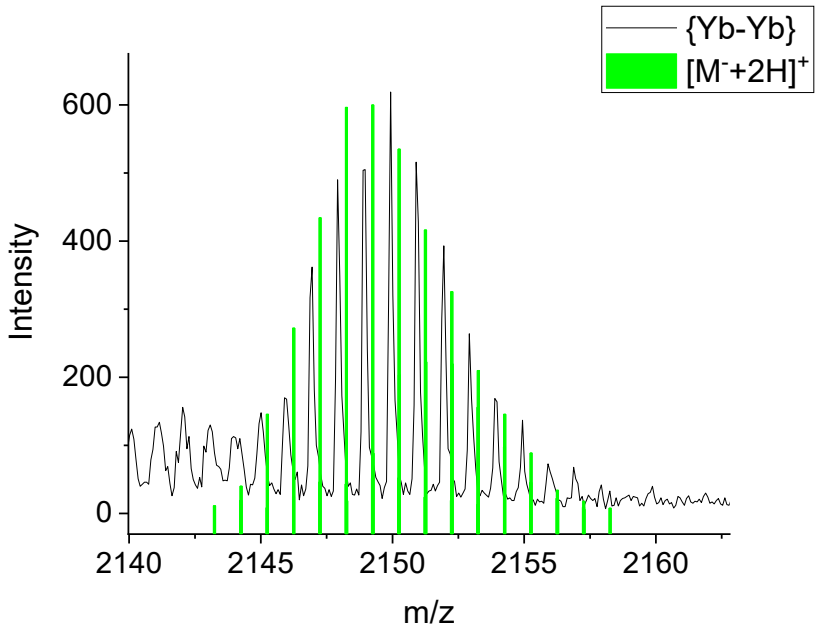
{Yb-Yb}
[M-+2H]+
Intensity
600
400
200
0
2140
2145
2150
2155
2160
m/z

c)

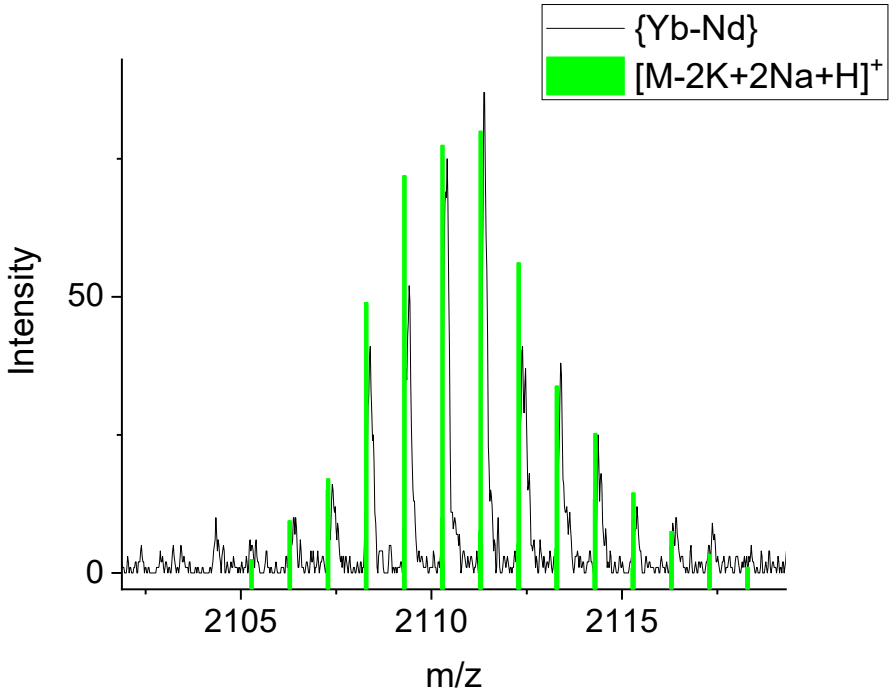
{Yb-Nd}
[M-2K+2Na+H]+
Intensity
50
0
2105
2110
2115
m/z

d)

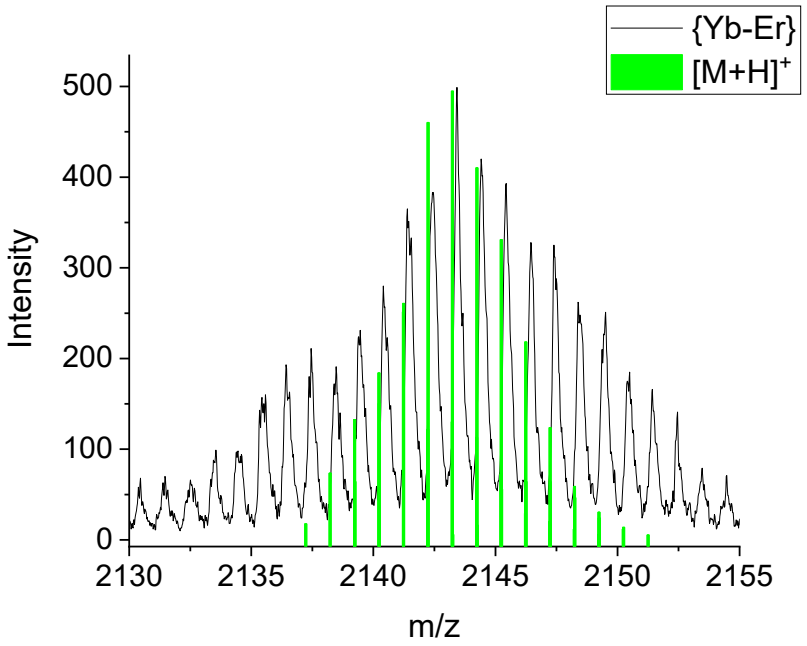

e)

Figure S 23. MALDI-TOF spectra of a) {Lu-Lu}, b) {Yb-Lu), c) {Yb-Yb}, d) {Yb-Nd}, e) {Yb-Er}.

IR spectroscopy of conjugates

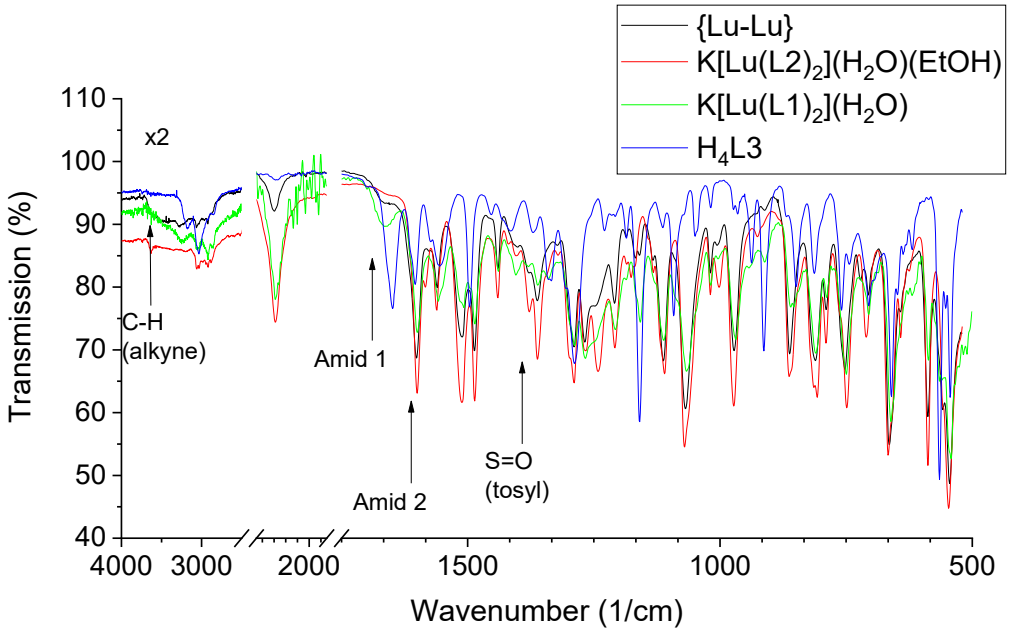

a)

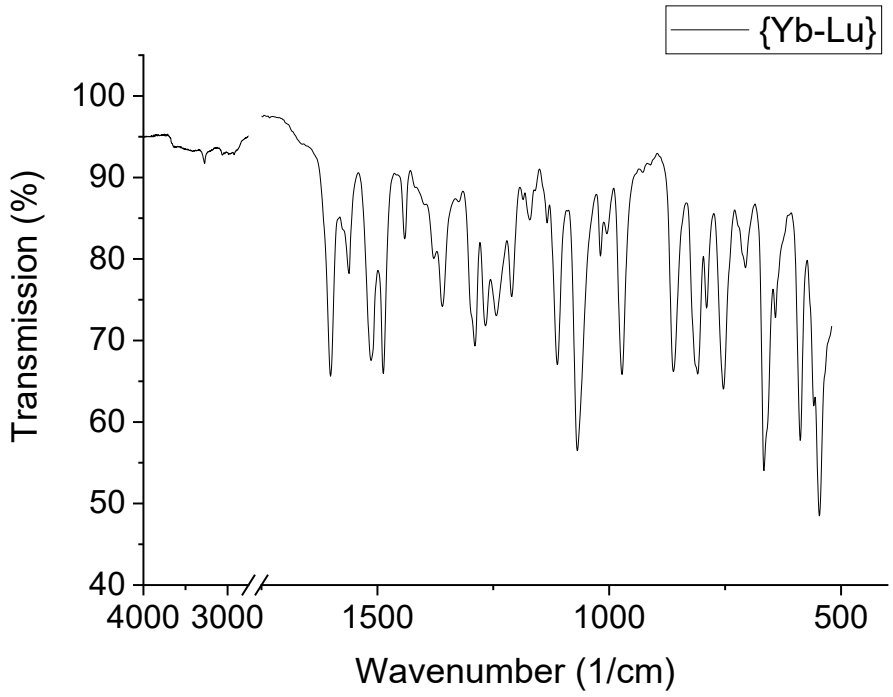

b)

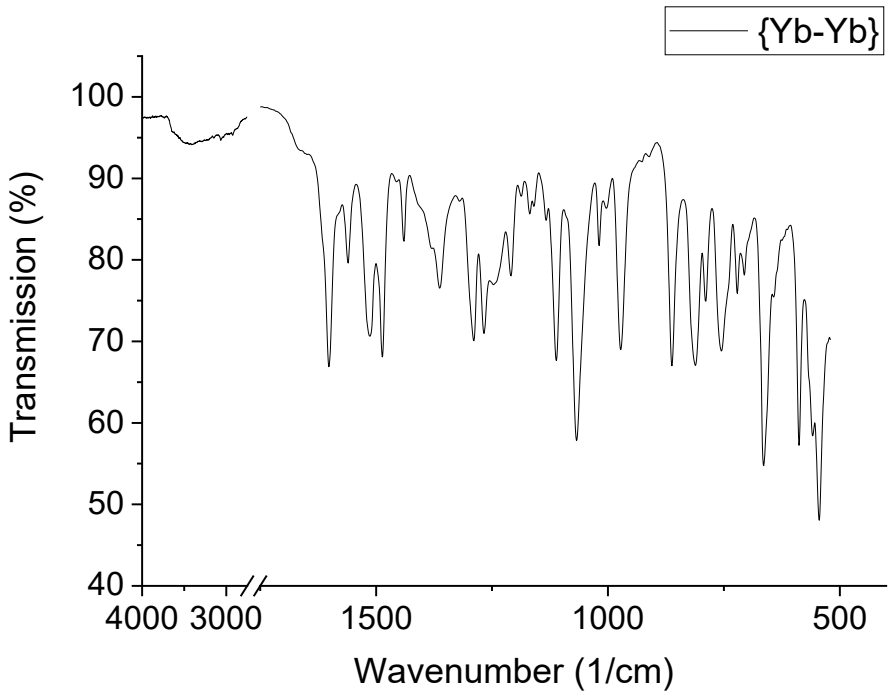
{Yb-Yb}
Transmission (%)
100
90
80
70
60
50
40
4000
3000
1500
1000
500
Wavenumber (1/cm)

c)

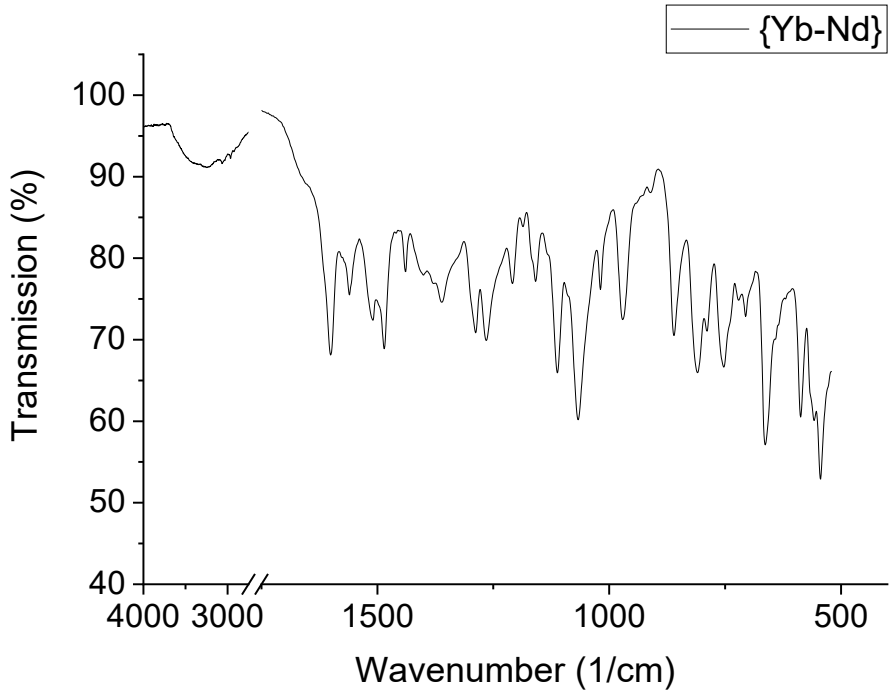
{Yb-Nd}
Transmission (%)
100
90
80
70
60
50
40
4000
3000
1500
1000
500
Wavenumber (1/cm)

d)

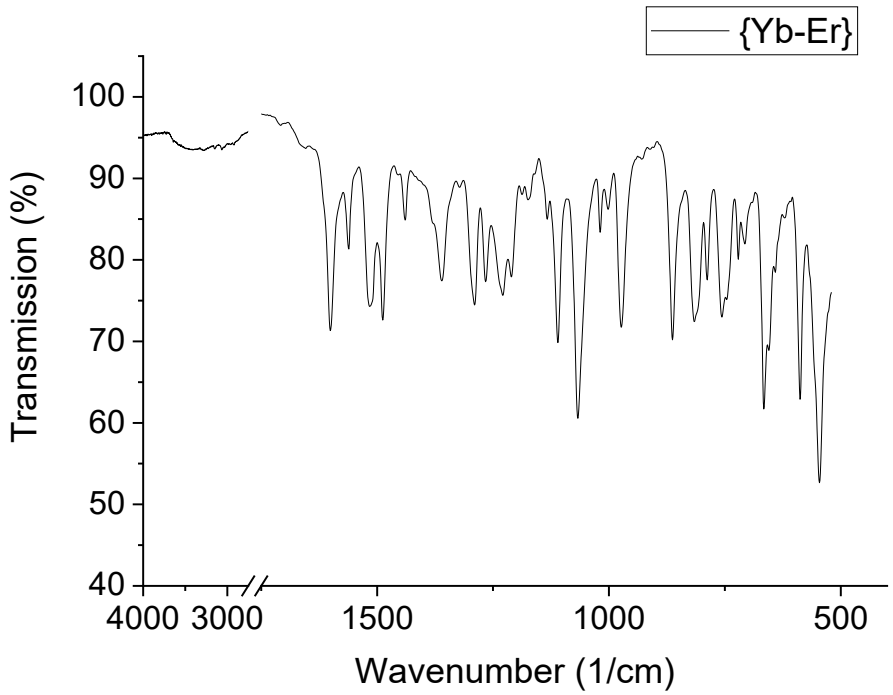

e)

Figure S 24. IR spectra of a) {Lu-Lu}, b) {Yb-Lu), c) {Yb-Yb}, d) {Yb-Nd}, e) {Yb-Er}.

PXRD data of conjugates

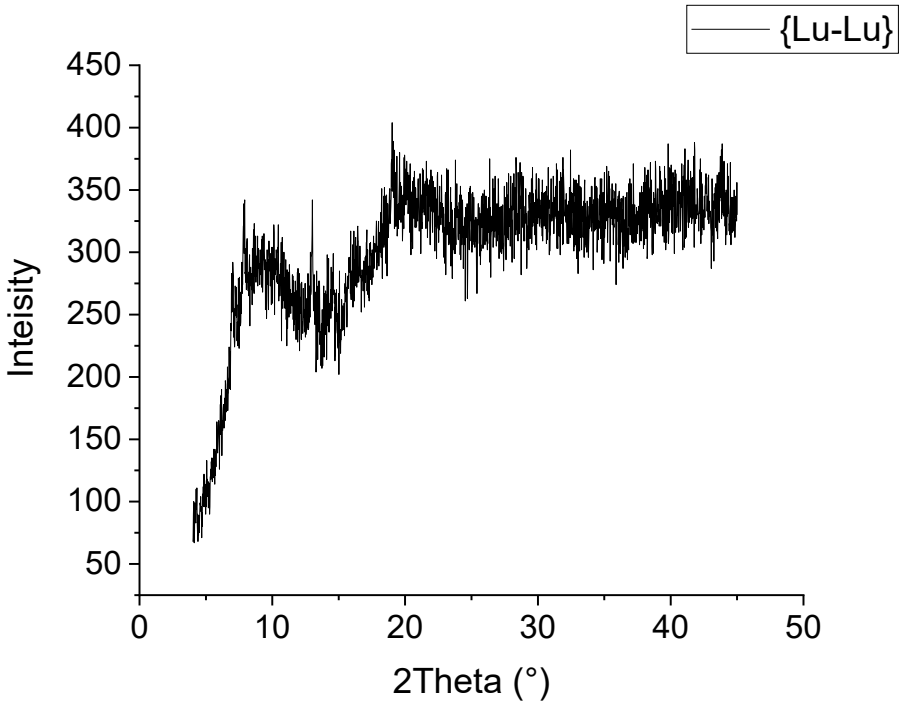

a)

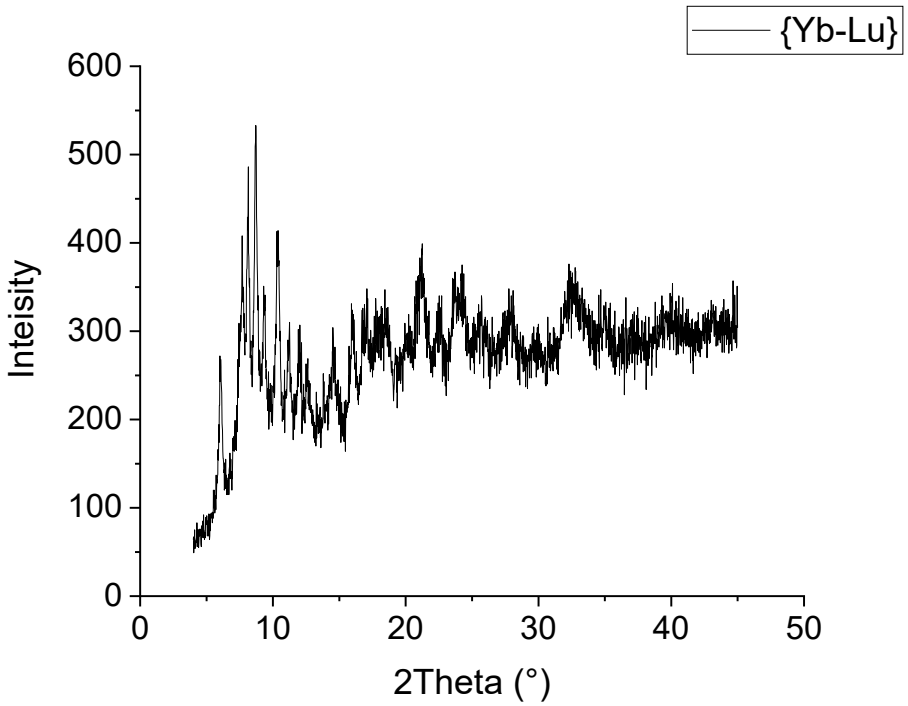

b)

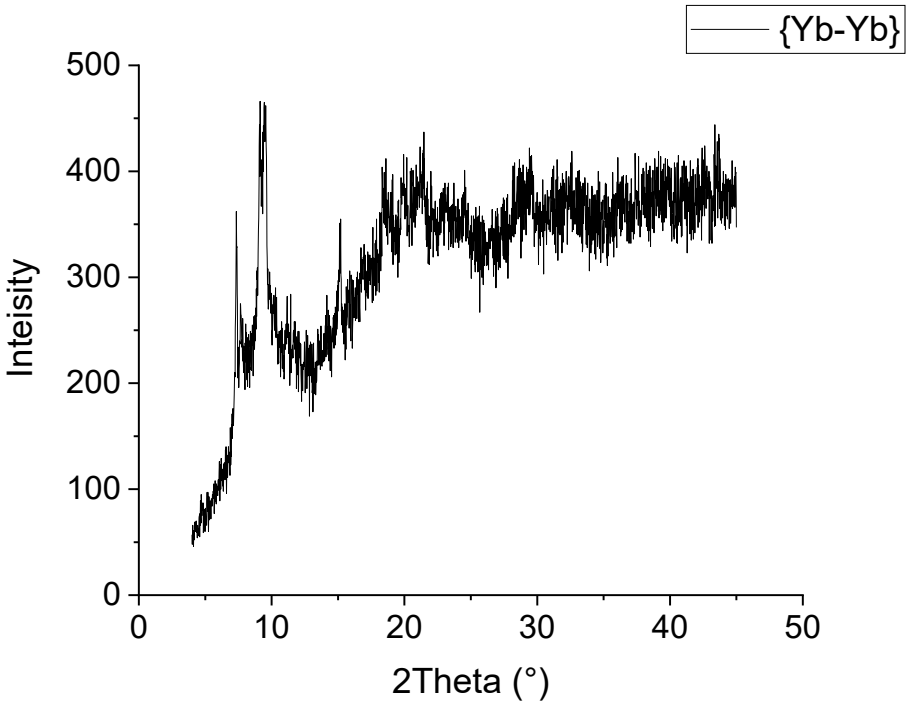
{Yb-Yb}
Inteisity
2Theta (°)
0
100
200
300
400
500
0
10
20
30
40
50

c)

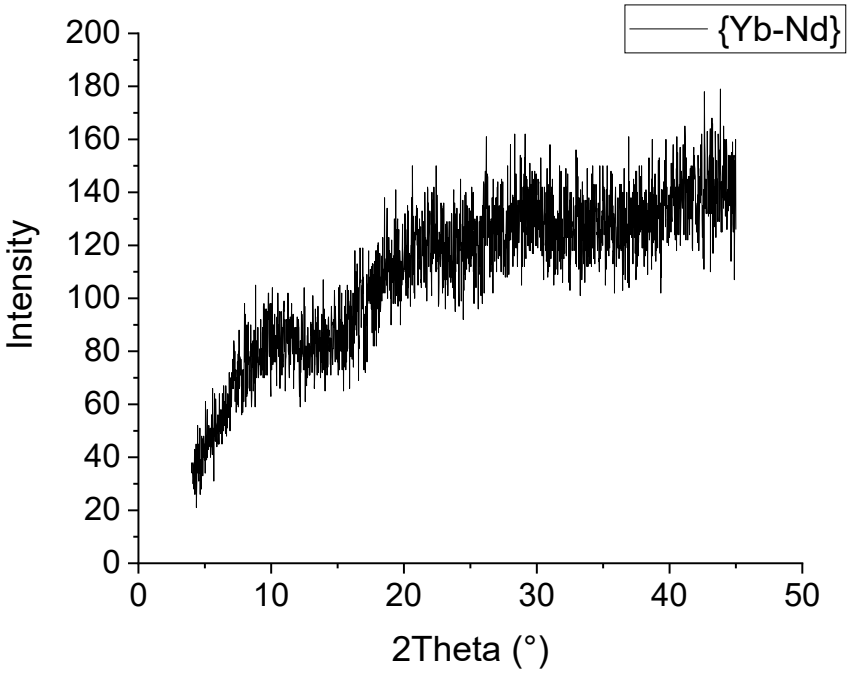
{Yb-Nd}
Intensity
2Theta (°)
0
20
40
60
80
100
120
140
160
180
200
0
10
20
30
40
50

d)

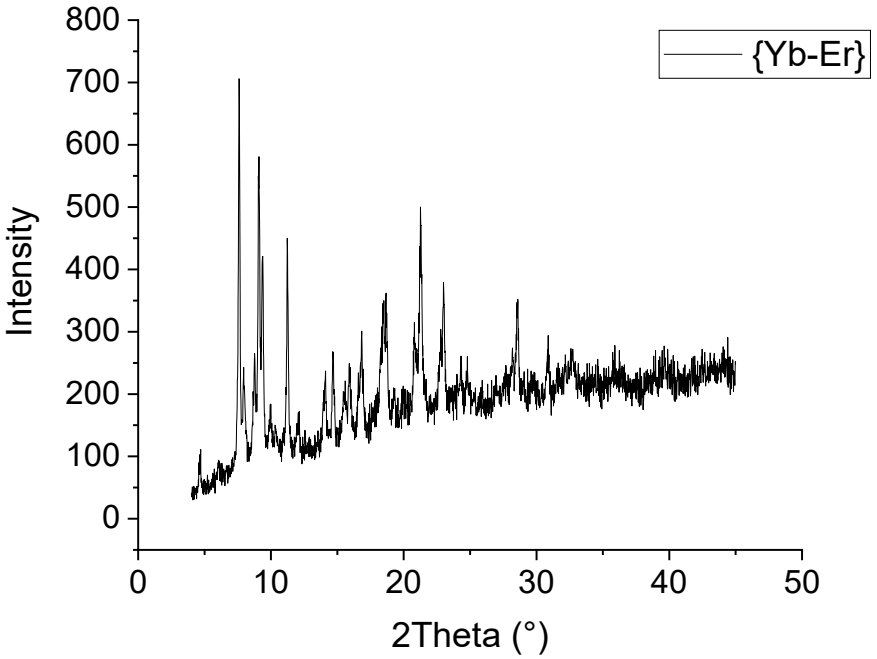

e)

Figure S 25. PXRD data of a) {Lu-Lu}, b) {Yb-Lu), c) {Yb-Yb}, d) {Yb-Nd}, e) {Yb-Er}.

Thermal analisys of conjugates

{Lu-Lu}

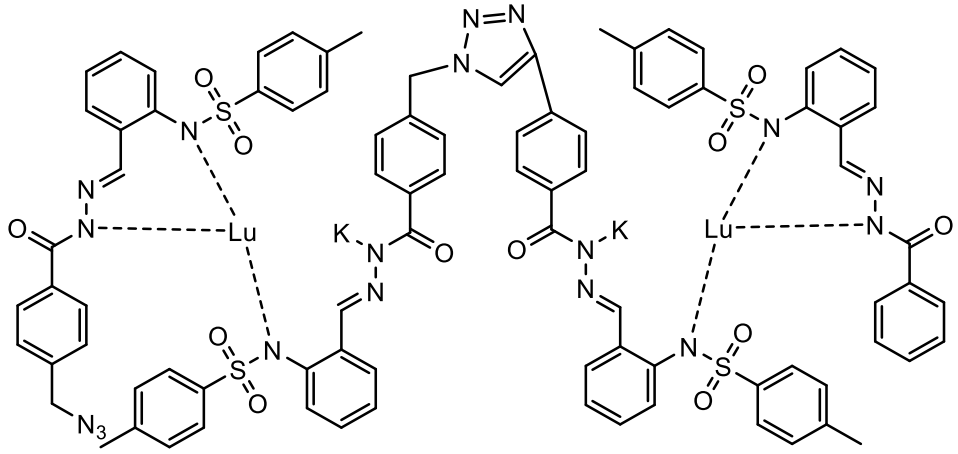

Exact Mass: 2126.2393

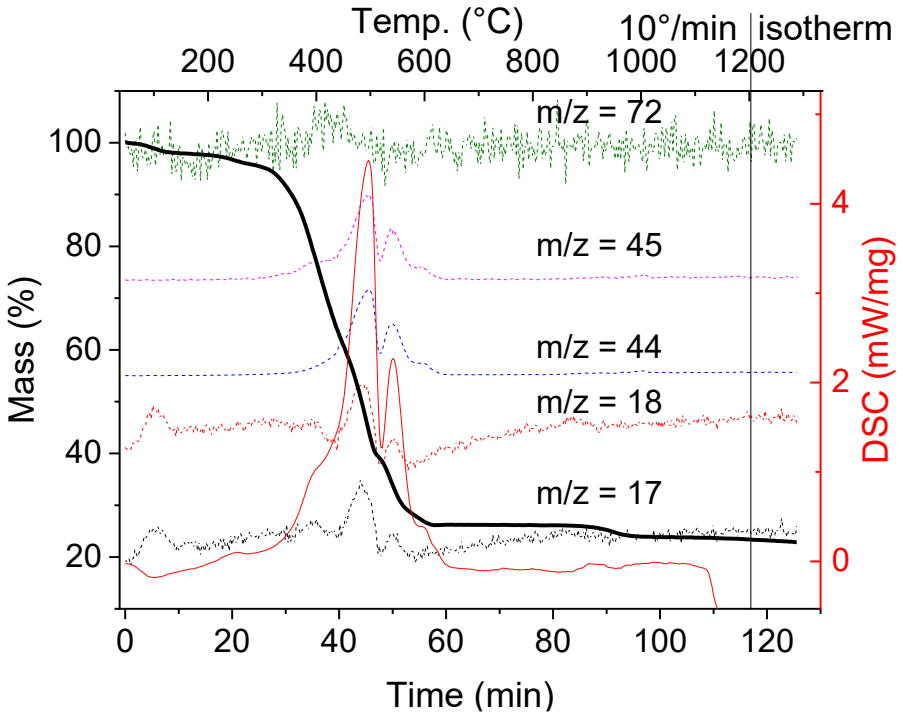

#	Temperature range (T_{max}), °C	Reaction	M(residue), % clcd	M(residue), % found
		{Lu-Lu} (M=2126+54=2180)		
1	40-224	-3H_2O (m/z= 17, 18)	97.5	97.2
2	224-700	ligands degradation		65.9
3	700-1200	→$K_2Lu_2O_4$	22.5	22.9

{Lu-Yb}

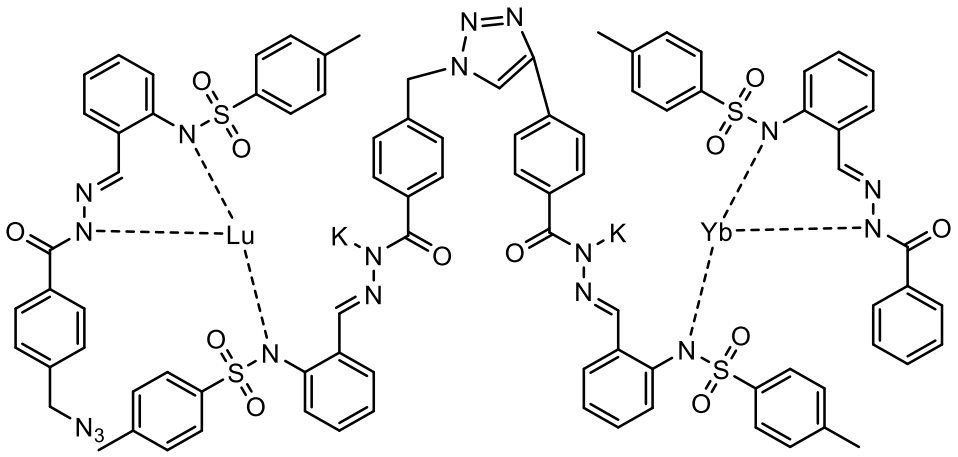

Exact Mass: 2125.2374

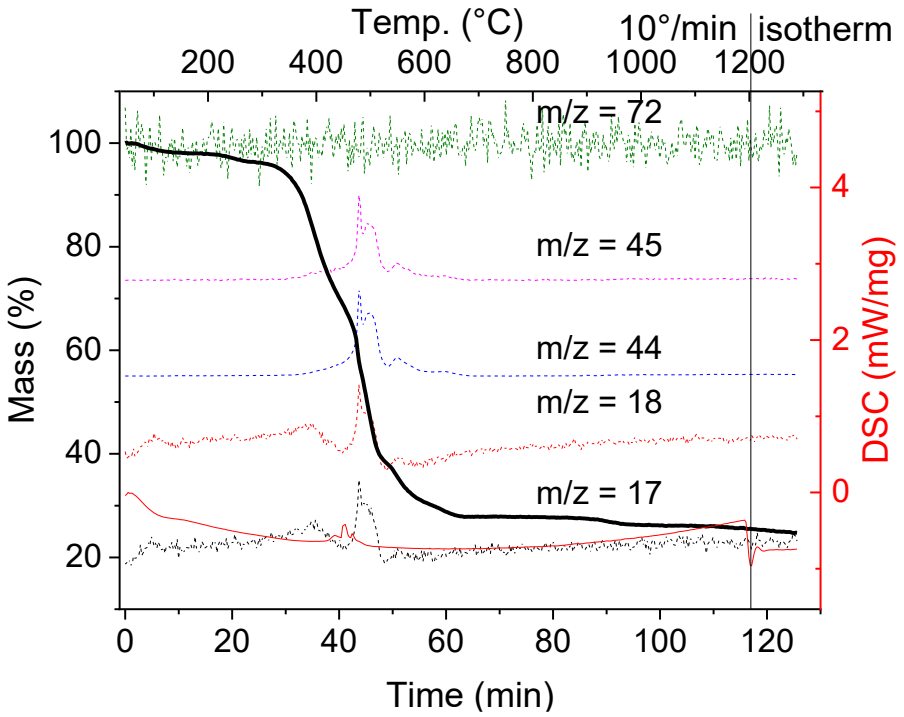

#	Temperature range (T_{max}), °C	Reaction	M(residue), % clcd	M(residue), % found
		{Yb-Lu} (M=2125+54=2179)		
1	40-200	-3H_2O (m/z= 17, 18)	97.8	97.5
2	200-780	ligands degradation		65.9
3	780-1200	→K_2LuYbO_4	23.2	24.77

{Yb-Yb}

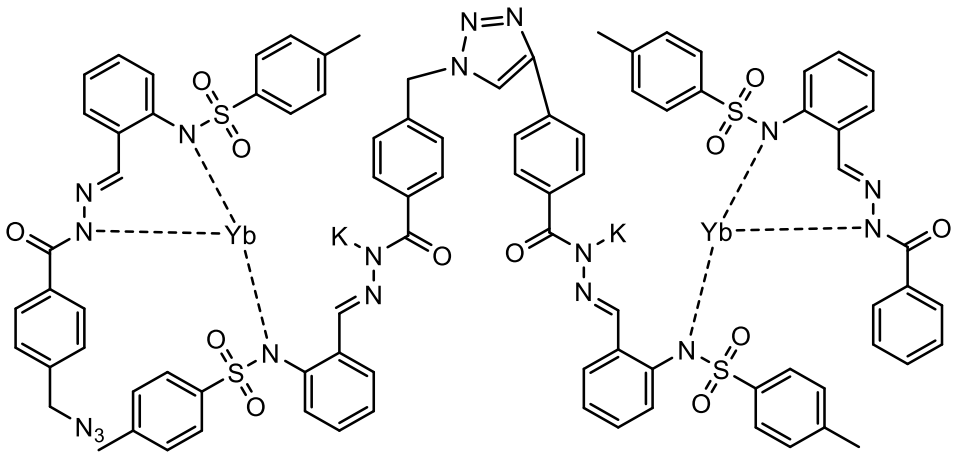

Exact Mass: 2124.2355

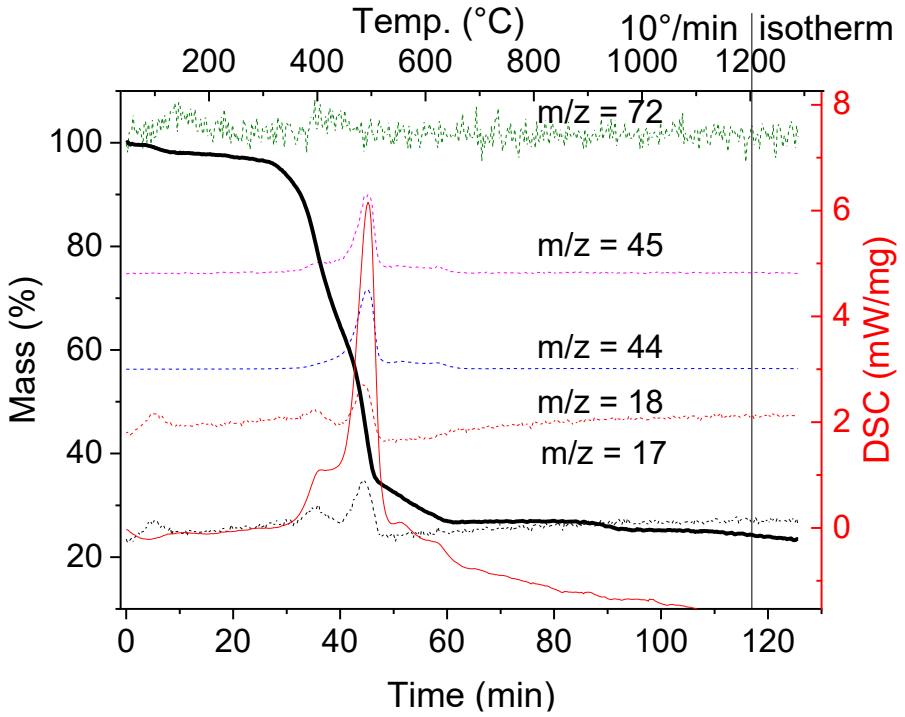

#	Temperature range (T_{max}), °C	Reaction	M(residue), % clcd	M(residue), % found
		{Yb-Yb} (M=2124+72=2196)		
1	40-170	-2H_2O (m/z= 17, 18)	98.3	97.8
2	170-256	-0.5THF (m/z= 72)	96.7	97.1
3	256-780	ligands degradation		27.0
4	780-1200	→$K_2Yb_2O_4$	23.0	23.6

{Yb-Nd}

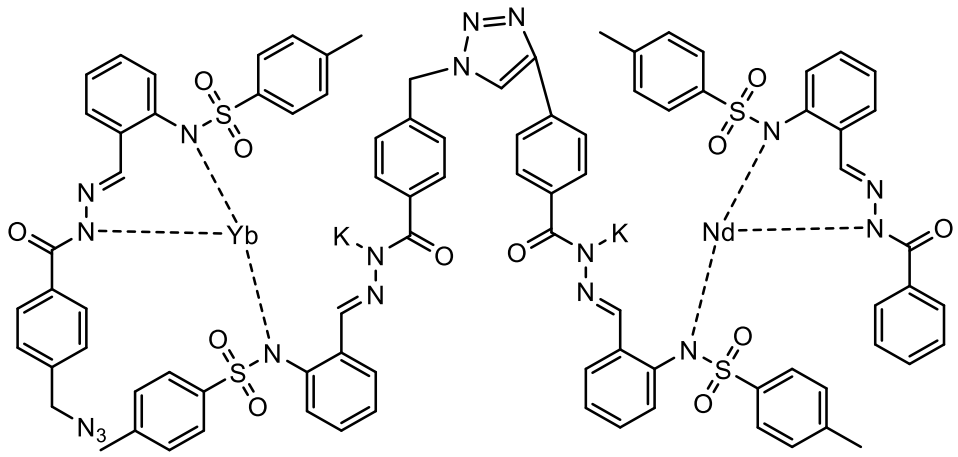

Exact Mass: 2092.2043

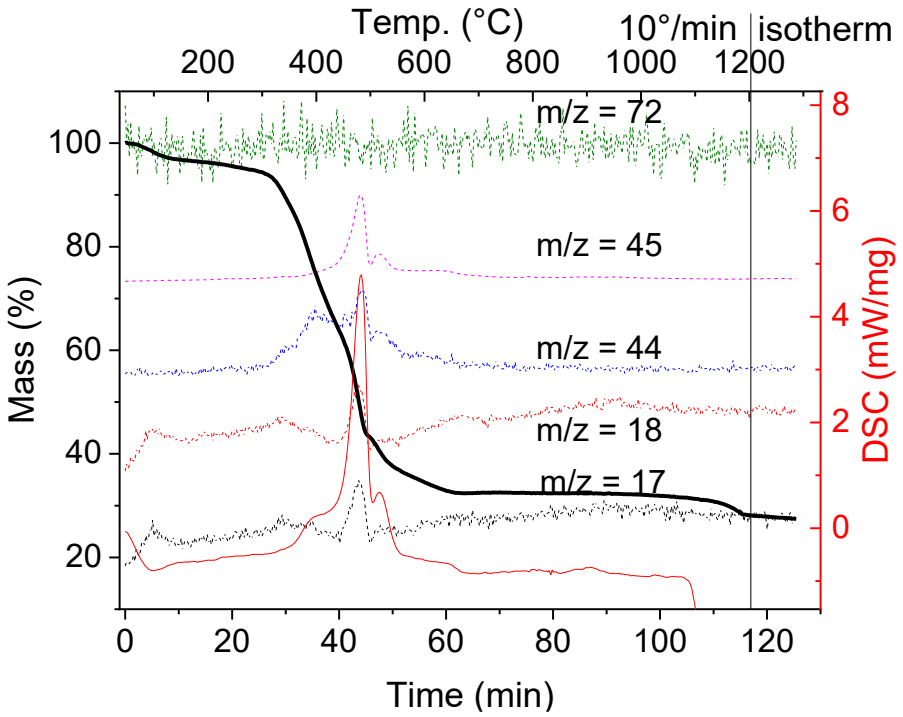

#	Temperature range (T_{max}), °C	Reaction	M(residue), % clcd	M(residue), % found
		{Yb-Nd} (M=2092+72=2164)		
1	40-167	-4H_2O (m/z= 17, 18)	96.5	96.5
2	167-690	ligands degradation		32.4
3	780-1200	→K_2NdYbO_4	21.8	27.6

{Yb-Er}

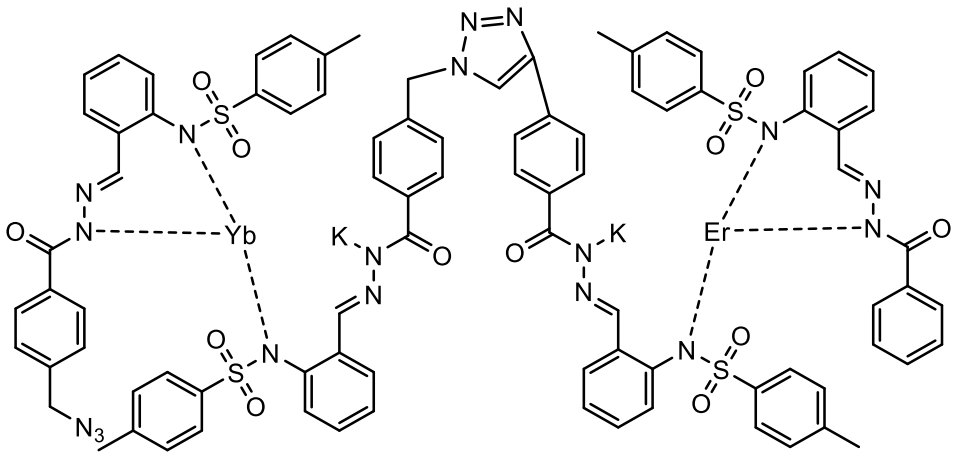

Exact Mass: 2116.2269

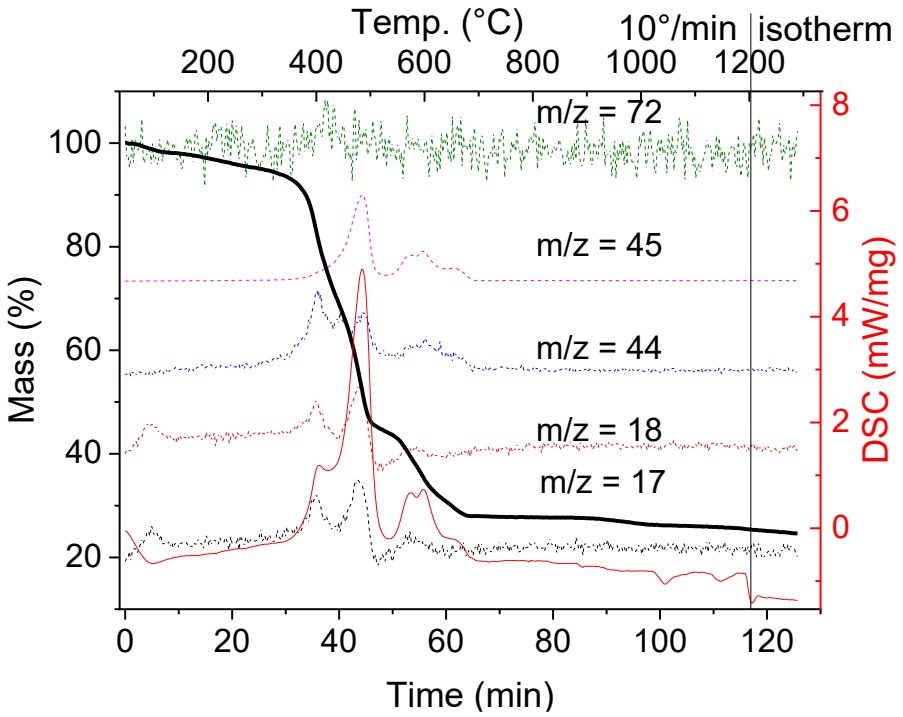

#	Temperature range (T_{max}), °C	Reaction	M(residue), % clcd	M(residue), % found
		{Yb-Er} (M=2116+72=2188)		
1	40-167	-4H_2O (m/z= 17, 18)	96.7	96.7
2	167-690	ligands degradation		27.8
3	780-1200	→K_2ErYbO_4	22.7	24.6

SEM and EDX of conjugates

{Yb-Lu}

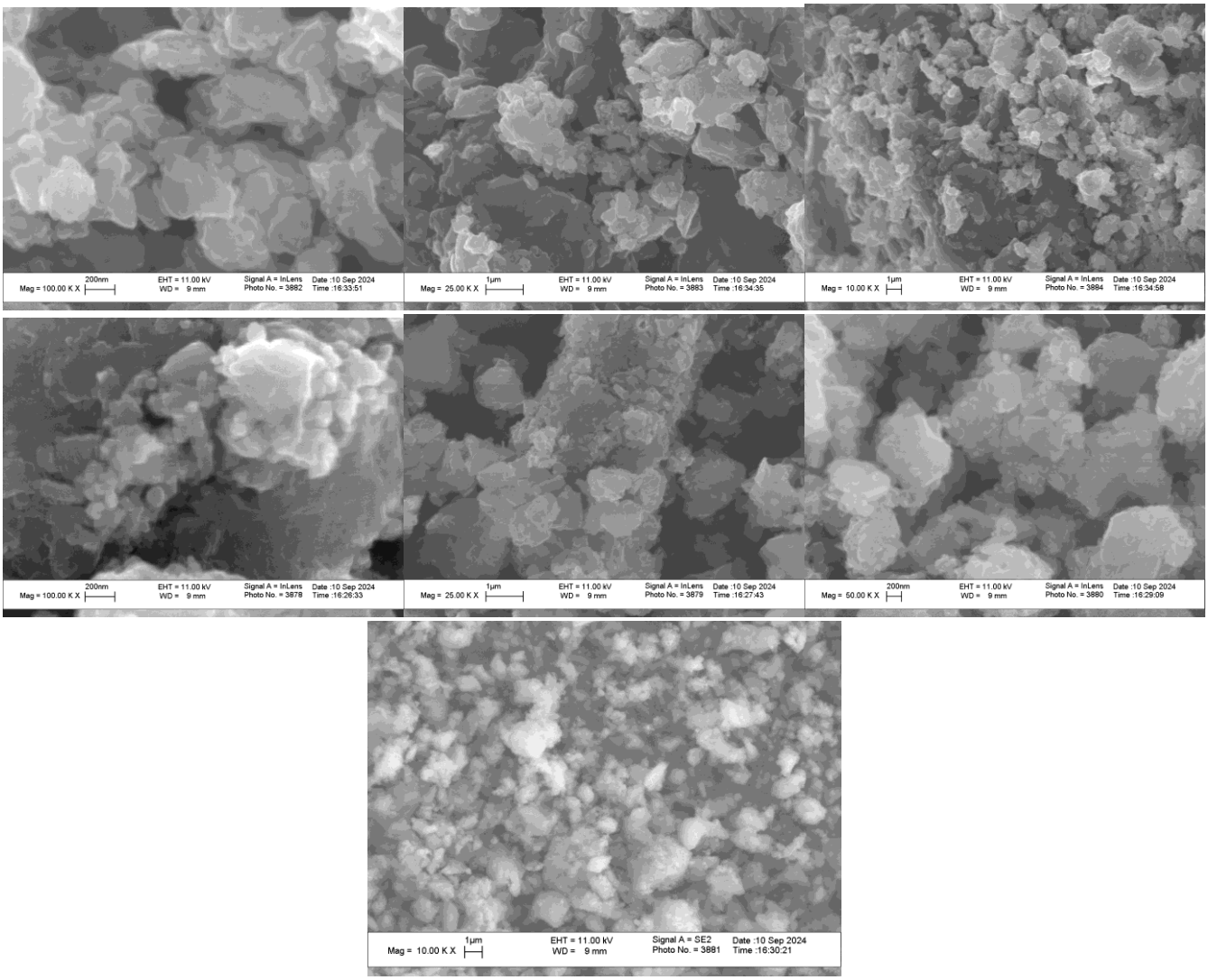

Figure S 26. SEM of {Yb-Lu}.

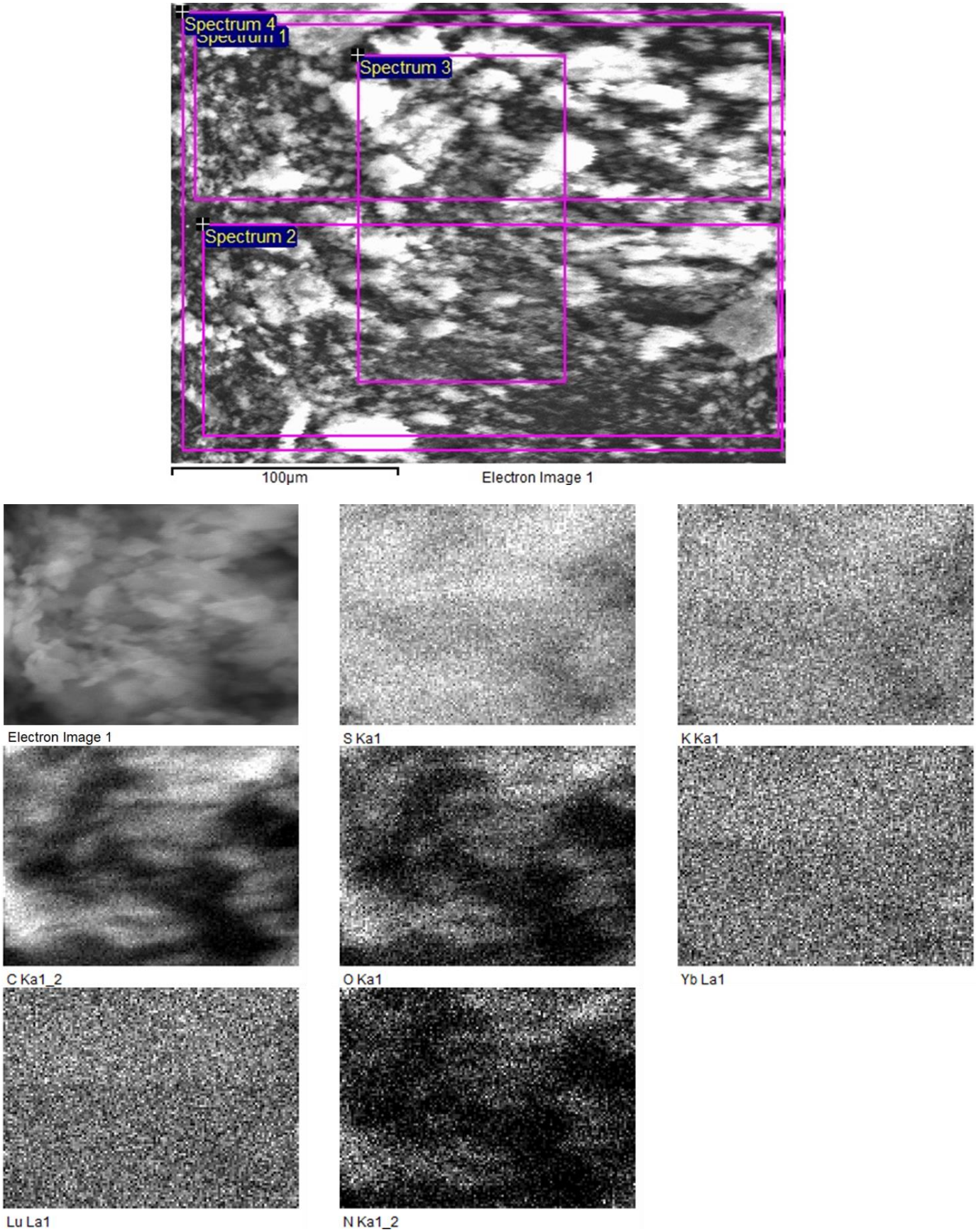

Figure S 27. EDX mapping for {Yb-Lu}.

Spectrum	In stats.	C	N	O	S	K	Yb	Lu
Spectrum 1	Yes	70.4146	14.4678	12.4263	1.4429	0.449	0.3878	0.4116
Spectrum 2	Yes	71.5875	13.0194	13.4035	1.0774	0.3213	0.2859	0.3051
Spectrum 3	Yes	72.0265	13.3956	11.9711	1.3862	0.4305	0.3871	0.403
Spectrum 4	Yes	72.1231	12.8821	12.7149	1.2359	0.3739	0.3242	0.3458
Theory		**45.00%**	**9.00%**	**6.00%**	**2.00%**	**1.00%**	**0.50%**	**0.50%**
Mean		**71.5379**	**13.4412**	**12.629**	**1.2856**	**0.3937**	**0.3463**	**0.3664**
Std. deviation		0.7843	0.718	0.6003	0.164	0.0579	0.0501	0.0502
Max.		72.1231	14.4678	13.4035	1.4429	0.449	0.3878	0.4116
Min.		70.4146	12.8821	11.9711	1.0774	0.3213	0.2859	0.3051

{Yb-Nd}

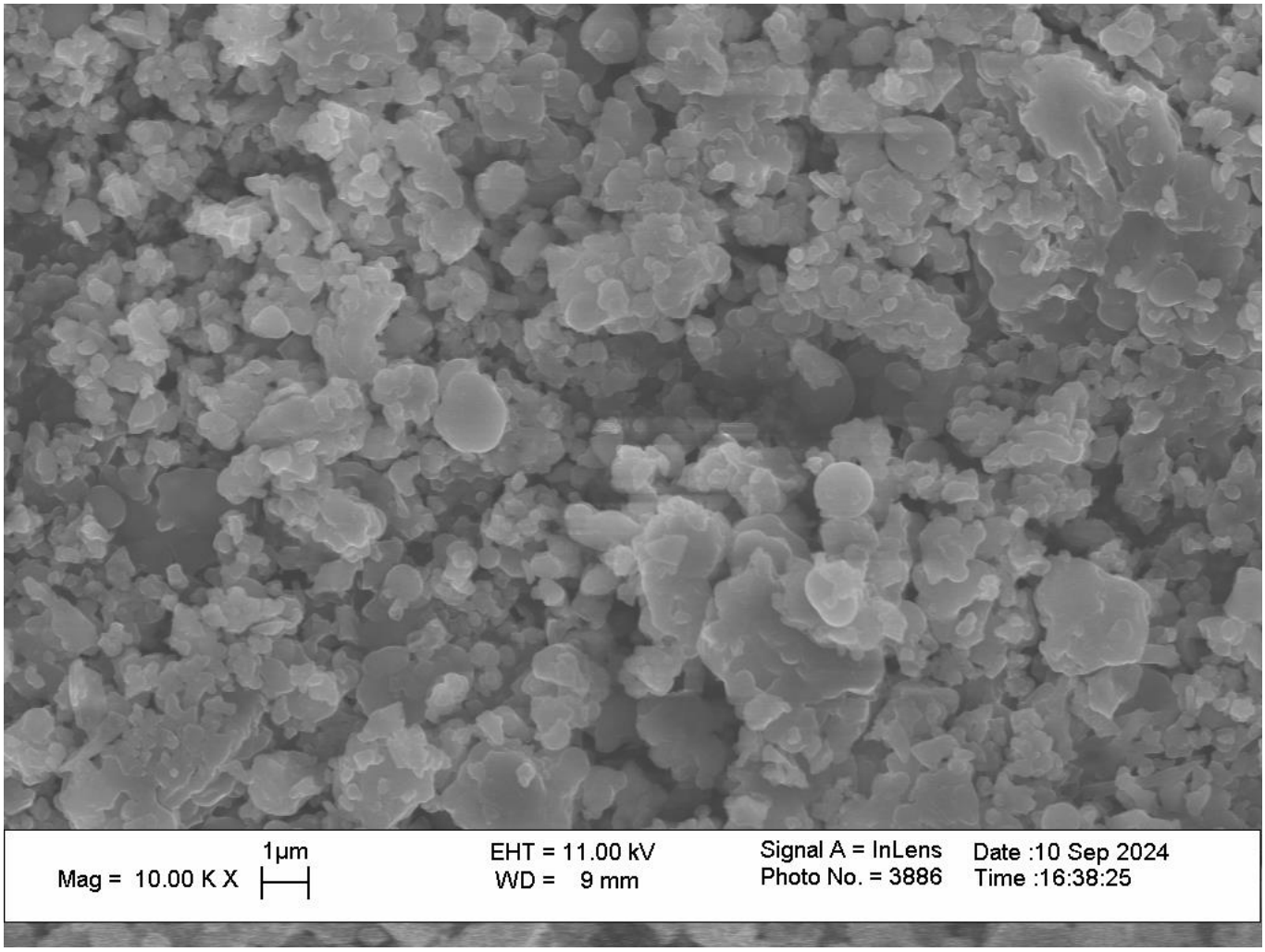

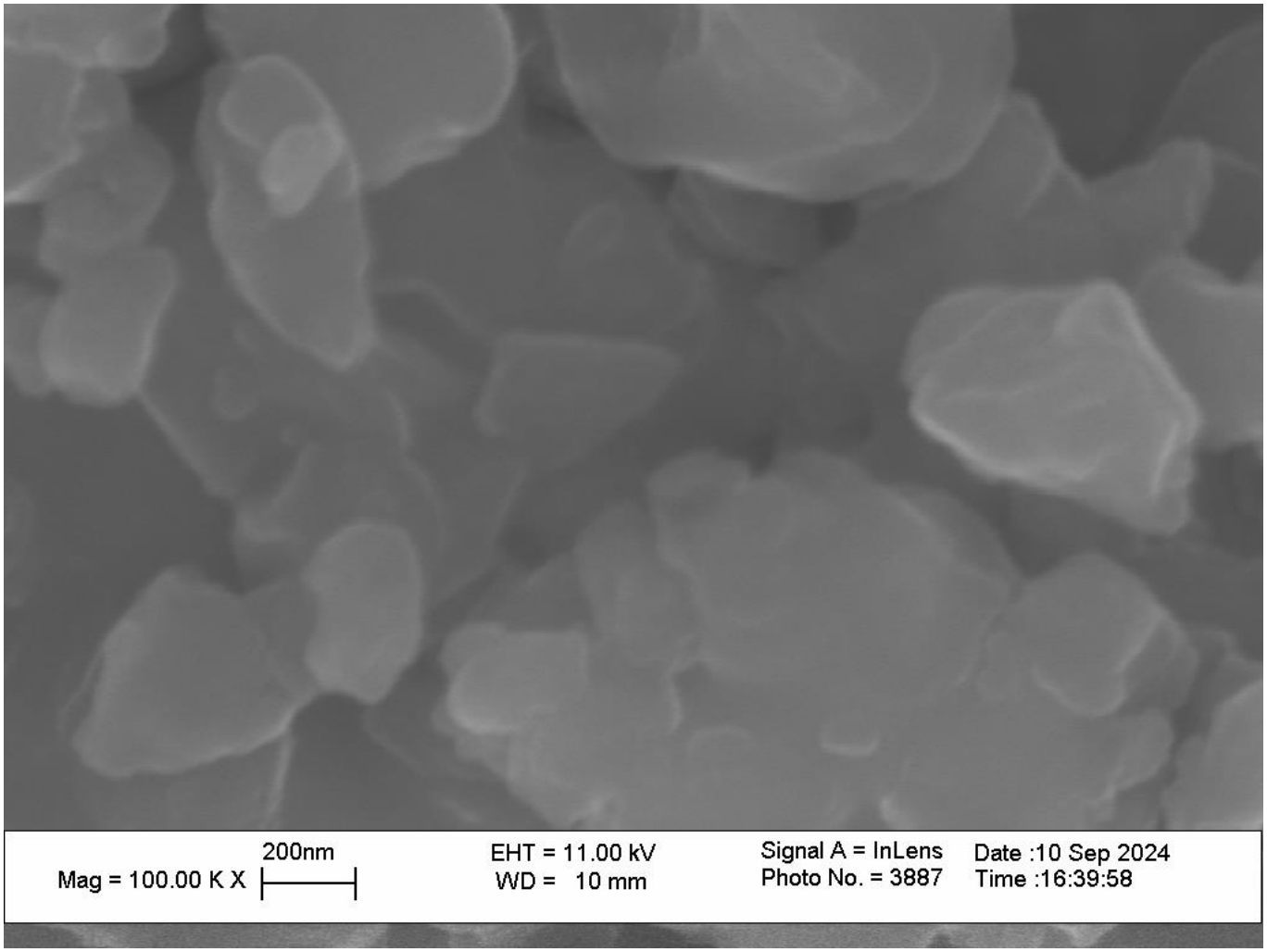
200nm
Mag = 100.00 K X
EHT = 11.00 kV
WD = 10 mm
Signal A = InLens
Photo No. = 3887
Date :10 Sep 2024
Time :16:39:58

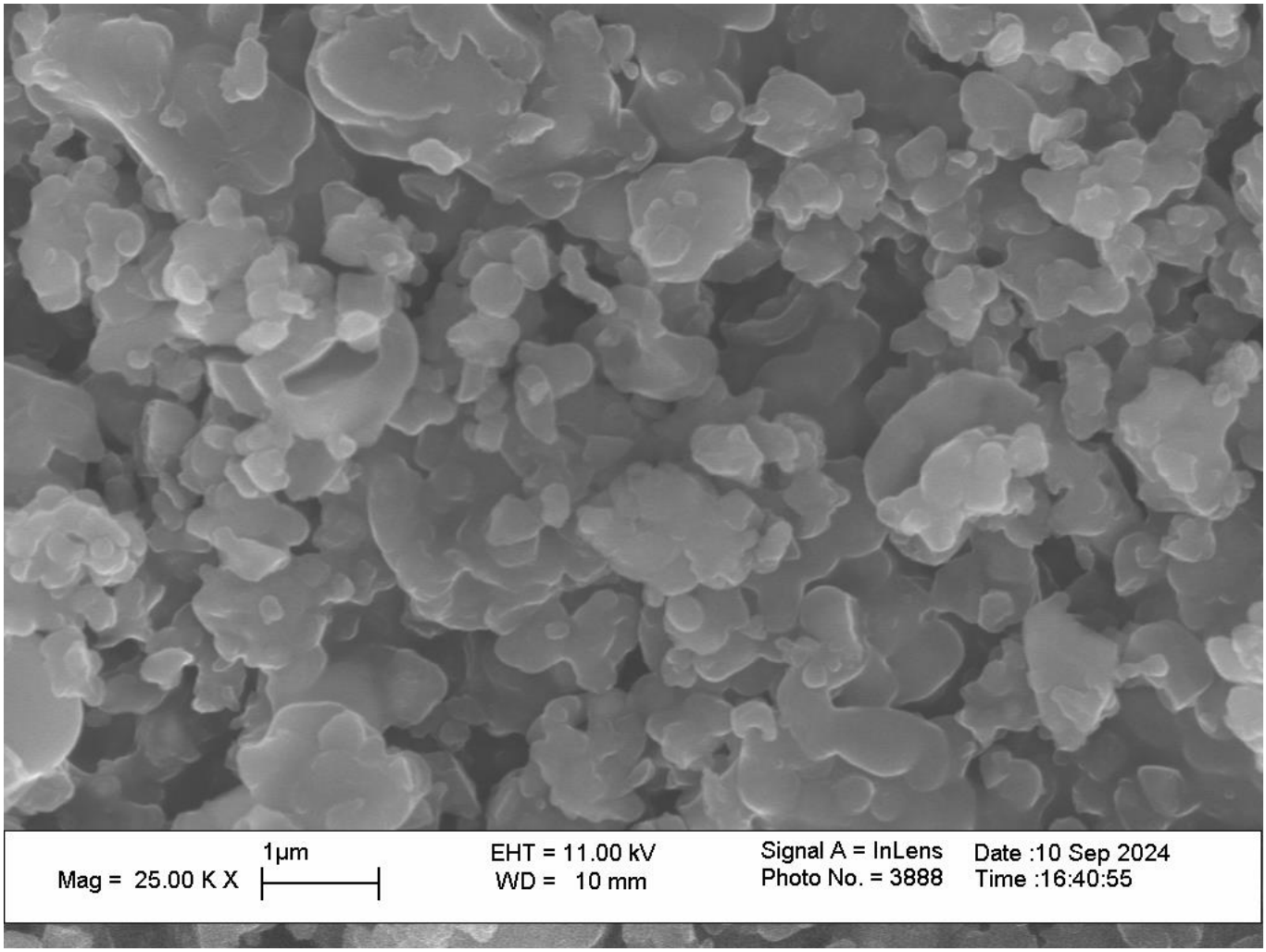
1µm
Mag = 25.00 K X
EHT = 11.00 kV
WD = 10 mm
Signal A = InLens
Photo No. = 3888
Date :10 Sep 2024
Time :16:40:55

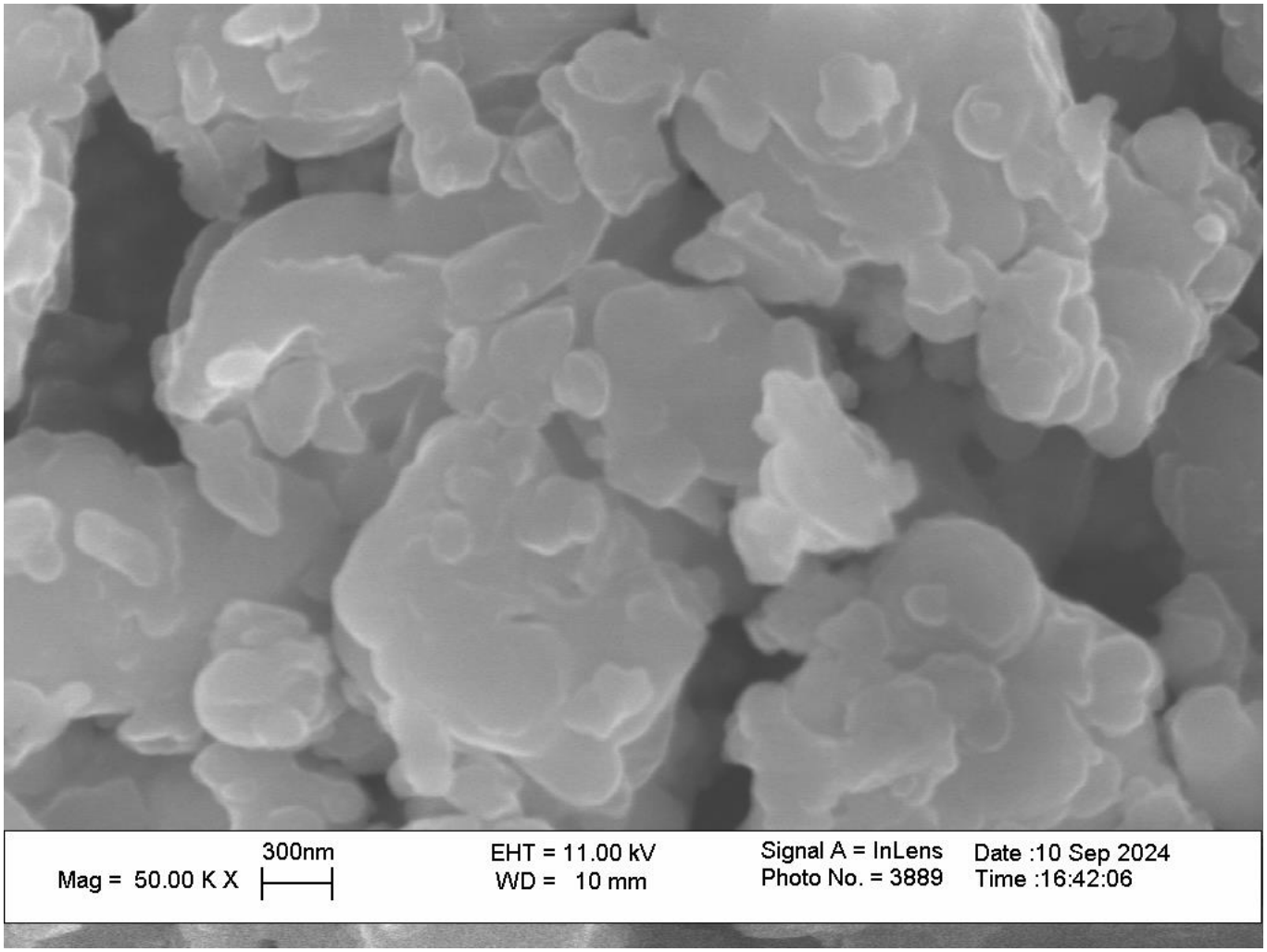
300nm
Mag = 50.00 K X
EHT = 11.00 kV
WD = 10 mm
Signal A = InLens
Photo No. = 3889
Date :10 Sep 2024
Time :16:42:06

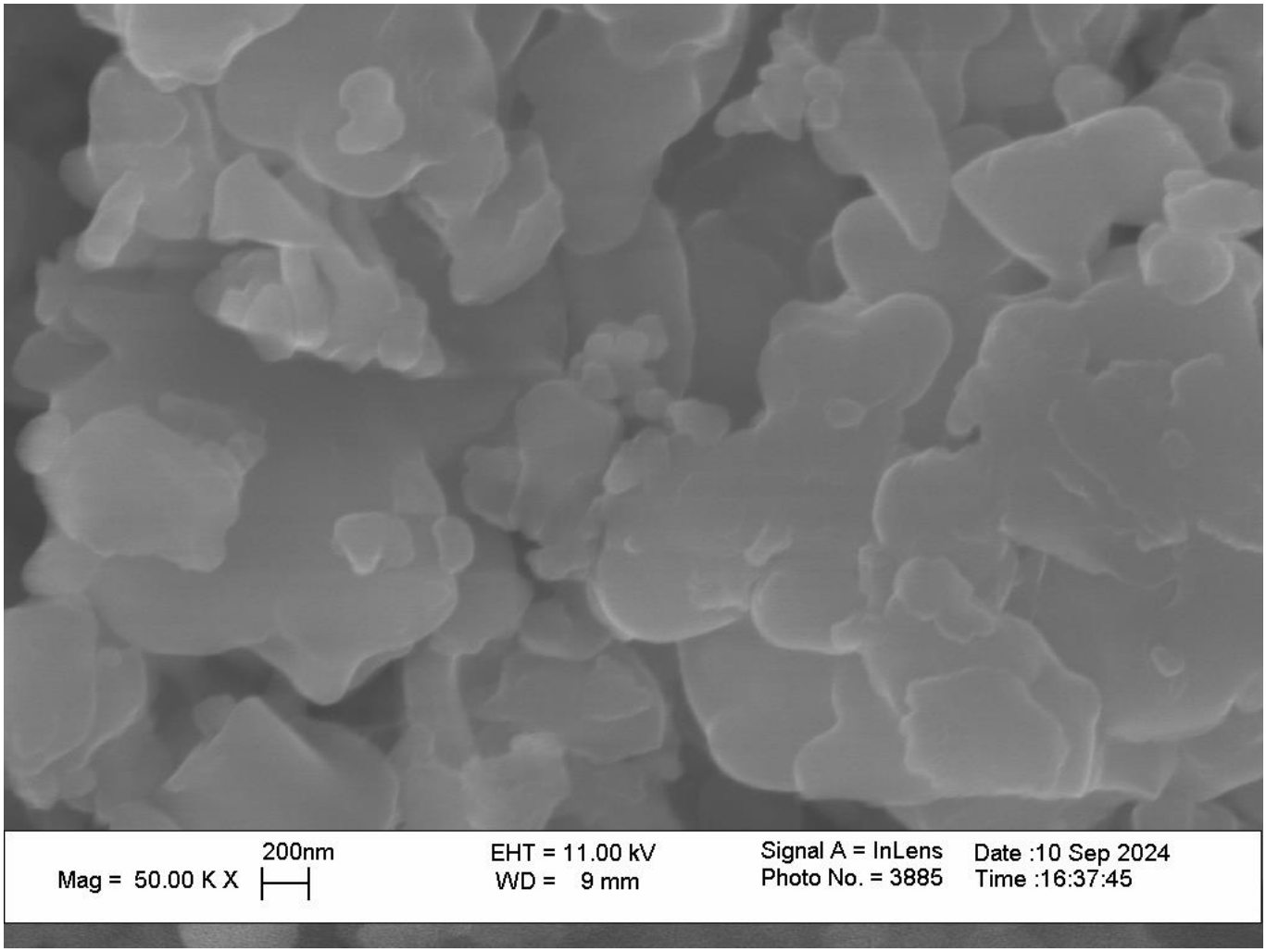

Figure S 28. SEM of {Yb-Nd}.

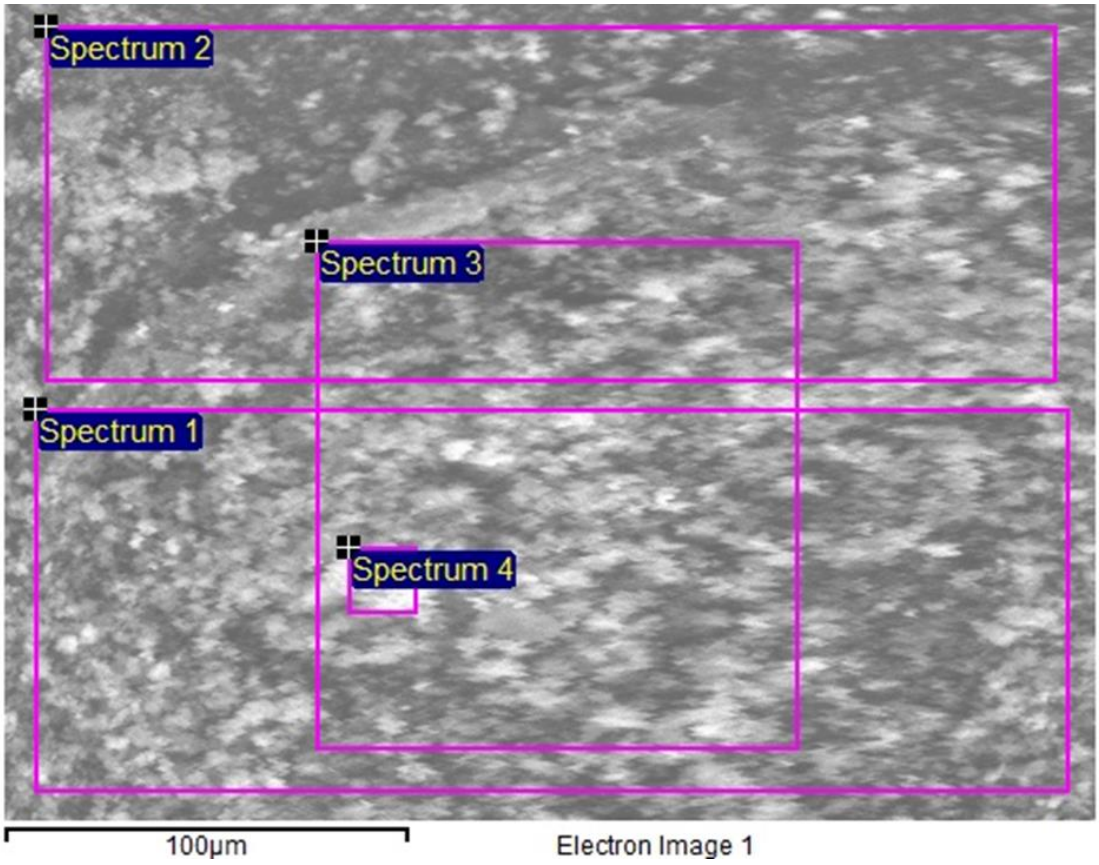

Spectrum	In stats.	C	O	S	K	Nd	Er	Yb
Spectrum 1	Yes	78.8522	18.7331	1.2583	0.2301	0.6304	-0.021	0.317
Spectrum 2	Yes	80.1864	18.1394	0.8543	0.1637	0.4507	-0.0145	0.2201
Spectrum 3	Yes	80.0289	17.2349	1.3985	0.2702	0.7354	-0.0122	0.3443
Spectrum 4	Yes	79.5706	17.4568	1.5689	0.2929	0.7296	-0.0203	0.4016
Theory		**45.00%**	**6.00%**	**2.00%**	**1.00%**	**0.50%**	**0.00%**	**0.50%**
Mean		**79.6595**	**17.891**	**1.27**	**0.2392**	**0.6365**	**-0.017**	**0.3208**
Std. deviation		0.5983	0.6806	0.3049	0.0566	0.1329	0.0043	0.0758
Max.		80.1864	18.7331	1.5689	0.2929	0.7354	-0.0122	0.4016
Min.		78.8522	17.2349	0.8543	0.1637	0.4507	-0.021	0.2201

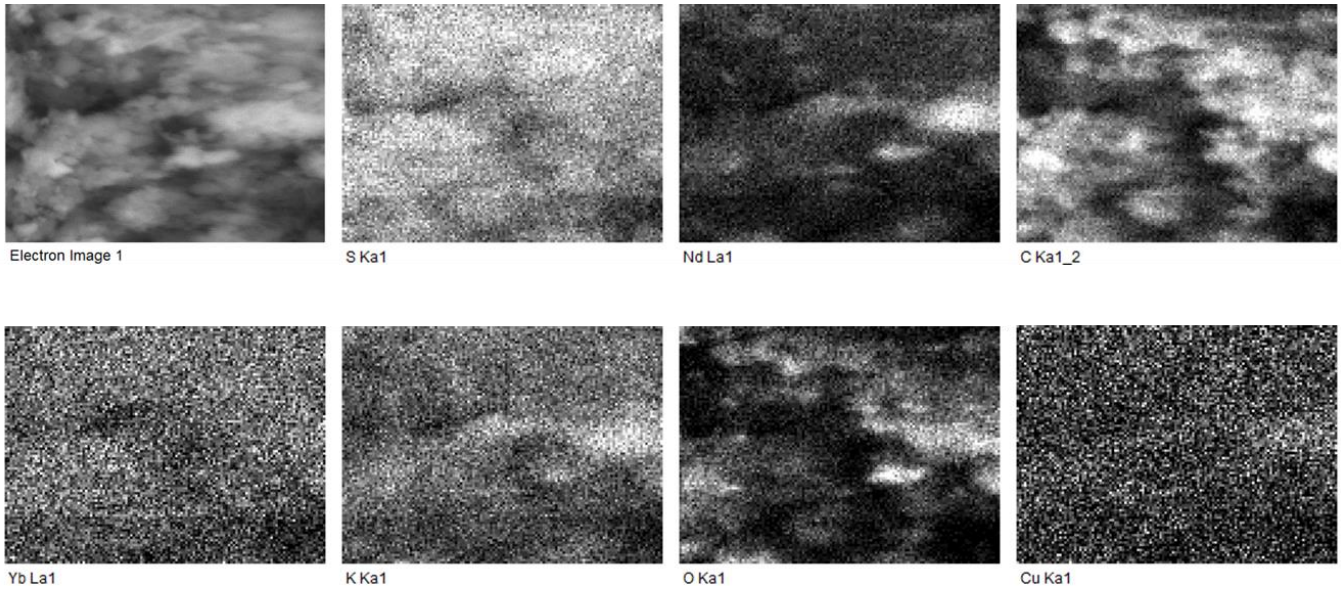

Figure S 29. EDX mapping of {Yb-Nd}.

{Yb-Er}

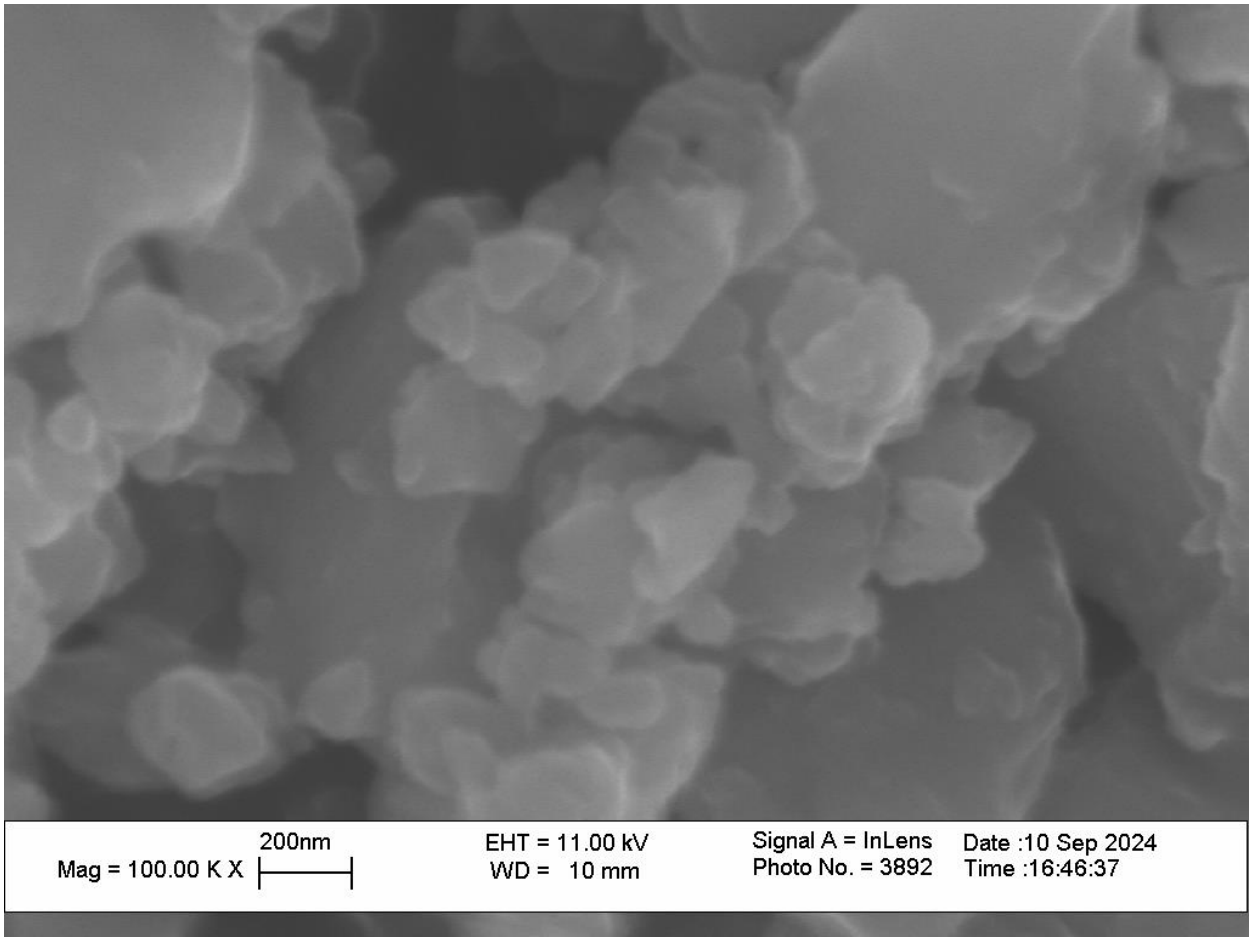

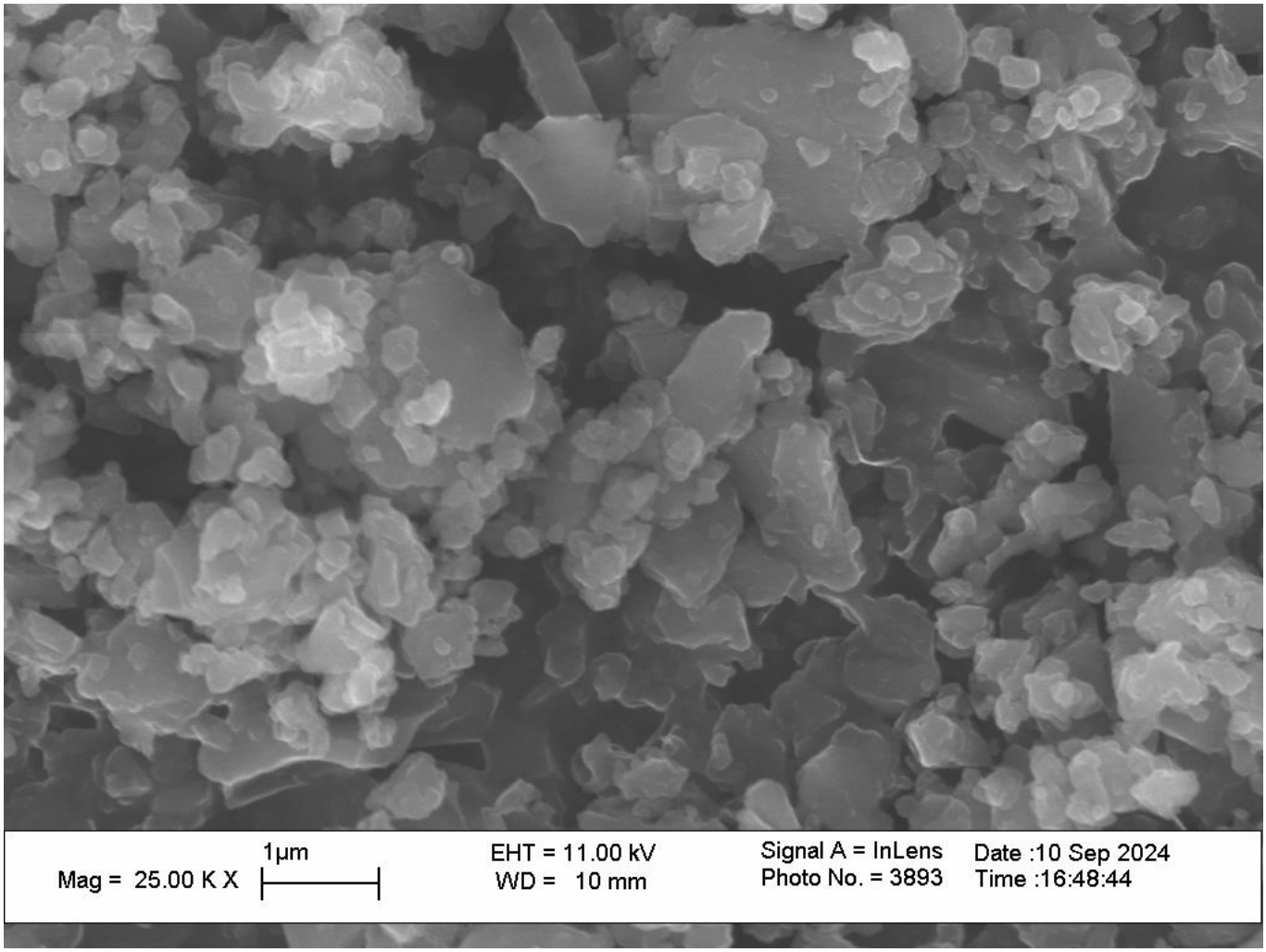
1µm
Mag = 25.00 K X
EHT = 11.00 kV
WD = 10 mm
Signal A = InLens
Photo No. = 3893
Date :10 Sep 2024
Time :16:48:44

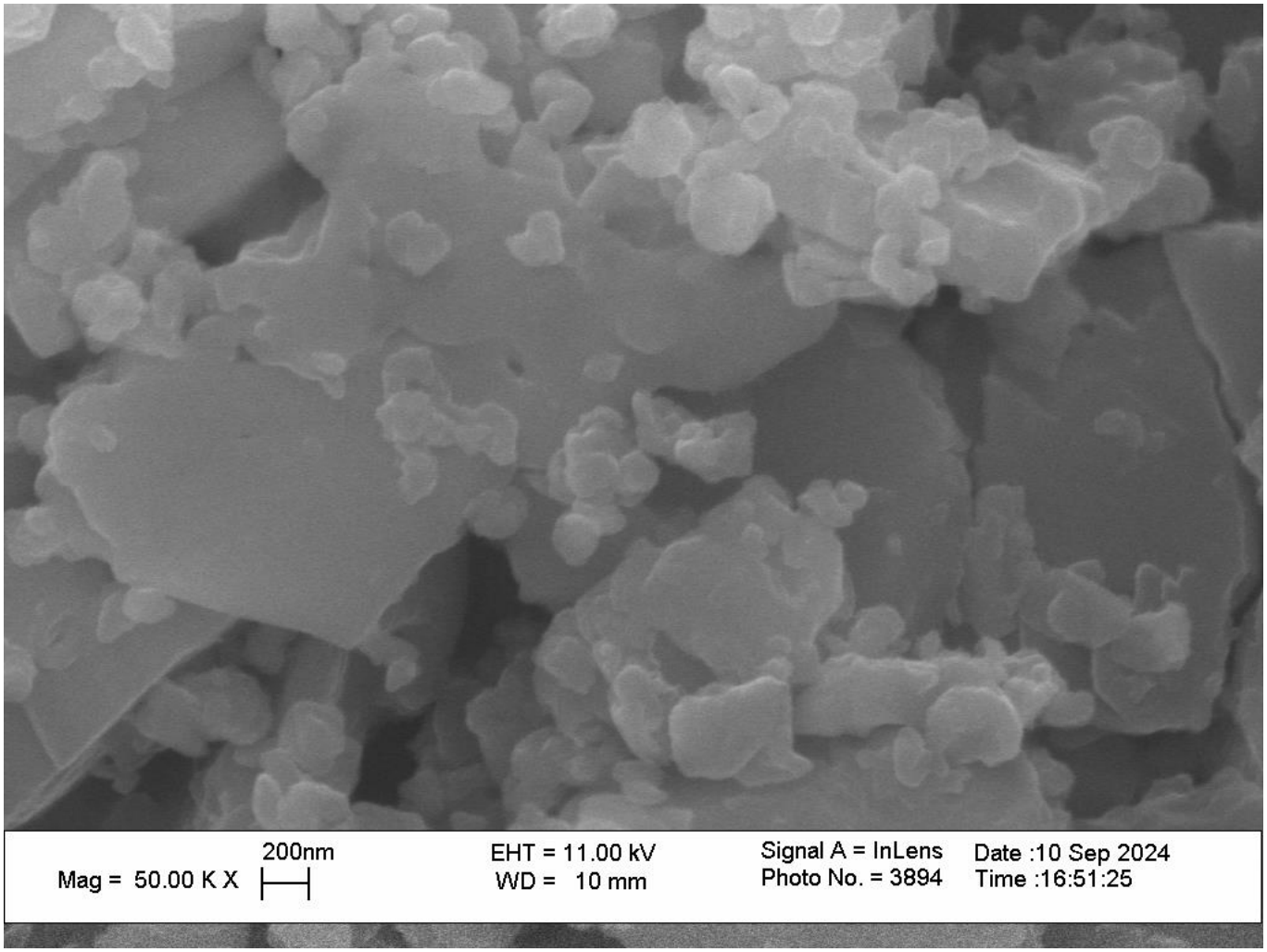
200nm
Mag = 50.00 K X
EHT = 11.00 kV
WD = 10 mm
Signal A = InLens
Photo No. = 3894
Date :10 Sep 2024
Time :16:51:25

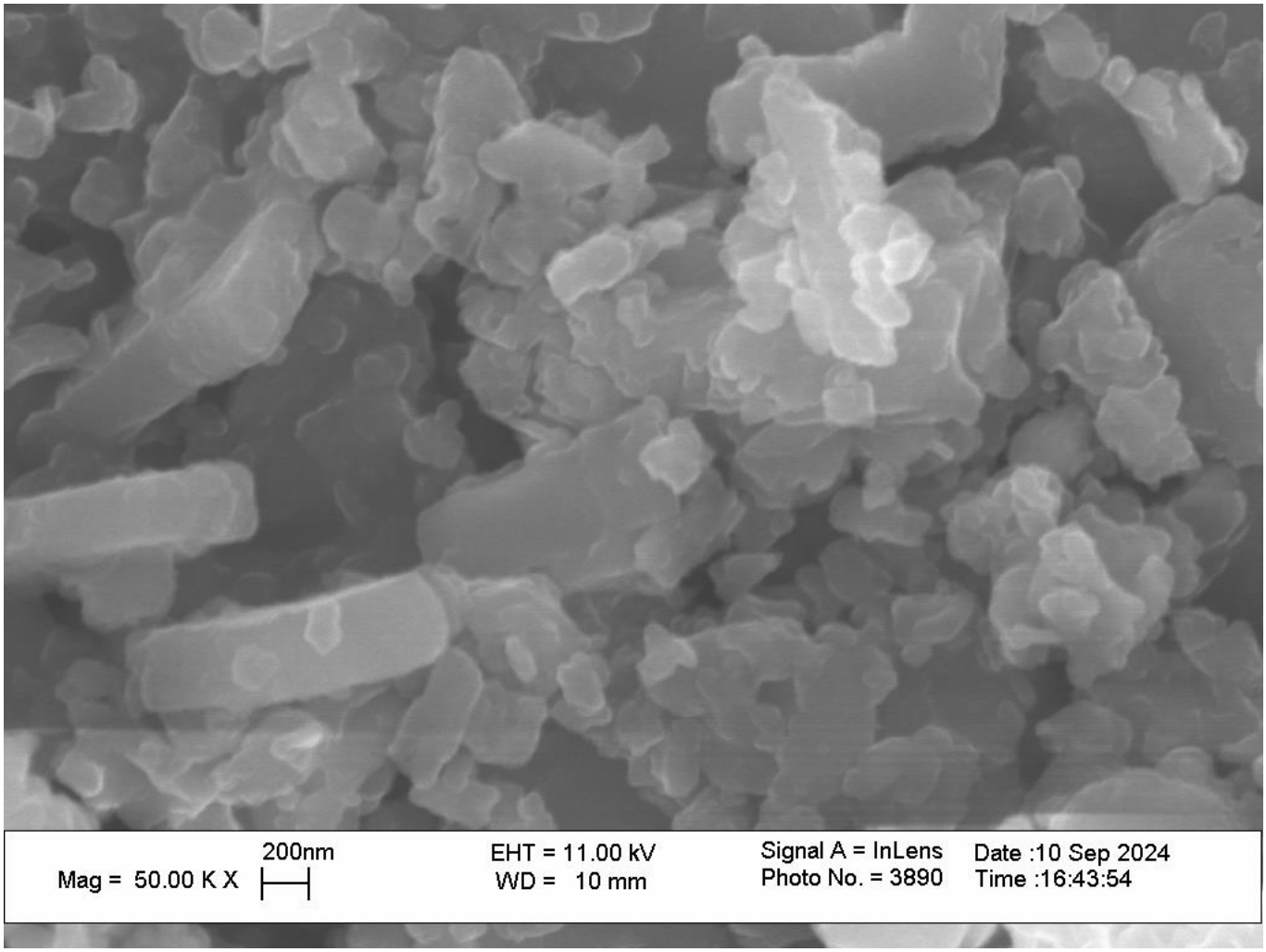
200nm
Mag = 50.00 K X
EHT = 11.00 kV
WD = 10 mm
Signal A = InLens
Photo No. = 3890
Date :10 Sep 2024
Time :16:43:54

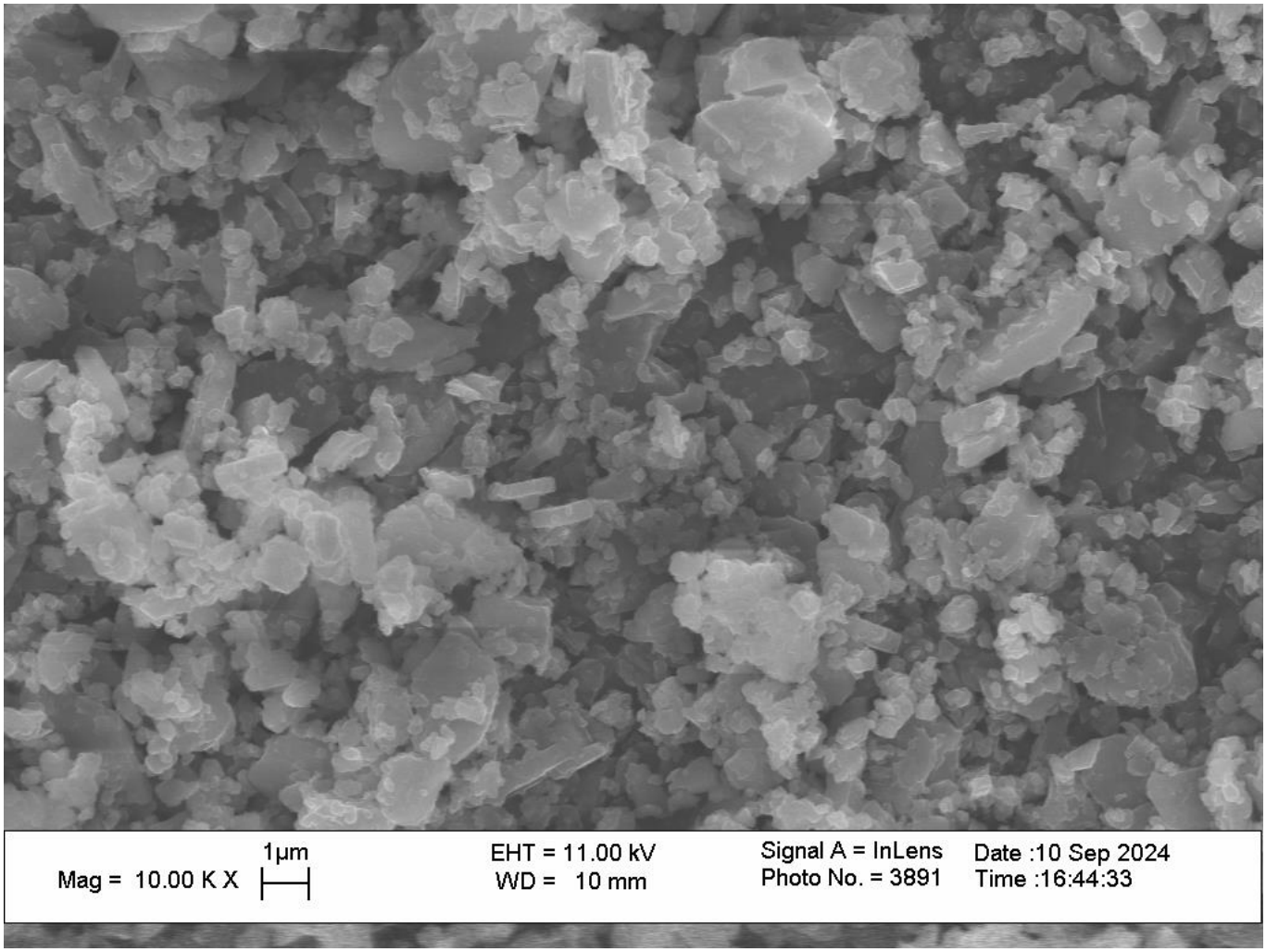

Figure S 30. SEM of {Yb-Er}.

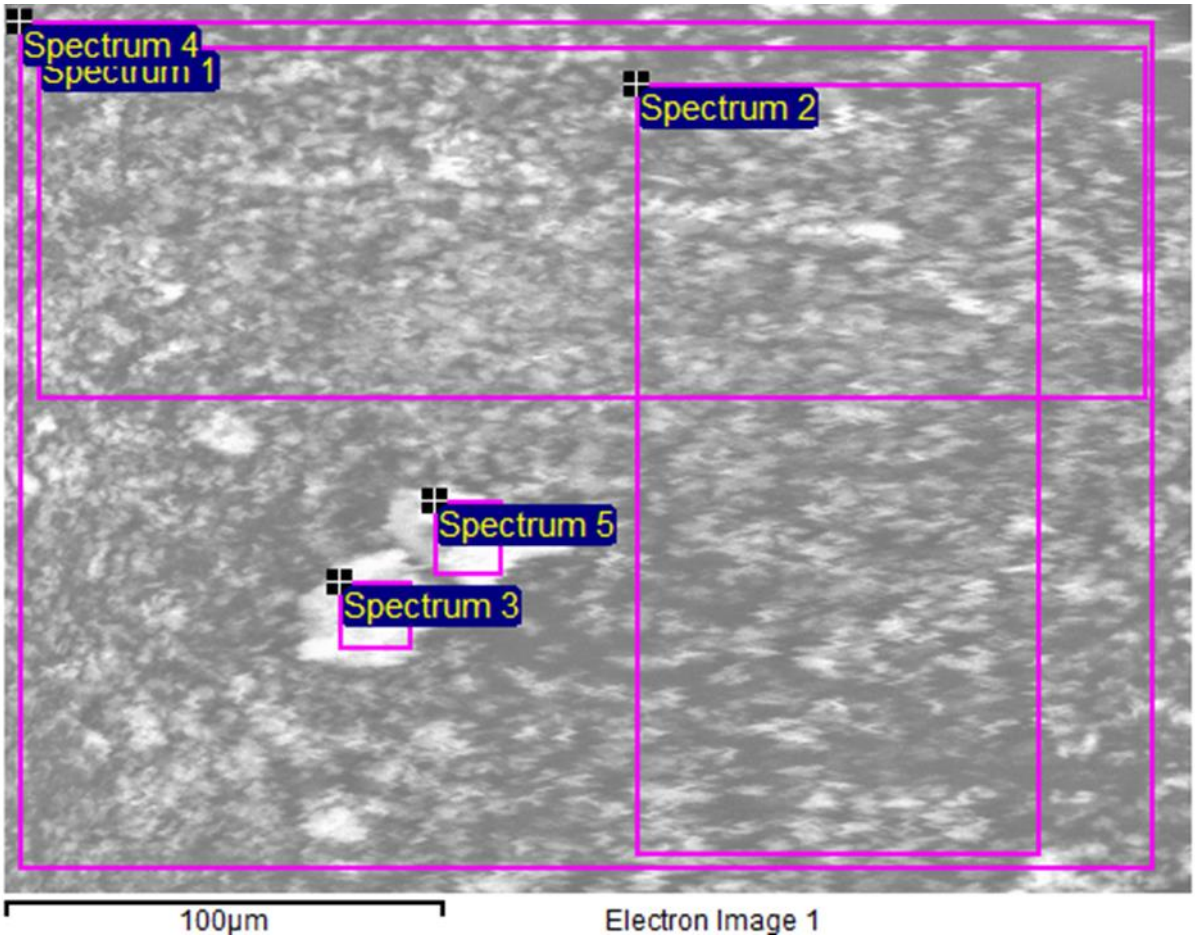

Spectrum	In stats.	C	N	O	S	K	Nd	Er	Yb
Spectrum 1	Yes	71.8022	12.6985	14.476	0.5348	0.1737	-0.0032	0.1556	0.1623
Spectrum 2	Yes	73.4992	11.2695	14.4528	0.3981	0.1326	-0.002	0.1219	0.128
Spectrum 3	Yes	72.6208	12.8248	11.5599	1.6524	0.5534	-0.0019	0.3791	0.4116
Spectrum 4	Yes	72.92	12.3391	13.7842	0.4888	0.1648	-0.001	0.148	0.1561
Spectrum 5	Yes	72.6632	13.0756	11.024	1.7682	0.5969	0.0008	0.4109	0.4604
Theory		45.00%	9.00%	6.00%	2.00%	1.00%	0.00%	0.50%	0.50%
Mean		72.7011	12.4415	13.0594	0.9685	0.3243	-0.0014	0.2431	0.2637
Std. deviation		0.6126	0.707	1.6481	0.6802	0.23	0.0015	0.1397	0.1588
Max.		73.4992	13.0756	14.476	1.7682	0.5969	0.0008	0.4109	0.4604
Min.		71.8022	11.2695	11.024	0.3981	0.1326	-0.0032	0.1219	0.128

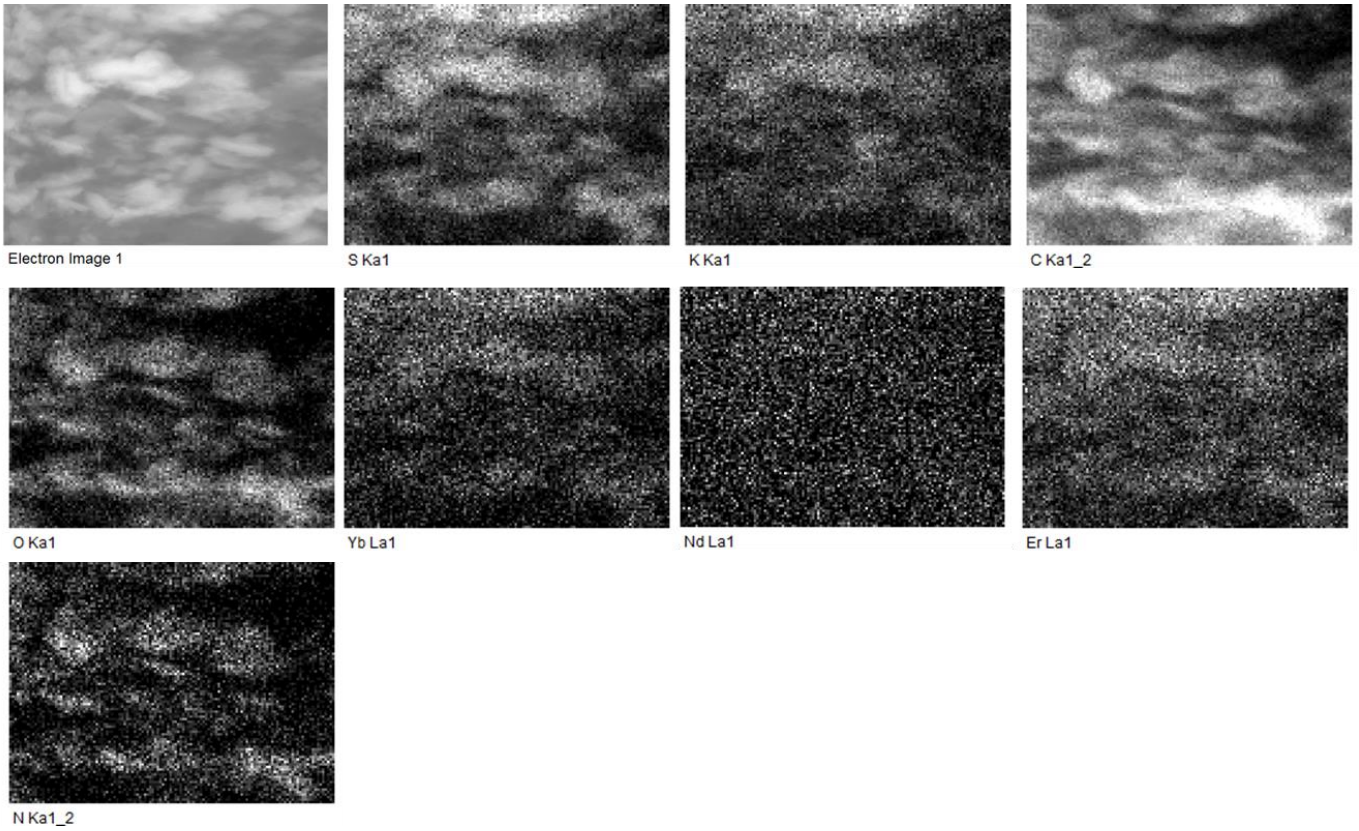

Figure S 31. EDX mapping for {Yb-Nd}.

^{1}H NMR for conjugates

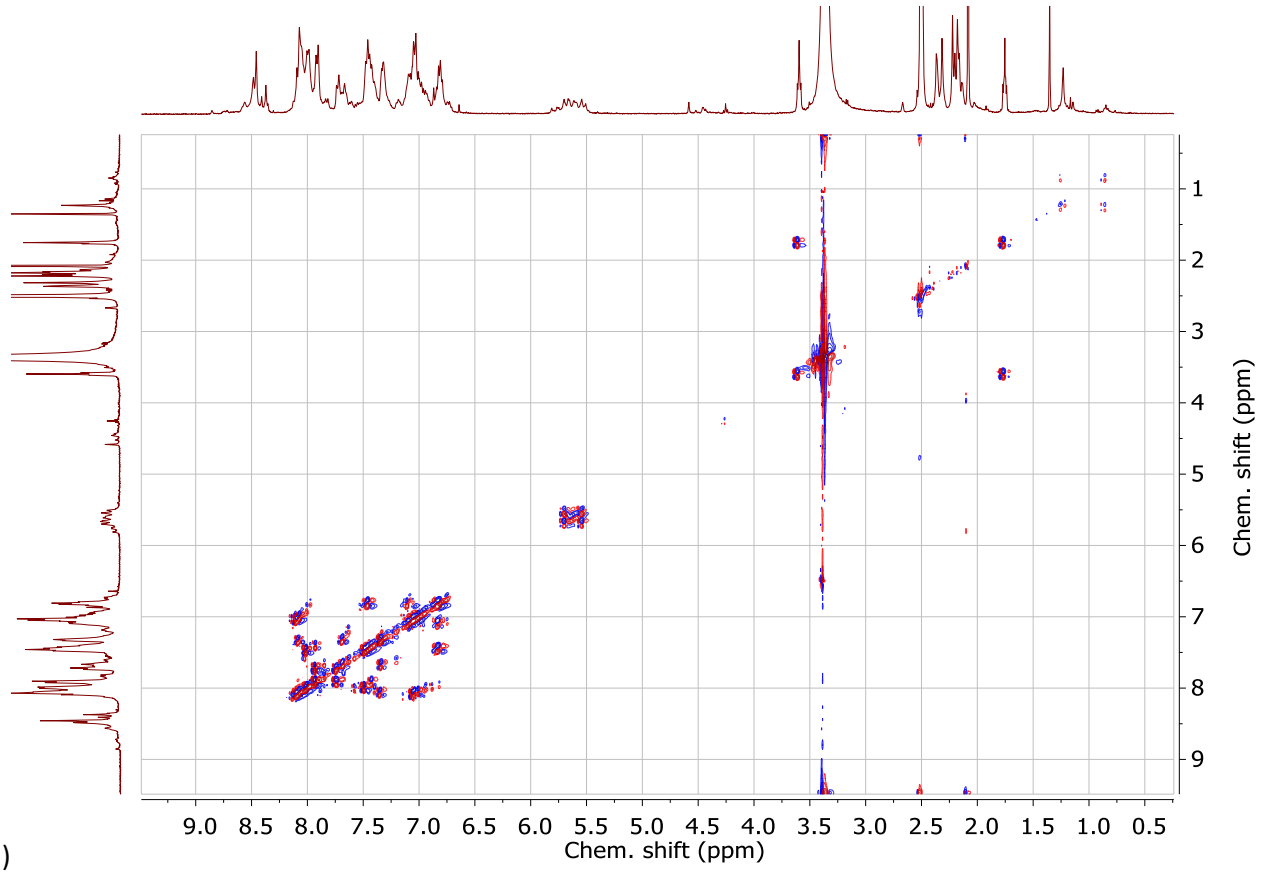

a)

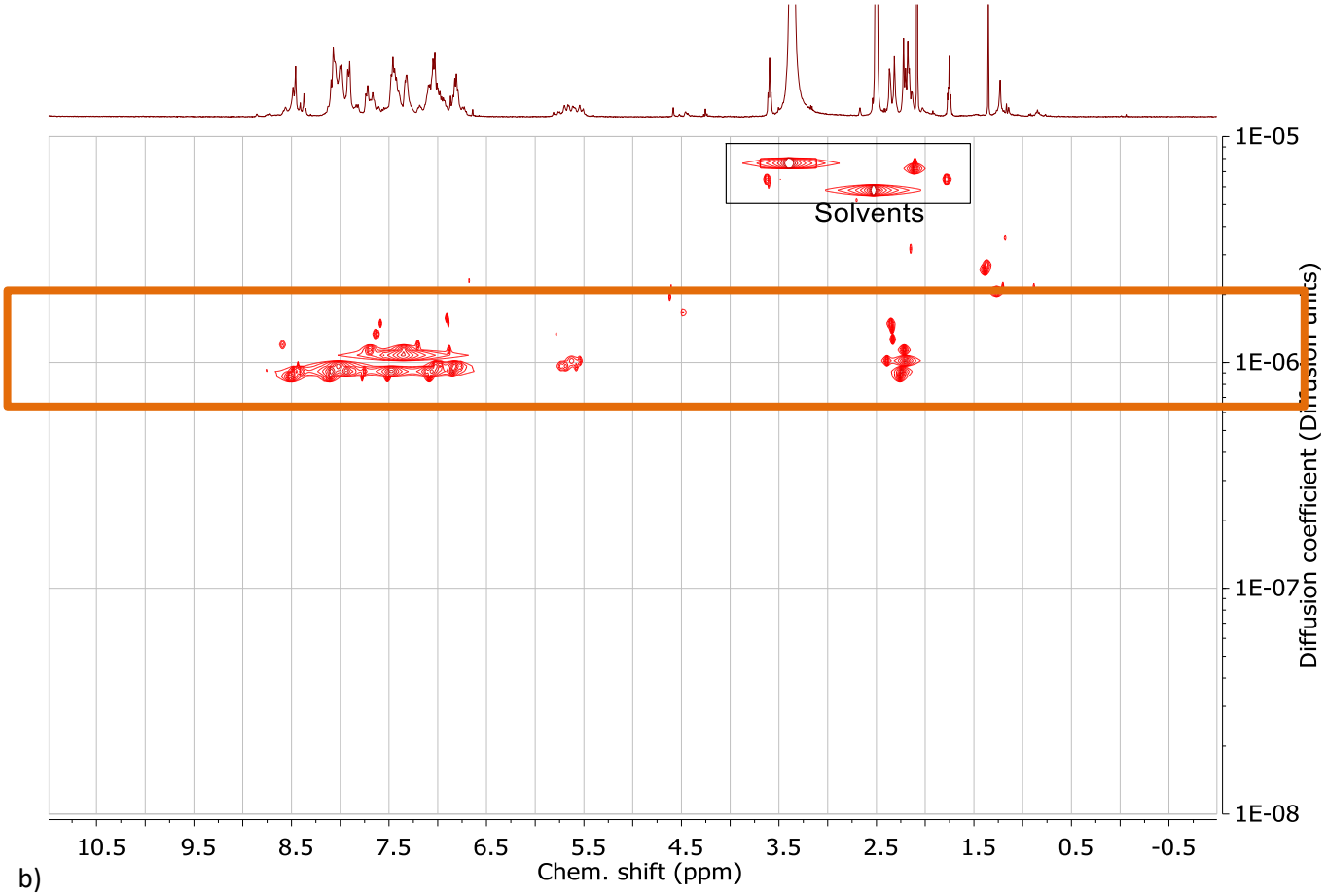
Solvents
1E-05
1E-06
1E-07
1E-08
Diffusion coefficient (Diffusion units)
10.5
9.5
8.5
7.5
6.5
5.5
4.5
3.5
2.5
1.5
0.5
-0.5
Chem. shift (ppm)

b)

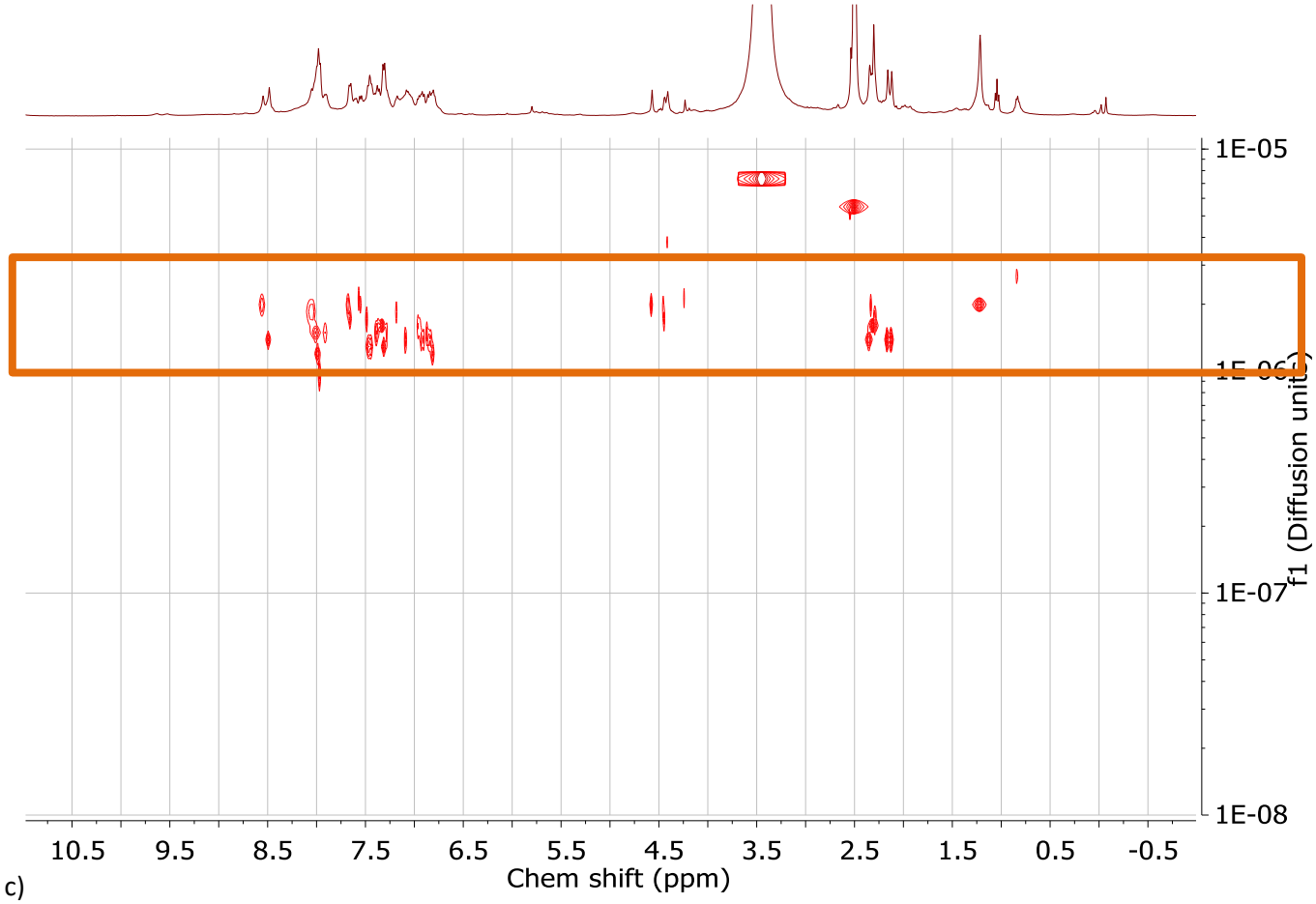

c)

Figure S 32. ^{1}H NMR spectra of {Lu-Lu} in regime a) COSY NMR, b) DOSY NMR. c)^{1}H DOSY NMR of {Yb-Lu}.

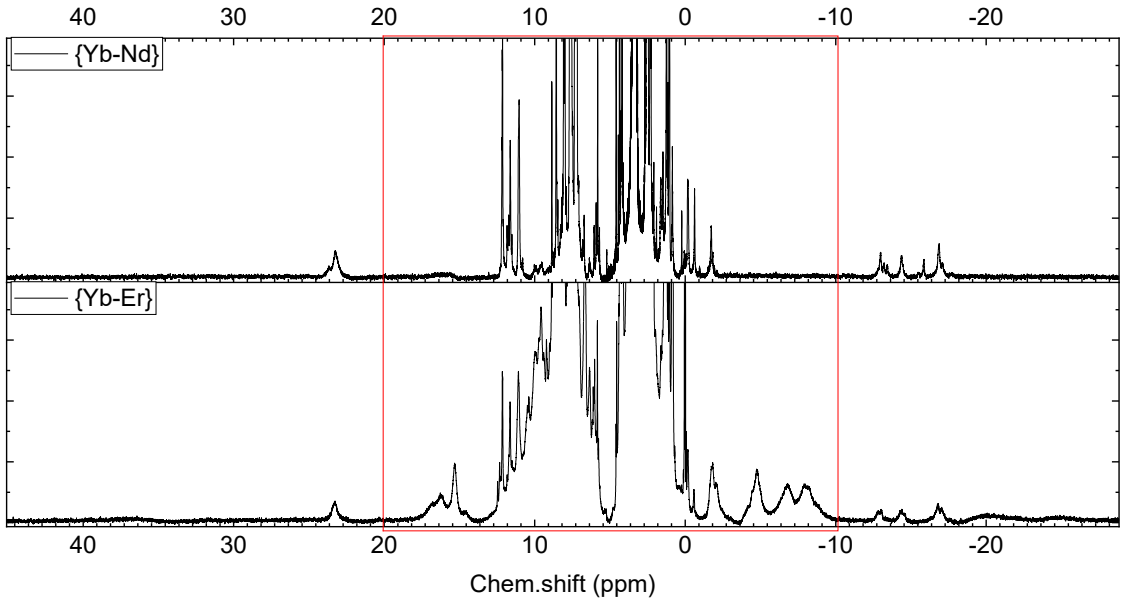

a)

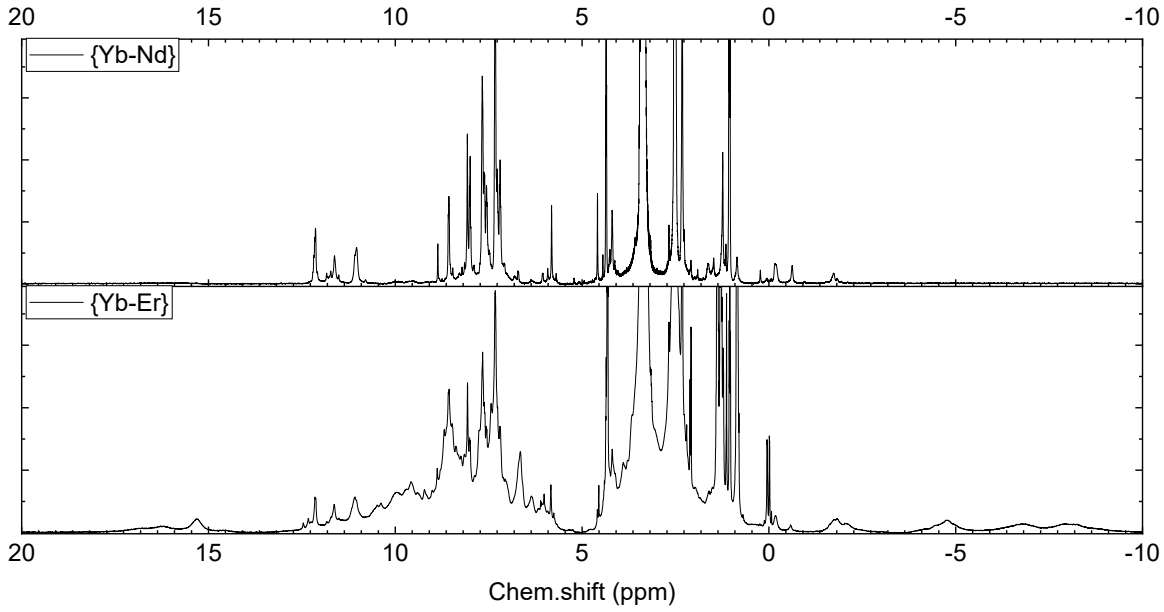

b)

Figure S 33. ^{1}H NMR spectra of {Yb-Nd} and {Yb-Er} in a) wide, b) short range. Red frame indicates short range.

Luminescence data of conjugates

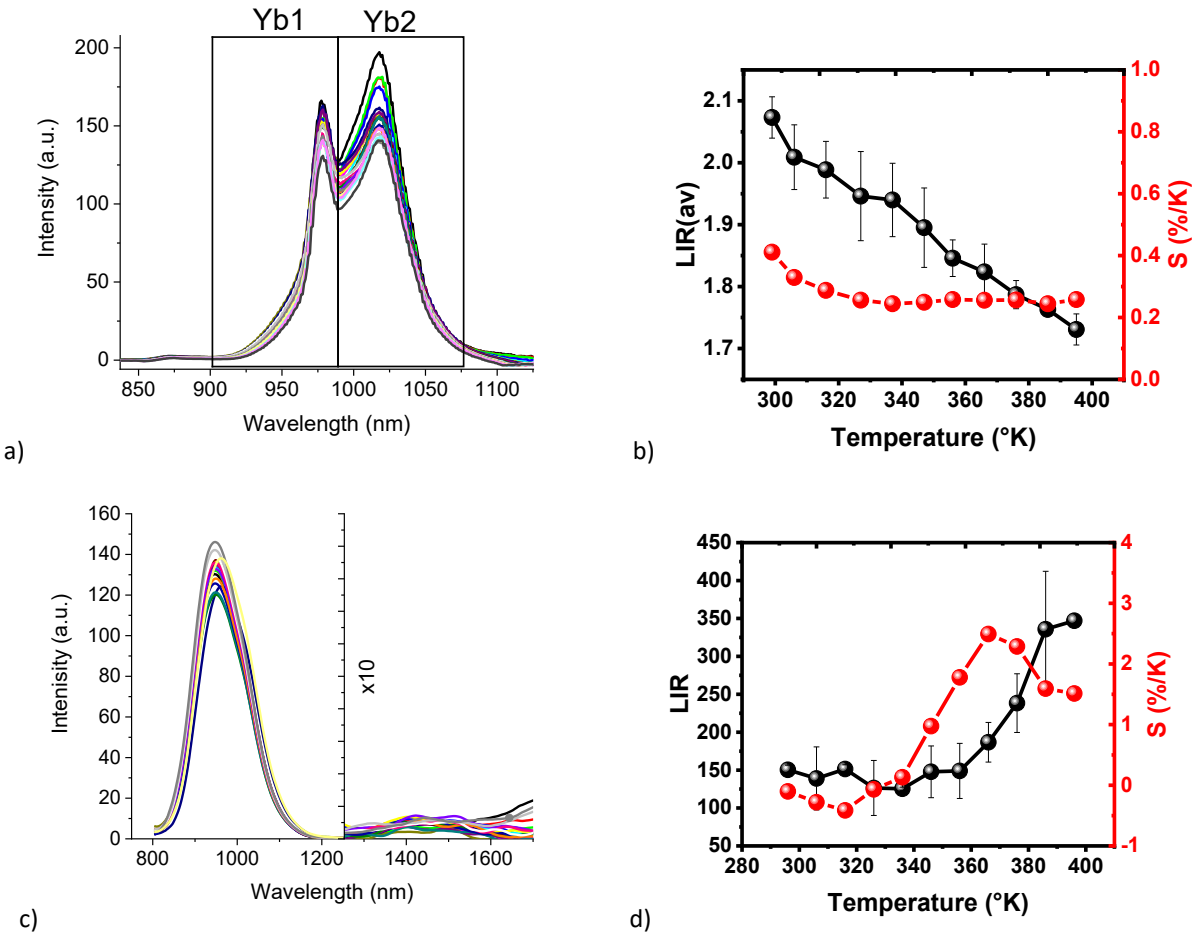

Figure S 34. Luminescence spectra change with the temperature and LIR of a), b) {Yb-Nd} and c),d) {Yb-Er}.

Table S 1. Luminescence data of the monometallic complexes and conjugates.

	ε_{max} (330-365 nm), $(M \cdot cm)^{-1}$	ε_{max}, (365-450 nm) $(M \cdot cm)^{-1}$	QY_{Ln}^{L}, %		QY_{Ln}^{Ln}, %	η_{sens}, %	τ_{obs}, μs	τ_{rad}, μs
			Pow.	DMSO				
Yb(L1)(HL1)*	33 000	38 400		1.04	2.4	43	15.7 (2)	659 (30)
$K[Yb(L1)_2](H_2O)_2$*	30 600	45 300	1.27	1.5	2.5	60	22.6 (2)	900 (78)
Yb(L2)(HL2)	30 100	26 300	1.1	0.85	1.2	73	11.3	968 (53)
$K[Yb(L2)_2](H_2O)$	42 300	48 000	1.0	0.58	1.3	45	14.0	1080 (58)
Nd(L1)(HL1)	43 000	23 000	0.11		-	-	1.4	-
$K[Nd(L1)_2](H_2O)$	39800	13200	0.10		-	-	1.2	-
Nd(L2)(HL2)	40 100	16 600	0.07		-	-	1.5	-
$K[Nd(L2)_2](H_2O)$	35 600	16 700	0.02		-	-	1.4	-
Er(L2)(HL2)	37 600	30 900	-		-	-	-	-
$K[Er(L2)_2](THF)_{0.5}$	29 800	31 800	-		-	-	-	-
$Yb_2(HL3)_2(THF)_{0.5}(H_2O)$	95900	60600	0.67	1.58	1.7	91	10.2	586
{Yb-Lu}	-	-	0.2				11.6	
{Yb-Yb}	-	-	0.16				8.8	
{Yb-Nd}	12 000	2 500	0.32	0.66	2.1/2.5	15/26	17.6/20.7	840 (46)

{Yb-Er}	12 000	5300	0.13	0.30	4.8	6.25	20.8	434 (31)

Luminescence decay of conjugates

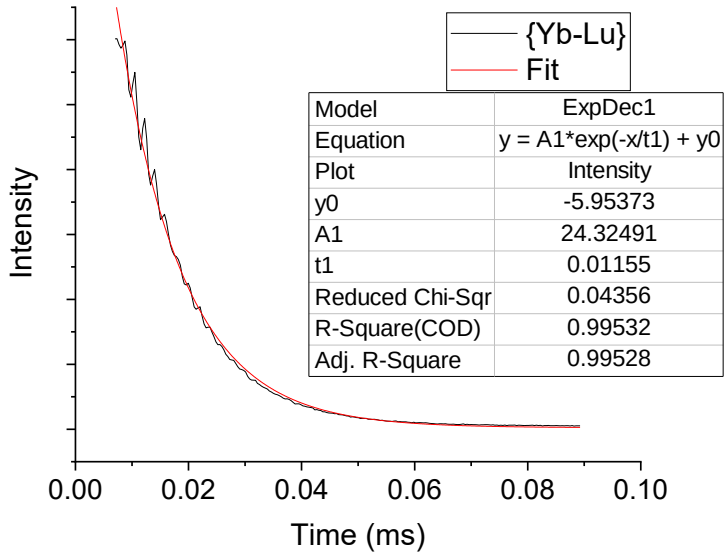

a)

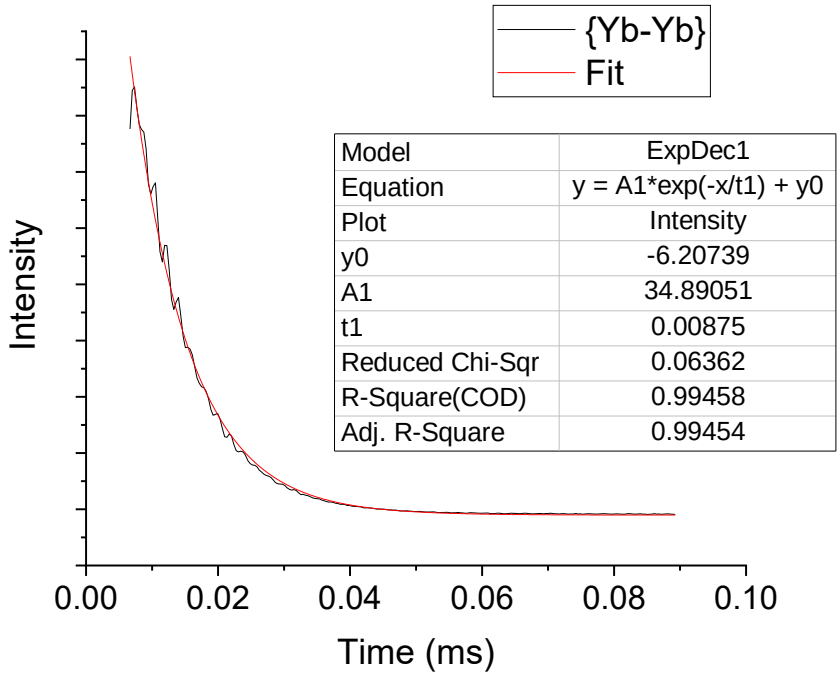

b)

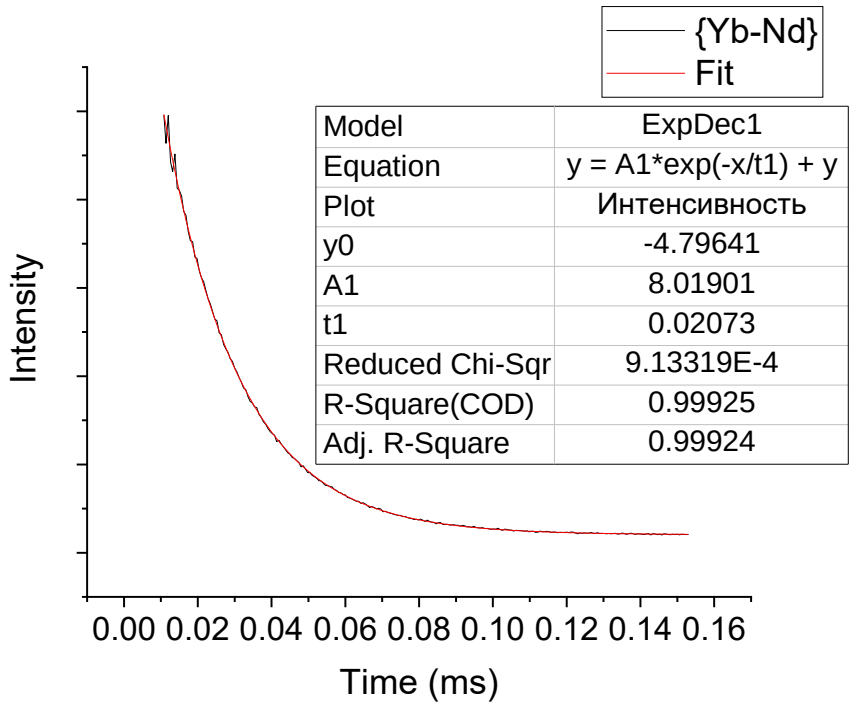

c)

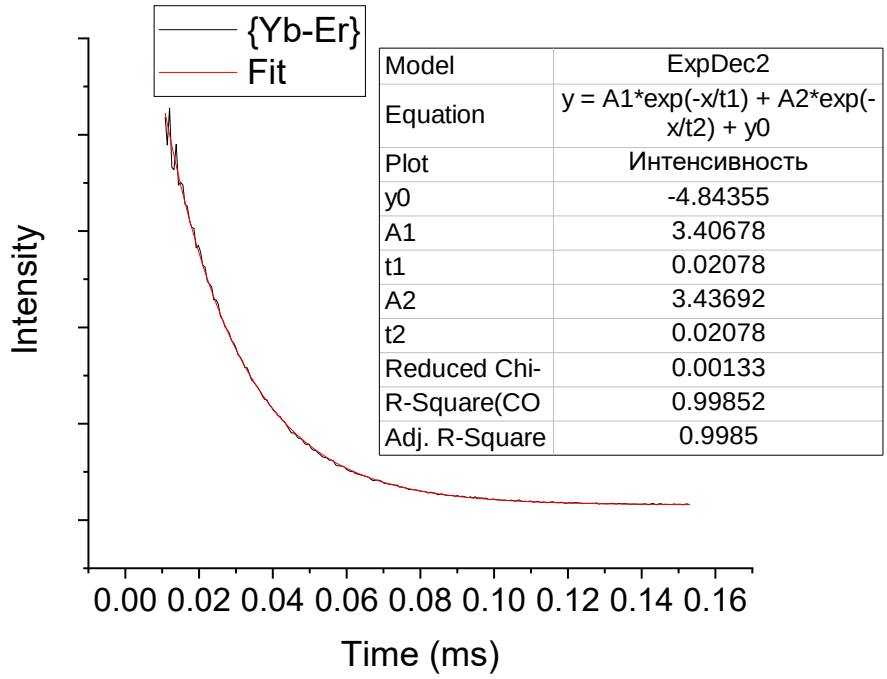

d)

Figure S 35. Lumnescence decay curves of a) {Yb-Lu}, b) {Yb-Yb}, c) {Yb-Nd}, d) {Yb-Er}.

VIS absorption spectra

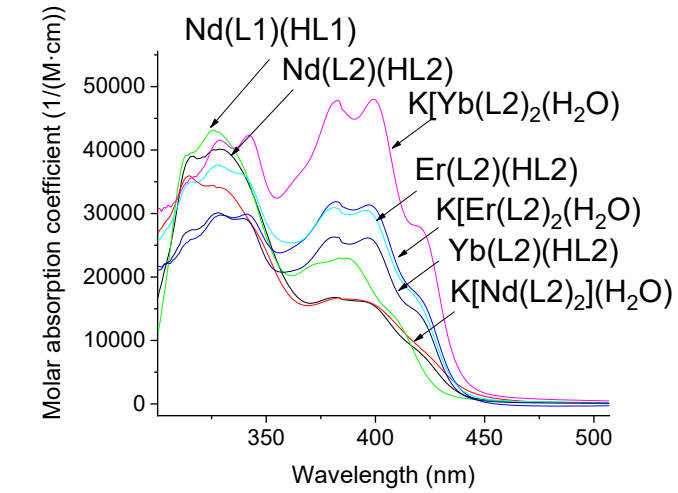

a)

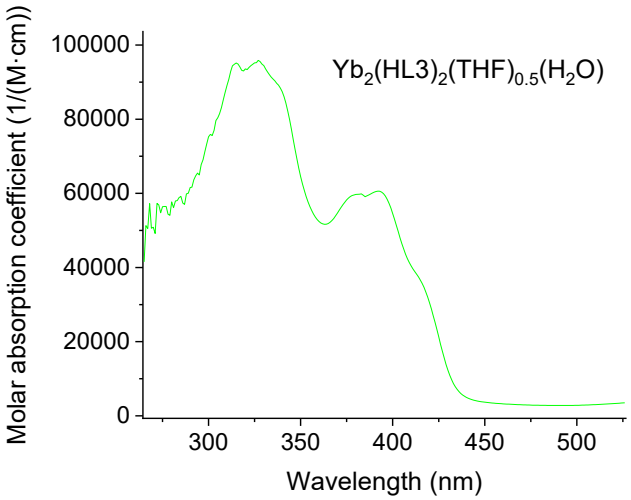

b)

Figure S 36. Vis absorption spectra of a) Ln(**L**)(H**L**) and K[Ln(**L**)$_2$](H$_2$O)$_n$ (**L** = L1, L2; Ln=Nd, Er, Yb), b) Yb$_2$(HL3)$_2$(THF)$_{0.5}$(H$_2$O).

NIR absorption spectra

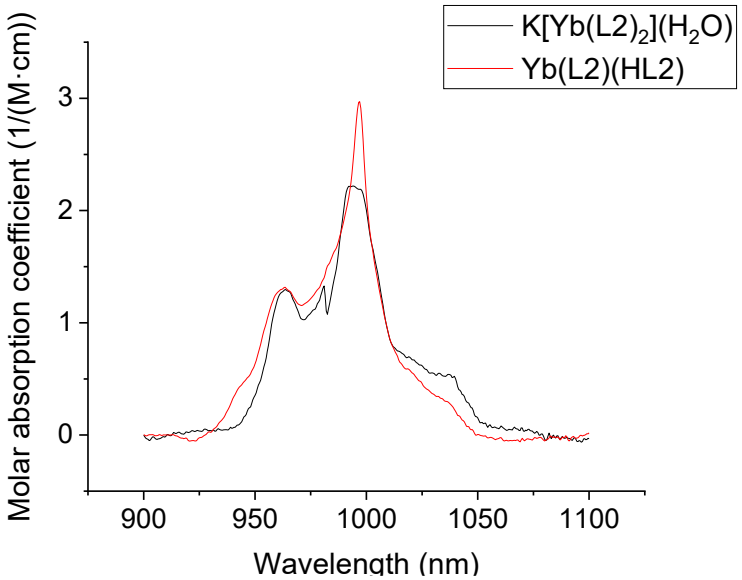

a)

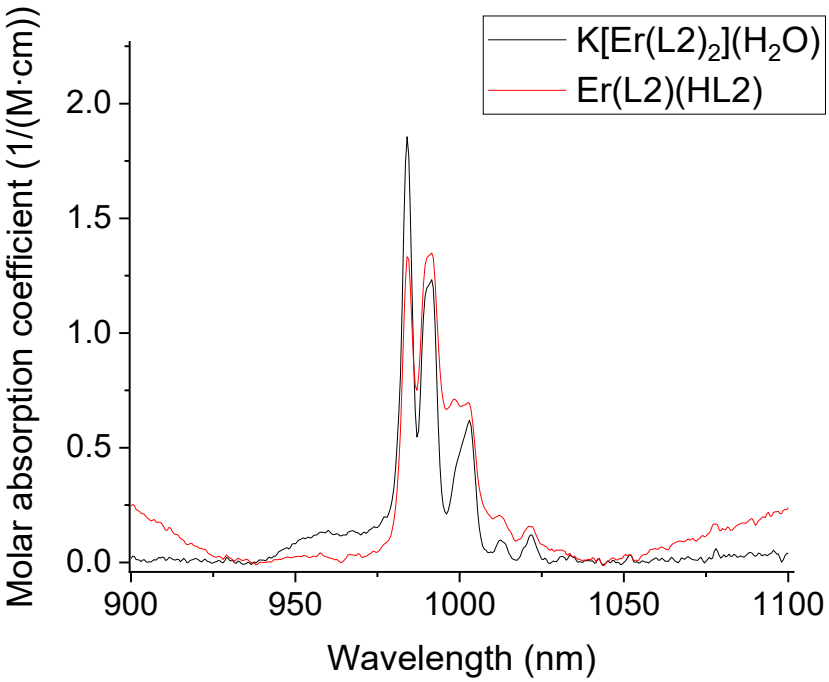

b)

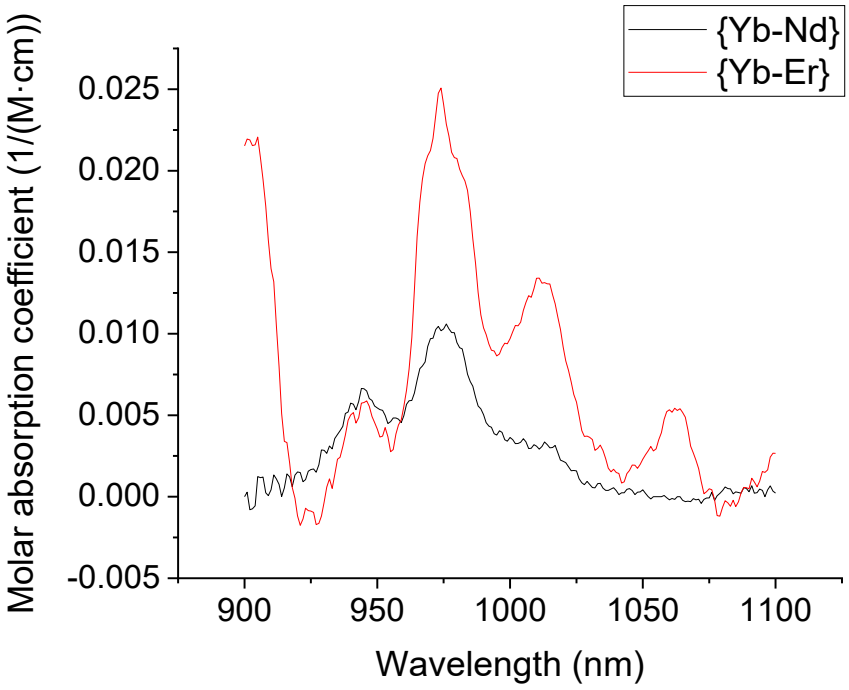

c)

Figure S 37. NIR absorption spectra of a) Yb(L2)(HL2) and $K[Yb(L2)_2](H_2O)$, b) Er(L2)(HL2) and $K[Er(L2)_2](THF)_{0.5}$, c) {Yb-Nd} and {Yb-Er}.

Triplet excited state energy determination

The complex of gadolinium with H_2L2 was used for ligand triplet state energy determination. The high paramagnetic effect of Gd^{3+} ion increases intersystem crossing and hence induces phosphorescence at low temperatures and even at normal conditions [19–21]. In the case of Gd(L2)(HL2), it was observer two emission bands with maximums on 460 and 520 nm. After cooling with liquid nitrogen emission band at 520 nm increased. This means that long-wave radiation originates from the triplet level, which is more effectively extinguished under normal conditions. The triplet excited state energy could be estimated by the maximum of phosphorescence emission band and appears to be equal to $T_1(L2) = 19\ 230\ cm^{-1}$.

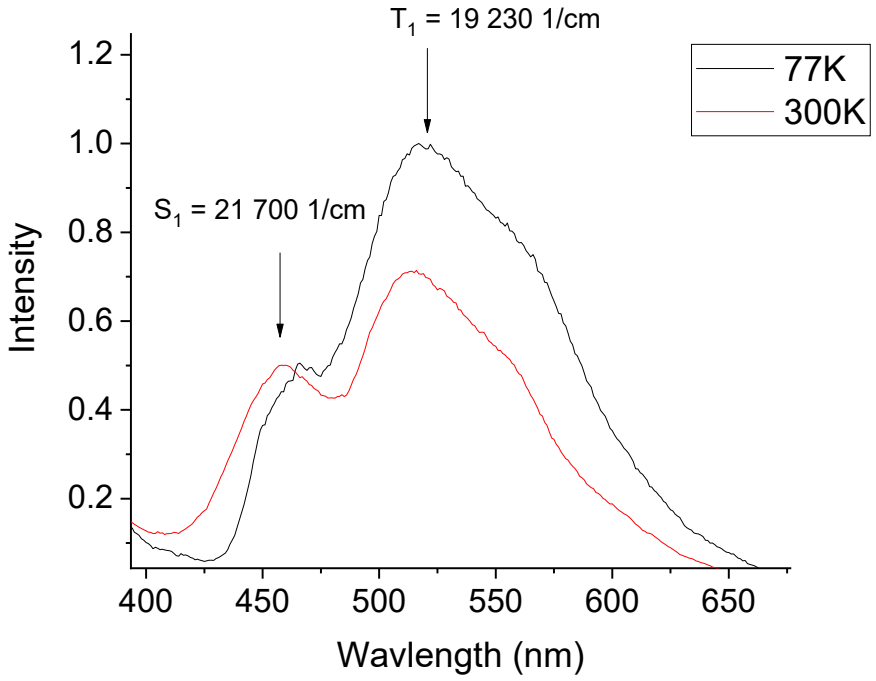

a)

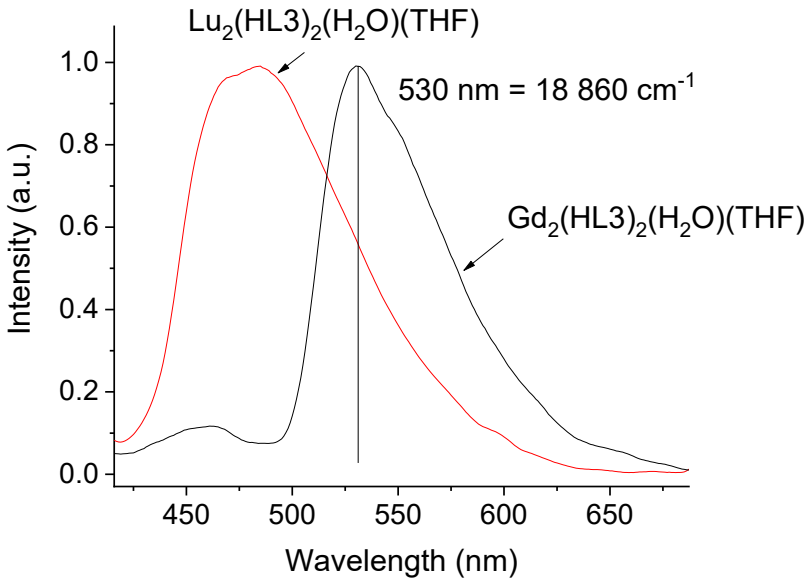

b)

Figure S 38. Luminescence spectra of a) Gd(L2)(HL2) at 300 and 77K, b) $Gd(HL3)_2(H_2O)(THF)$ and $Lu(HL3)_2(THF)$.

Cytotoxicity

Cytotoxicity of the compounds was measured in standard MTT test on cancer (A549, non-small cell lung carcinoma; HCT116, colorectal carcinoma; MCF-7, breast adenocarcinoma) and non-cancer cells (WI-38, diploid human cell line) (**Ошибка! Источник ссылки не найден.**).

Table S 2. MTT test results for conjugates; n/a = non-active.

	IC_{50}, μM			
Cell line /Compound	A549	HCT116	MCF-7	WI-38
{Yb-Nd}	92.2±3.3	90.6±2.9	86.9±2.6	n/a
{Yb-Er}	30.4±2.0	101.8±5.5	n/a	n/a
Cisplatin	2.6±0.8	6.6±0.4	4.8±0.5	5.2±1.1

Both tested compounds appeared to be not active (marked as n/a in the table) for the WI-38 cell line, with {Yb-Nd} also showing no activity for MCF-7 cells. Both conjugates showed activity on A549 and HCT116 lines with IC_{50} values (inhibitor concentration for 50% cell viability) in the submillimolar range. Despite this rather low toxicity, such a different activity in cancer cells and WI-38 cells allows considering them as selective chemotherapy agents.